

Selection and characterization of llama-derived anti-P2X7 single domain antibodies

Dissertation

Zur Erlangung der Würde des Doktors der Naturwissenschaften
des Fachbereichs Biologie, der Fakultät für Mathematik, Informatik und
Naturwissenschaften,
der Universität Hamburg

vorgelegt von

Welbeck Owusu Danquah

aus Kumasi, Ghana

Hamburg, August 2012

Genehmigt vom Fachbereich Biologie
der Fakultät für Mathematik, Informatik und Naturwissenschaften
an der Universität Hamburg
auf Antrag von Professor Dr. F. NOLTE
Weiterer Gutachter der Dissertation:
Professor Dr. W. STREIT
Tag der Disputation: 12.10.2012

Hamburg, den 21.09.2012



Professor Dr. J. Fromm

Vorsitzender des Promotionsausschusses
Biologie

Eidesstattliche Versicherung

Hiermit erkläre ich an Eides statt, dass ich die vorliegende Dissertationsschrift selbst verfasst und keine anderen als die angegebenen Quellen und Hilfsmittel benutzt habe.


HAMBURG, 08.10.2013

First Examiner:

Prof. Dr. Friedrich Koch-Nolte

University Medical Center (UKE), Hamburg-Eppendorf

Martinistr. 52, 20246 Hamburg

Second Examiner:

Prof. Dr. Wolfgang Streit

Biozentrum Klein Flottbek

Ohnhorstr. 18, 22609 Hamburg

Date of Final Oral Defence:

12th October 2012

Acknowledgements

Special thanks go to Prof. Dr. Friedrich Koch-Nolte for providing me the opportunity to pursue such an exciting field of science. I am thankful for his constant readiness during this whole pursuit, to listen and to provide fresh impulse and for his support in acquiring the skill of independent scientific research. I am also thankful for his encouragement and provision for the means to take part in international scientific congresses by which my scientific horizon was expanded.

My thanks also go to Prof. Dr. Wolfgang Streit for showing interest in my thesis and for his willingness to assume the role of the second examiner.

I am thankful to Prof. Dr. Friedrich Haag, Prof. Dr. Hans-Willi Mittrücker and Dr. Eva Tolosa for the countless scientific discussions - I always learnt something new.

I am also grateful for all the colleagues of the Institute of Immunology with whom I worked in the last years and for the constructive atmosphere in which a lot of progress was made. I especially thank Mandy Unger, a comrade in Nanobody research for the many tips shared; Björn Rissiek for his enthusiasm and help with flow cytometry techniques; Marion Nissen, Gudrun Dubberke, Fabienne Seyfried and Joanna Schmidt for their excellent and patient technical assistance in acquiring important experimental skills.

To Cathy Meyer-Schwesinger and her group for the teamwork on the EAG model.

To Ablynx, especially Toon Laeremans, Catelijne Stortelers and Joanna Assunção for the fruitful collaboration.

To my wife and friend, Jana, for her support through all the years, and to our daughter Yovela Hope, for being such a joy.

Table of Contents

Abstract	10
1 Introduction	12
1.1 Purinergic signaling by nucleotides released from cells	12
1.2 The nucleotide-gated P2X7 ion channel	13
1.2.1 Secondary responses of P2X7 activation	14
1.2.2 Splice variants and single nucleotide polymorphisms	15
1.2.3 P2X7 in diseases	17
1.2.4 P2X7 antagonism	17
1.3 Antibodies in the immune response	18
1.3.1 Conventional antibodies	19
Antibody architecture	20
Antibody classes	20
1.3.2 Llama heavy chain antibodies and nanobodies	22
1.4 Phage display	24
1.4.1 Bacteriophages: biology and structure	25
1.4.2 Generation of phage libraries	25
1.4.3 Selection by bio-panning	26
1.5 Autoimmune glomerulonephritis	27
2 Goals of the project	29
3 Materials	30
3.1 Lab Equipment	30
3.2 Consumables	31
3.3 Chemicals	31
3.4 Affinity Chromatography matrices	33
3.5 Media, buffers and solutions	33
3.5.1 Eukaryotic cell culture media	33

3.5.2 Bacterial culture media	33
3.5.3 Eukaryotic cell lysis buffer	34
3.5.4 Bacterial cell lysis buffer	34
3.5.5 Antibody staining buffers	34
3.5.6 SDS-PAGE and western blot buffers	35
3.5.7 DNA agarose gel electrophoresis buffer	35
3.5.8 Affinity chromatography buffers	35
3.6 DNA and protein standards	36
3.7 Enzymes	36
3.8 Oligonucleotides and plasmids	36
3.9 Kits	36
3.10 Antibodies	37
3.11 Helperphages	37
3.12 Cell lines	37
3.13 E. coli strains	38
3.14 Mouse strains	38
4 Methods	39
4.1 Methods in molecular biology	39
4.1.1 Transformation of bacteria	39
<i>Transformation of chemically competent bacteria</i>	<i>39</i>
<i>Transformation of electro-competent bacteria</i>	<i>39</i>
4.1.2 Cultivation of bacterial culture	39
4.1.3 Cryopreservation of bacteria	40
4.1.4 Preparation of plasmid DNA	40
4.1.5 Quantification of DNA and RNA	40
4.1.6 Restriction digestion of DNA	40
4.1.7 Dephosphorylation of DNA fragments	40
4.1.8 Agarose gel electrophoresis of DNA and RNA fragments	41
4.1.9 Extraction of DNA fragments from agarose gel	41

4.1.10 Ligation of DNA fragments	41
4.1.11 Polymerase chain reaction (PCR)	41
4.1.12 DNA sequencing	43
4.1.13 Preparation of RNA from peripheral llama blood lymphocytes	43
4.1.14 Reverse transcription of RNA to cDNA	43
4.1.15 Construction of anti-P2X7 VHH library	44
4.1.16 Phage rescue (generation of VHH phage library)	45
4.1.17 Phage precipitation	45
4.2 Methods in cell biology	46
4.2.1 Cell culture of eukaryotic cells	46
4.2.2 Determination of cell number using Neubauer chamber	47
4.2.3 Transfection of eukaryotic cells	47
4.2.4 Preparation of HEK cell lysates	47
4.2.5 Enrichment of P2X7-specific HEK cells per Easy-Sep	47
4.2.6 Panning of phages on cells and phage rescue	48
4.2.7 Flow cytometry (FACS)	49
4.2.8 Preparation of leukocytes from peripheral blood (mouse and human)	50
4.2.9 Preparation of splenocytes	50
4.2.10 Preparation of liver leukocytes	50
4.2.11 Staining of cell surface proteins	51
<i>Cell lines</i>	51
<i>Peripheral blood</i>	51
<i>Mouse splenocytes and liver leukocytes</i>	52
4.2.12 P2X7-mediated shedding of cell surface proteins and exposition of phosphatidylserine – blockade by Nanobodies	53
<i>Yac-1 cell line</i>	53
<i>Transfected HEK cells</i>	54
<i>Human peripheral blood</i>	55
<i>Mouse splenocytes and liver leukocytes</i>	55
4.2.13 P2X7-mediated apoptosis assays	56
4.2.14 Screening for P2X7-specific Nanobody clones	56

4.3 Methods in protein biochemistry	57
4.3.1 Preparation of bacterial periplasma lysates	57
4.3.2 Protein purification by affinity chromatography	57
<i>Immobilized metal affinity chromatography (Nickel-NTA)</i>	57
<i>M2 anti-FLAG affinity chromatography</i>	58
<i>Hano43/Hano44-coupled AminoLink affinity immunoprecipitation</i>	58
4.3.3 Sodium dodecyl sulfate polyacrylamide gel electrophoresis (SDS-PAGE)	58
4.3.4 Coomassie blue staining	59
4.3.5 Desalting of protein elution fractions	59
4.3.6 Quantification of proteins	59
4.4 Methods in animal experiments	60
4.4.1 Immunization of llamas	60
4.4.2 Injection of mice with anti-P2X7 nanobodies	60
4.4.3 Induction of anti-podocyte nephritis in mice	60
5 Results	62
5.1 Cloning, selection, reformatting and expression of anti-P2X7 Nbs	62
5.1.1 Immunized llamas show P2X7-specific antibody response	62
5.1.2 Cloning of PCR-amplified VHH coding regions yields immune libraries	65
5.1.3 Panning of phage libraries on P2X7-expressing cells yields 18 families of mP2X7-specific and 3 families of hP2X7-specific Nbs	67
5.1.4 Reformatting, expression and purification of Nanobodies in monomeric, dimeric, bi-specific and Nb-Fc fusion formats	72
5.1.5 Nb 1c81 recognizes mouse, rat and human P2X7, four other Nbs show selective reactivity with mouse or human P2X7	74
5.2 Molecular and functional characterization of hP2X7-specific Nanobodies	76
5.2.1 Cross-blockade binding analyses show that Nbs 1c81 and 1c113 share an overlapping binding site with the anti-hP2X7 mAb L4	76
5.2.2. Combination of epitope-independent Nbs permits visualization of P2X7 on human peripheral blood lymphocytes and monocytes	77
5.2.3 Fc-fusion proteins of Nanobodies 1c81 and 3c23 inhibit ATP-induced shedding of CD62L by hP2X7 and CD62L co-transfected HEK cells	80
5.2.4 In a dose-response assay, Nbs 1c81 and 3c23 inhibit shedding of CD62L in transfected HEK cells more efficiently than mAb L4	81

5.2.5 Nb-Fc fusion proteins of Nanobodies 3c23 and 1c81 inhibit ATP-mediated externalization of phosphatidylserine by RPMI 8226 myeloma cells	82
5.2.6 Nb-Fc fusion proteins of Nbs 1c81 and 3c23 prevent P2X7-mediated cell death of RPMI 8226 cells	83
5.2.7. Nb-Fc fusion proteins of Nbs 1c81 and 3c23 block ATP-induced externalization of PS and shedding of CD62L by primary human T cells	85

5.3 Biochemical and functional characterization of mouse P2X7-specific Nbs **87**

5.3.1 At saturating doses, several mP2X7-specific Nbs inhibit P2X7 mediated shedding of CD62L by Yac-1 lymphoma cells	87
5.3.2 Dose-response analyses reveal a rank order of inhibitory potencies of five families of anti-mP2X7 Nbs	89
5.3.3 Titrations ATP and NAD ⁺ at fixed Nb concentration reveal rank order of inhibitory and enhancing potencies of anti-mP2X7 Nbs	91
5.3.4 Reformatting of Nbs into dimeric molecules increases potency	92
5.3.5 Nb 13A7 and 8G11 block, Nb 14D5 potentiates nucleotide-induced shedding of CD62L by primary Balb/c T cells	95
5.3.6 Intraperitoneal injection of Nb 13A7-13A7 blocks P2X7 activation ex vivo in B6 mice	96
5.3.7 Genetic fusion of dimers of Nbs 13A7 and 14D5 to albumin-specific Nb, ALB8, does not reduce the capacity of these Nbs to block or potentiate P2X7	100
5.3.8 Intravenous injections of ALB8-linked dimeric Nbs 13A7 and 8G11 block activation of P2X7 ex vivo 2 h post injection	101
5.3.9 Intravenous injection of 13A7-13A7-ALB blocks P2X7 activation whereas 14D5-14D5-ALB results in loss of CD4 ⁺ CD25 ⁺ Tregs in vivo	103

6 Discussion **109**

6.1 Selected Nbs modulate P2X7 activation **109**

6.2 Applications of anti-P2X7 Nbs in research **115**

6.2.1 Nbs permit detection of P2X7 in native conformation	115
---	-----

Monomeric, dimeric and Nb-Fc constructs 116

Nb-Alkaline phosphatase (PhoA, ALPP) fusion proteins 116

Nb-AviTag-biotin-streptavidin constructs 117

6.2.2 Anti-P2X7 Nbs as specific inhibitors in vitro and in vivo	118
---	-----

Extending the in vivo half-life of Nbs 118

6.2.3 Use of P2X7-blocking Nbs to protect Tregs from NAD-induced cell death in experimental set-ups	119
---	-----

6.3 Nb-mediated antagonism of P2X7 as a therapeutic approach **120**

6.3.1 Potential application of P2X7-blocking Nbs in Glomerulonephritis	121
6.3.2 Potential application of P2X7-blocking Nbs in Multiple sclerosis	122
6.4 Nb potentiation of P2X7 activation as a therapeutic approach	123
6.4.1 Combining Nb-mediated potentiation of P2X7 activation with chemotherapy to improve tumor therapy	124
<i>Enhancing uptake and reducing expulsion of chemotherapeutic compounds</i>	124
<i>Depletion of Tregs</i>	124
6.4.2 Nb-mediated potentiation of P2X7 as a therapeutic approach in the clearance of intracellular pathogens	125
6.5 Perspectives	125
7 Appendix	126
<i>7.1 Oligonucleotides (Primers)</i>	<i>126</i>
<i>7.2 Plasmid maps</i>	<i>127</i>
<i>7.3 Sequences of isolated Nanobody clones</i>	<i>128</i>
<i>7.4 Abbreviations</i>	<i>131</i>
8 References	133

Abstract

P2X7 is an ATP-gated ion channel that is widely expressed on cells of the immune system. ADP-ribosylation by the toxin-related ADP-ribosyl transferase 2 (ART2) at Arg-125 also gates the purine receptor, likely by presenting the covalently linked ADP-ribose as an ATP-analog to the ligand binding pocket. P2X7 mediates shedding of cell surface antigens and cell death and reportedly is involved in several autoimmune and inflammatory diseases. Specific antagonists of the receptor have therefore been proposed as potential new therapeutics. Our research group and others have previously demonstrated that single domain antibodies (V_HHs or Nanobodies) derived from llama heavy chain only antibodies (hcAbs) exhibit a propensity to bind to and block functional crevices on proteins such as the active site of an enzyme. In this study, Nanobodies (Nbs) were generated from P2X7-immunized llamas and tested for their capacity to specifically bind and functionally modulate P2X7. To induce antibodies against native P2X7, llamas were immunized with cDNA expression vectors for mouse and human P2X7 and with HEK cells transfected to stably express these receptors. The P2X7-specific antibody response was verified by FACS-analyses of sera obtained from immunized llamas. RNA was isolated from llama peripheral blood lymphocytes and reverse transcribed into cDNA. The V_HH repertoire was PCR-amplified and cloned into the pAX50 phagemid vector. Panning phage libraries on lymphoma cells endogenously expressing P2X7 and on P2X7-transfected cell lines yielded 31 distinct Nb families. Eighteen of these were verified to specifically bind mouse P2X7, three to specifically bind human P2X7. Half of the anti-mP2X7 Nb families were found to modulate NAD⁺- and ATP-mediated activation of the ion channel: six families inhibited P2X7-mediated shedding of CD62L while three families potentiated the activation of P2X7. Two of three anti-hP2X7 Nb families blocked P2X7-mediated shedding of CD62L and cell death, with 10-50 fold higher potencies than the previously described L4 monoclonal antibody. The third hP2X7-specific Nb family antagonized the purine receptor with a potency similar to that of mAb L4. Following intravenous or intraperitoneal injection, the two most potent mP2X7-antagonizing (13A7) or potentiating Nbs (14D5) specifically targeted P2X7 *in vivo* and demonstrated inhibition or potentiation of P2X7-mediated nucleotide-induced shedding of CD27 and exposition of phosphatidylserine *ex vivo*. *In vivo* targeting of P2X7 by synergistic Nbs resulted in partial depletion of regulatory T cell subset. In a pilot experiment to test the potential therapeutic utility of P2X7-Nbs in the mouse model of anti-podocyte antibody mediated glomerulonephritis, the P2X7 inhibiting Nb 13A7 attenuated disease while the synergistic Nb 14D5 mediated an early onset and a more severe disease course. The Nbs generated in this project have demonstrated utility as new research tools hold promise as novel therapeutic tools.

Zusammenfassung

P2X7 ist ein ATP-gesteuerter Ionenkanal, der auf einer Vielzahl von Immunzellen exprimiert wird. Durch die ADP-Ribosylierung von Arg-125 durch die Toxin verwandte ADP-Ribosyltransferase 2 (ART2) kann der Purinrezeptor ebenfalls aktiviert werden. P2X7 vermittelt sowohl die Abspaltung von Zelloberflächenantigenen als auch den NICD induzierten Zelltod und wird mit unterschiedlichen Autoimmun- und inflammatorischen Krankheiten in Verbindung gebracht. Aufgrund dessen werden P2X7 Antagonisten als neue Therapeutika in Betracht gezogen.

Einzeldomänenantikörper (V_HHs oder Nanobodies) leiten sich von der variablen Domäne der Lama Schwerekettenantikörper (hcAbs) ab. Arbeiten aus unserer und anderen Arbeitsgruppen konnten nachweisen, dass V_HHs die Eigenschaft aufweisen funktionelle Bereiche von Proteinen, wie das katalytische Zentrum von Enzymen zu binden und zu blockieren. In dieser Arbeit wurden aus P2X7 immunisierten Lamas, Nanobodies (Nb) generiert und auf ihre Fähigkeit getestet P2X7 spezifisch zu binden und dessen Funktionalität zu modulieren. Für die Induktion von Schwerekettenantikörpern gegen natives murines und humanes P2X7 wurden Lamas mit cDNA Expressionsvektoren bzw. mit P2X7 stabil transfizierten Zellen immunisiert. Die spezifische P2X7 Antikörperantwort wurde mittels FACS-Analysen der Lamaimmunseren bestätigt. RNA wurde aus peripheren Blutlymphozyten isoliert und über Reverse Transkription in cDNA umgeschrieben. Das V_HH-Repertoire wurde per PCR amplifiziert und in den Phagemid-Vektor, pAX50 kloniert. Die Phagenbibliotheken wurden auf Lymphomzellen, die endogen P2X7 exprimieren bzw. auf P2X7 transfizierten Zellen selektioniert. Es wurden 31 unterschiedliche Nb-Familien gewonnen, von denen 18 spezifisch murines P2X7 und drei spezifisch humanes P2X7 binden. Die Hälfte der anti-mP2X7 Nb-Familien beeinflussen die NAD⁺ und ATP vermittelte Aktivierung des Ionenkanals. Sechs Familien inhibieren die P2X7 vermittelte Abspaltung von CD62L, während drei andere die Aktivierung von P2X7 verstärken. Zwei der drei hpP2X7 Familien blockieren die durch den Purinrezeptor vermittelte Abspaltung von CD62L und den Zelltod mit einer 10-50 fach höheren Wirkung als der beschriebene monoklonale Antikörper, L4. Die dritte spezifische hpP2X7 Nb-Familie wirkt ähnlich wie der mAb L4 antagonistisch zum Purinrezeptor. Eine spezifische Bindung der beiden potenten mP2X7 Nbs (13A7 - Antagonist, 14D5 - Agonist) konnte *in vivo* nach intravenöser oder intraperitonealer Injektion nachgewiesen werden. Des Weiteren zeigte sich *ex vivo* eine Inhibierung bzw. Potenzierung der P2X7 vermittelten Abspaltung von CD27 und die Exposition von Phosphatidylserin. Es konnte gezeigt werden, dass die *in vivo* Bindung von 14D5 an P2X7 in der Maus zur partiellen Depletion der regulatorischen T Zellen führt. Um das therapeutische Potential der P2X7 Nbs zu untersuchen, wurden diese in einem Mausmodell der anti-Podozyten vermittelten Glomerulonephritis getestet. Hierbei konnte durch die Verwendung des inhibierenden Nbs 13A7 der Krankheitsverlauf gemildert werden, wobei der synergistische Nb 14D5 zu einem früheren und schwereren Krankheitsverlauf führte. Die in diesem Projekt generierten Nbs konnten ihren Nutzen als neue Forschungswerkzeuge bestätigen und zeigen Potential für die Anwendung in der Therapie.

1 Introduction

1.1 Purinergic signaling by nucleotides released from cells

Nucleotides such as ATP and NAD⁺ are released from cells during various physiological and pathological conditions (Haag *et al*, 2007; Adriouch *et al*, 2012; Wilhelm *et al*, 2010; Di Virgilio, 2007; Hubert *et al*, 2010; Wang *et al*, 2004; la Sala *et al*, 2003; Adriouch *et al*, 2007; Scheuplein *et al*, 2009). These extracellular nucleotides transmit signals via various receptors and ecto-enzymes. Purine receptors are a family of ligand-gated transmembrane proteins widely expressed in the body that mediate a plethora of cellular and physiological effects (Fredholm *et al*, 1994; Burnstock, 2007). Signaling via purine receptors potentiates insulin secretion by islet β -cells (Richards-Williams *et al*, 2008) and nitric oxide production by lung endothelial cells (Kiefmann *et al*, 2009); mediates platelet activation and aggregation in blood clotting (Dorsam & Kunapuli, 2004); plays a role in the immune suppressive effects by regulatory T cells (Csóka *et al*, 2008); mediates development of allergic contact dermatitis (Weber *et al*, 2010) and is involved in sensation to neuropathic pain (Trang *et al*, 2012). Purine receptors comprise two subtypes, designated P1 and P2, reflecting their gating by adenosine (nucleoside) or ADP/ATP (nucleotide) respectively. The P2 subtype is further divided into P2X and P2Y receptors based on structural differences and the different cellular responses mediated upon gating (Burnstock, 2007). Both P1 and P2Y receptors are G protein-coupled seven-pass transmembrane receptors (GPCRs) mediating metabotropic cellular effects whereas P2X receptors are a unique family of homo- and heterotrimeric ion channels.

P2X receptors

P2X receptors are ligand-activated ion channels gated by ATP and other nucleotides. Most mammalian genomes encode seven members of the P2X family designated P2X1 – P2X7 (Burnstock, 2007). P2X receptors are widely expressed by smooth muscles, cells of the nervous system, testis, colon, gut, skin and cells of the immune system (Surprenant & North, 2009). All P2X receptors show a common topology composed of intracellular N- and C-termini, two hydrophobic transmembrane domains and a highly glycosylated extracellular domain containing 10 conserved cysteine residues. The full length protein of P2X receptors range from 384 (P2X4) to 595 (P2X7) amino acids encoded by 11 – 13 exons. The basic architecture of a functional P2X ion channel is a trimer, either homomeric

or heteromeric. Gating of P2X receptors is accompanied by the influx and efflux of ions, predominantly Ca^{2+} , Na^+ and K^+ ions with the respective receptors showing differing levels of ion selectivity, nucleotide selectivity and sensitivity (Burnstock, 2007).

1.2 The nucleotide-gated P2X7 ion channel

P2X7 is the seventh member of the family of ATP-gated ion channels (**Fig. 1.1**). Each subunit of the trimeric P2X7 ion channel has a molecular weight of 72 kDa comprising 595 amino acids. While formation of heteromeric trimers has been documented for all other P2X receptors, evidence points to a predominantly homomeric architecture in the P2X7 ion channel (Torres *et al*, 1999; Dubyak, 2007; Nicke, 2008). A structural peculiarity of P2X7 among all the other P2X receptors is the long C-terminus which has been shown to play important roles in P2X7 signaling, pore-formation, and cytotoxicity (Becker *et al*, 2008; Adriouch *et al*, 2002; Smart *et al*, 2003).

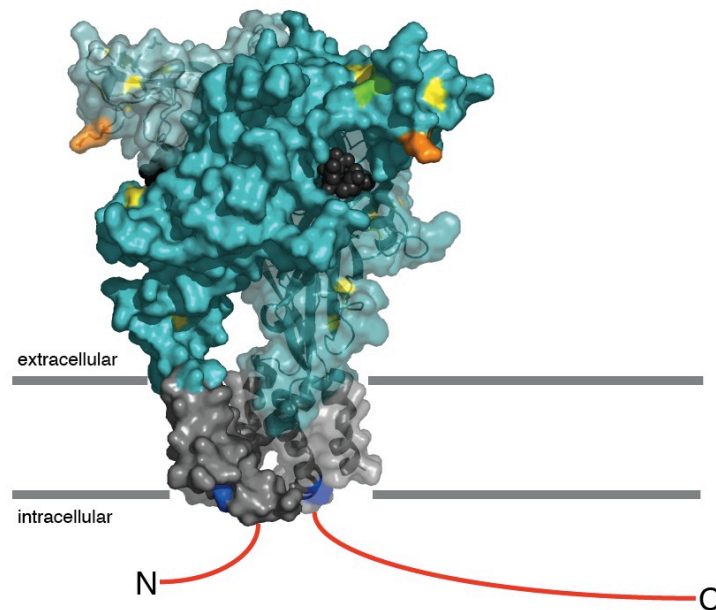


Figure 1.1. Structural characteristics of P2X7. Murine P2X7 was modeled based on the crystal structure of the zebra fish P2X4 (pdb code 4DW1, side view) using PyMOL. P2X7 forms homotrimers with each polypeptide clasping the other subunits like three dolphins with their flippers. The cytosolic N- and C-termini which were deleted for crystallization purposes are indicated by red lines (for clarity, the termini for only one of the three subunits are indicated). Peculiar to P2X7 among the P2X class of purine receptors is the long intracellular C-terminal tail which is a regulatory module necessary for pore formation. ATP (shown in black) binds in a pocket located at the interface between two interacting subunits. The site of ADP-ribosylation of P2X7 by the toxin-related murine ectoenzyme, ART2, is marked in orange (Arg-125). Proximally above the ATP-binding pocket, an ADP-ribose group bound to Arg-125 could present ADP-ribose as an ATP analog in the ATP-binding pocket. The positions of two allelic variants of human P2X7 that influence ATP sensitivity are shown in green (H155Y) and blue (A348T). Whereas the H155Y site is found in the ectodomain, the A348T site is found in the second transmembrane domain. Ten conserved cysteine residues that form five disulfide bridges in the ectodomain are coded yellow. The transmembrane domains are shaded gray.

P2X7 is a non-selective ion channel, gating by its cognate ligand, ATP, results in the influx of Ca^{2+} and Na^{+} ions and the efflux of K^{+} ions (Surprenant & North, 2009). In mice, an alternative mode of activation of the receptor has been demonstrated: a toxin-related ectoenzyme, ART2, expressed on T cells and iNKT cells transfers an ADP-ribose moiety from NAD^{+} to Arg125 of P2X7. This covalent modification presumably mimics ligand-binding and thereby elicits receptor activation (Adriouch *et al*, 2008; Young, 2010). P2X7 was initially described as a cytotoxic receptor in cells of hematopoietic lineage. Subsequent analyses have shown that P2X7 is expressed also by epithelial, mesenchymal and neural cellular lineages.

1.2.1 Secondary responses of P2X7 activation

In the event of cellular injury or inflammation, ATP and other nucleotides are released into the extracellular milieu as danger signals. P2X7 has been postulated as a sensor for these danger associated molecular patterns (DAMPs) (Haag *et al*, 2007; la Sala *et al*, 2003; Hoque *et al*, 2012). Sensing the presence of extracellular ATP and the mobilization of the immune response is mediated by P2X7 expressed on cells of the immune system. In macrophages and dendritic cells, P2X7 activation results in the processing of the leaderless 31kDa pro-IL1- β and the release of the mature 17 kDa IL1- β via activation of the NALP3 inflammasome (Di Virgilio, 2007). It has been demonstrated that the efflux of K^{+} ions which accompanies the activation of the purine receptor, is responsible for the assembly and the activation of the NALP3 inflammasome (Pétrilli *et al*, 2007; Jin & Flavell, 2010). This induces the cleavage of pro-caspase 1 to its active form which in turn cleaves IL1- β . Moreover, other pro-inflammatory cytokines such as IL-18 as well as soluble IL-6R and TNF- α have been demonstrated to be released in a P2X7-dependent manner (Perregaux *et al*, 2000; Mehta *et al*, 2001; Garbers *et al*, 2011; Suzuki *et al*, 2004). The release of soluble TNF- α and IL6R is attributed to metalloproteases of the ADAM family (Blobel, 2005). ADAM 17 (also TACE, TNF- α converting enzyme) and ADAM 10 have been demonstrated to be responsible for the ATP-induced, P2X7-mediated shedding of L-selectin (CD62L) and CD27 by T cells and iNKT cells as well the shedding of the low affinity IgE receptor, CD23, by B lymphocytes (**Fig. 1.2**)(Le Gall *et al*, 2009; Lemieux *et al*, 2007; Moon *et al*, 2006). Furthermore, P2X7 activation leads to a transient reversible exposition of phosphatidylserine on the outer leaflet of the plasma membrane, likely induced by the influx of Ca^{2+} ions (Seman *et al*, 2003; Scheuplein *et al*, 2009; Fadeel,

2004). Sustained activation of the purine receptor results in (i) the mobilization of pannexin hemichannels permeable to large organic cationic molecules up to 900 Da in size, (ii) disruption of the integrity of the plasmamembrane and (iii) cell death (Pelegrin & Surprenant, 2006; Scheuplein *et al*, 2009; Seman *et al*, 2003; Hubert *et al*, 2010; Baroja-Mazo *et al*, 2012; Gulbransen *et al*, 2012).

1.2.2 Splice variants and single nucleotide polymorphisms

The P2X7 gene is located on chromosome 12 in humans and on chromosome 5 in mice (Wiley *et al*, 2011). The full length protein is encoded by 13 exons interspaced by long stretches of non-coding sequences (introns). The intracellular N-terminus and part of the first transmembrane domain are encoded by exon 1, the ectodomain is by exons 2- 10, the second transmembrane domain by exons 10 and 11, and the intracellular C-terminal tail by exons 11-13 (Sluyter & Stokes, 2011). Several isoforms of P2X7 resulting from alternative splicing, have been reported in mouse, rat and human. Most of the minor splice variants lead to a reduced or complete loss of function (Sluyter & Stokes, 2011; Wiley *et al*, 2011). One splice variant, P2X7k has been described in rodents harboring an alternative exon 1 encoding the N-terminus and first transmembrane domain. P2X7k has been demonstrated to show increased ligand sensitivity and P2X7 signaling as compared to the major isoform, P2X7a (Nicke *et al*, 2009).

Numerous non-synonymous single nucleotide polymorphisms (SNPs) have been reported for the murine and human P2X7 gene. Some SNPs in human P2X7 result in loss of function (Sluyter & Stokes, 2011). The SNP rs3751143 (E496A) is associated with increased susceptibility to tuberculosis, likely due to impaired killing of intracellular mycobacteria (Fernando *et al*, 2007). Two common SNPs encoding the allelic variants H155Y and A348T influence ligand sensitivity, pore formation and secretion of IL-1 β by monocytes (Cabrini *et al*, 2005; Stokes *et al*, 2010). The chimpanzee, mouse and rat P2X7 orthologues each encompass Y155 and T348 at these positions, corresponding to the higher sensitive human P2X7 variants.

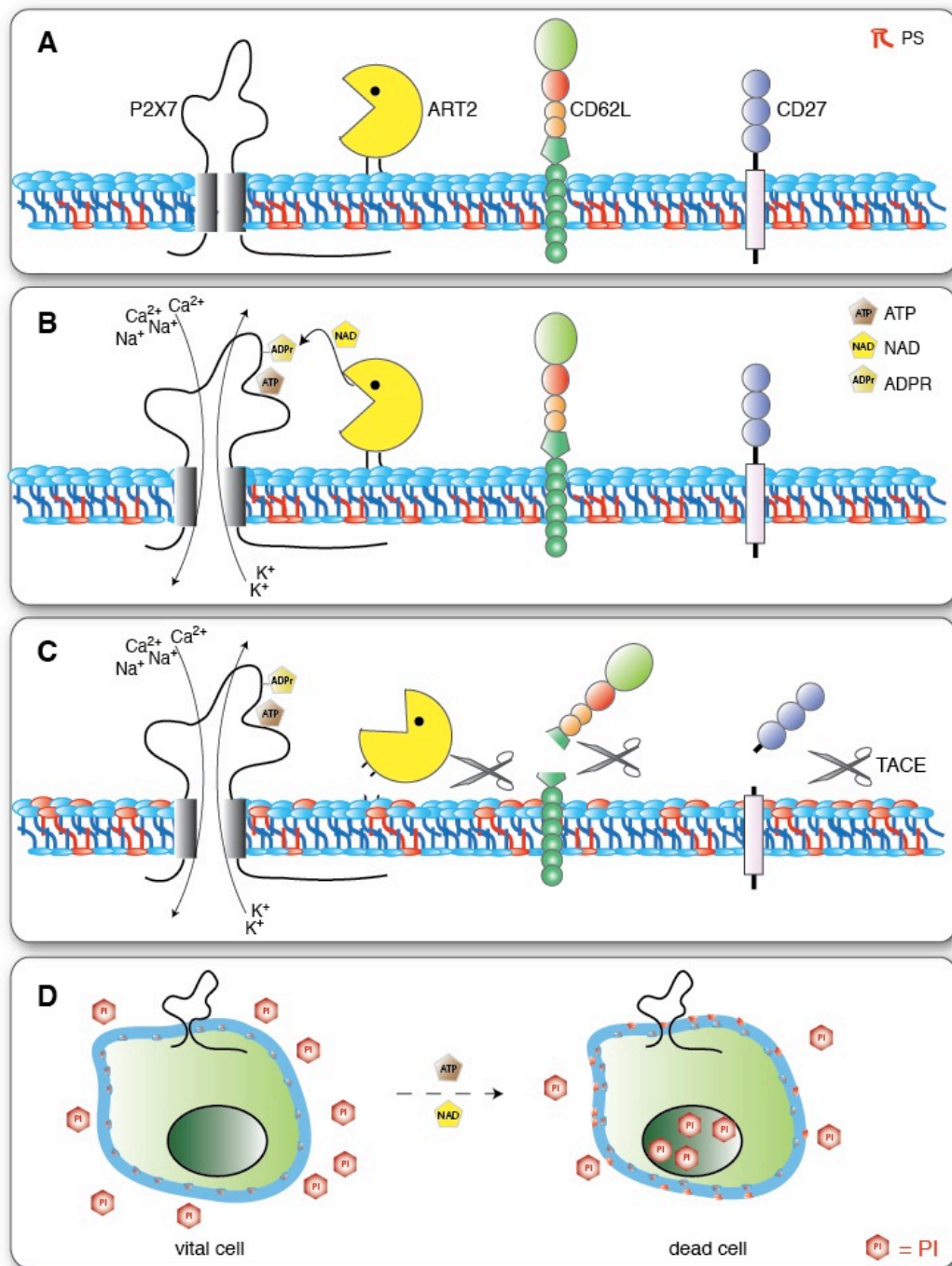


Figure 1.2. P2X7 mediates ectodomain shedding and cell death. (A) T cells express P2X7 together with the ectoenzyme, ADP-ribosyltransferase 2 (ART2), L-selectin (CD62L) and the TNF- α receptor family member, CD27. Moreover, the plasmamembrane is polarized: phosphatidylserine (PS) is found on the inner leaflet of the plasmamembrane. (B) P2X7 gating via binding by ATP or ADP-ribosylation of Arg-125 by ART2 leads to the influx of Ca²⁺ and Na⁺ ions and the efflux of K⁺ ions. (C) Activation of P2X7 leads to the shedding of the ectodomains of several cell surface proteins, including those of ART2, CD62L and CD27 by metalloproteases of the ADAM family such as the TNF- α converting enzyme (TACE, also ADAM17). Moreover, gating of P2X7 induces the externalization of PS to the outer leaflet of the plasmamembrane. (D) Living cells are impermeable to the DNA-intercalating compound, propidium iodide (PI). Sustained activation of P2X7 leads to cell death resulting in irreversible staining of DNA by PI. The latter is used as a marker for cell death.

1.2.3 P2X7 in diseases

Participation of P2X7 in several inflammatory diseases has been inferred from studies of P2X7 knock-out mice and from association studies of human P2X7 SNPs. P2X7-deficient mice were found to be less susceptible to experimental models of multiple sclerosis (Sharp *et al*, 2008), auto-immune nephritis (Taylor *et al*, 2009), and antibody-induced arthritis (Labasi *et al*, 2002). Activation of the NALP3 inflammasome mediated by P2X7 has been implicated to play a pivotal role in T-cell mediated type IV allergic contact dermatitis (Weber *et al*, 2010). P2X7 activation in neurons and the resulting pannexin-1 activation was demonstrated to mediate death of enteric neurons in colitis (Gulbransen *et al*, 2012). Moreover, the P451L allelic variant in the C-terminal tail of mouse P2X7 (Adriouch *et al*, 2002), was found to be associated with different sensitivities to sensory pain of B6 versus Balbc mice (Sorge *et al*, 2012). Similar associations were found also for human P2X7: following mastectomy, patients expressing more sensitive P2X7 variants reported more pronounced pain sensation as compared to those with less sensitive variants (Sorge *et al*, 2012). Less sensitive forms of P2X7 were reported to support tumor growth by reducing P2X7-mediated cell death whilst upregulation of P2X7 was found in certain tumors such as early forms of gastric cancer, colon cancer, breast carcinoma and kidney carcinoma (Di Virgilio *et al*, 2009; Adinolfi *et al*, 2012). Moreover, Tregs, which support tumor growth have been shown to be more sensitive to P2X7-mediated death than other T cell subsets (Hubert *et al*, 2010). Consequently, P2X7 antagonism has been proposed to be useful in treatment of many inflammation-based conditions while augmentation of P2X7 activation may support tumor clearance (Fu *et al*, 2009).

1.2.4 P2X7 antagonism

Reports suggesting a central role of P2X7 in inflammation and neuropathic conditions, has spurred research and development of P2X7 blocking small-molecule compounds. Three main groups of P2X7 antagonists can be defined. The first group entails ions such as calcium, zinc, magnesium and protons (Guile *et al*, 2009; Friedle *et al*, 2010). The second group includes ATP analogs and other small molecule compounds including the generic non-selective molecules such as PPADS, Brilliant Blue G, suramin, KN-62 and a range of more selective drugs discovered in high throughput screening assays such as A-740003, A-438079 and A-839977 (Abbot Labs) which have already been shown to provide therapeutic benefit in kidney inflammation (Taylor *et al*, 2009). Clinical studies have also

been conducted with similar compounds to probe the potential benefit of P2X7 antagonists in human clinical trials. AZD9056 (Astra Zeneca) was probed in Phase II clinical trials with patients suffering from chronic obstructive pulmonary disease (COPD) without any therapeutic benefit (Study code: D1521C00002). However, the same compound tested in Phase II trials in patients with Crohns disease, resulted in significant decrease in the disease activity index in patients (Study code: D8830C00002). Moreover treatment with AZD9056 resulted in reduced swollen and tender joints in a Phase II clinical trials with patients with rheumatoid arthritis (RA) receiving background treatment with methotrexate (Study code: D1520C05287). RA patients demonstrating lack of improvement following treatment with methotrexate were enrolled in Phase IIa/III clinical trials to probe the benefit of the P2X7 antagonist CE-224,535 (Pfizer). The study has been completed, pending analysis of outcome (Study code: NCT 00628095). Clinical applications of these molecules are hampered by unpredictable toxic side effects *in vivo* requiring tedious safety pre-trials (Arulkumaran *et al*, 2011). Antibodies constitute a third group of emerging P2X7 antagonists. So far, a single monoclonal antibody, L4, was shown to (partially) block P2X7 receptor function in human monocytes *in vitro* (Buell *et al*, 1998). Antibodies offer several advantages over small molecule compounds, including higher selectivity for their target antigens and lower toxicity. The goal of this project was to generate antibody-derived antagonists of P2X7 from immunized llamas and to characterize their specificity and possible therapeutic application.

1.3 Antibodies in the immune response

The immune system consists of the innate and adaptive systems. The innate immune system is already in place by birth and responds rapidly to common pathogenic structures with the help of germline-encoded pathogen recognition receptors (Kumar *et al*, 2011). This suffices to prevent most pathogens from causing infection. The innate immune system is however limited in diversity and is unable to keep up with rapidly evolving pathogens. In vertebrates, the adaptive arm of the immune system evolved as a more effective means to control infections (Rodríguez *et al*, 2012). The adaptive immune response comprises T cell mediated cellular and B cell mediated antibody responses. T and B cells carry highly diverse receptors that permit specific binding to antigens. T cells recognize antigens presented by antigen presenting cells (APCs) in context of major

histocompatibility complex molecules (MHC). CD4⁺ and CD8⁺ T cells recognize antigens in context of MHC class II and class I molecules, respectively (Janeway *et al*, 2005). Antibodies bind and neutralize viruses, bacteria and other microorganisms as well as secretory toxins by preventing interaction with the host. Moreover, antibodies bind to the surface of pathogens and opsonize them for clearance by phagocytes. Antibodies can also mediate activation of the complement pathway resulting in further opsonization of the pathogen and the formation of a lytic membrane attack complex which kills the pathogen (Janeway *et al*, 2005).

Antibodies are produced as soluble glycoproteins from terminally differentiated B cell-derived plasma cells. Upon binding of an antigen by the B cell receptor, the antigen is internalized, processed and presented in context of MHC II molecules on the surface of the cell. A primed T cell with the cognate T cell receptor recognizes and binds the complex of antigen-MHC II presented by the B cell and forms an immunological synapse. Interaction between CD40 expressed by the B cell and CD40 ligand expressed by the T cell, potentiates the T cell to locally release IL4 and other cytokines in the microenvironment of the immunological synapse. IL4 drives proliferation of the B cell and differentiation to antibody-producing plasma cells. Secretory antibodies carry the same antigen specificity as the B cell receptor (Noelle *et al*, 1992; Vallé *et al*, 1989).

1.3.1 Conventional antibodies

Conventional antibodies are glycosylated proteins of the immunoglobulin superfamily with a basic structure composed of two copies of two different polypeptide chains designated light and heavy chains. The light chain of a mammalian IgG antibody has a molecular weight of approximately 25 kDa whereas the heavy chain has a molecular weight of approximately 50 kDa. An identical pair each of light and heavy chains combine to form a Y-shaped 150 kDa IgG antibody (**Fig. 1.3**). Heavy and light chains associate by hydrophobic interactions and by a conserved inter-polypeptide disulphide bond connecting the C-terminal domains. The two heavy chain polypeptides are usually linked by two or more disulphide bonds in the hinge region (Davies & Chacko, 1993).

Antibody architecture

Light and heavy chains are composed of so called immunoglobulin domains of about 100-110 amino acids with a characteristic protein fold composed of two β -sheets (Janeway *et al*, 2005). Mammalian light chains consist of 2 such domains whereas heavy chain polypeptides are composed of 4 or 5 immunoglobulin domains depending on the antibody class. The N-terminal immunoglobulin domain of both light and heavy chains show highest sequence variability and is called variable domains (denoted V_L and V_H for light and heavy chains, respectively), whereas the less variable distal C-terminal domains are the constant domains. Each light chain possesses one constant domain (C_L) whereas 3 or 4 constant domains ($C_{H1} - C_{H3}/C_{H4}$) are found in antibody heavy chains. Each C_{H1} is linked to C_{H2} by a flexible proline-rich stretch of amino acids referred to as the hinge region. The $C_{H2} - C_{H3}$ (or $C_{H2} - C_{H4}$) tail domains of the antibody comprise the Fc domain. Induction of effector responses upon antigen binding is mediated by the Fc domain. The disulfide linked V_L-C_L and V_H-C_{H1} arms generated *in vitro* by proteolytic cleavage of the Y-shaped antibody are referred to as the Fab fragments (fragment of antigen binding) (**Fig. 1.3**) (Edelman, 1971). Antigen binding by the combined V_L and V_H domains is mediated by three highly variable loops in each variable domain, termed complementary determining regions (CDR). The 3 CDR loops connect β -strands of the more conserved framework regions (FR1 – FR4). The third complementary determining region, CDR3, is encoded by newly formed segments of the genome generated by DNA recombination and nucleotide insertions during early B cell development. The CDR3 region shows the highest diversity and usually forms the core of the contact region with the antigen (Davies & Cohen, 1996; Kabat & Wu, 1991).

Antibody classes

Most mammals express one or more members of five distinct classes of antibodies differing in structures of the CH domains and effector functions determined by the Fc domain. IgM and IgD are expressed as cell surface receptors by mature B cells before contact with antigen. Alternative splicing of the exon encoding the transmembrane region generates a secretory form of IgM, which is found as soluble serum antibody early in the immune response. IgMs can form pentameric structures and induce activation of the complement system. IgGs are the most abundant serum immunoglobulins comprising 75% of all serum antibodies (Reeves & Todd, 1996). IgGs exhibit the longest serum half life (21

days) and function as pathogen neutralizers, opsonizers as well as activators of complement. IgAs are the second most abundant antibody class and are translocated through epithelial cells to the surfaces of mucosal tissues. IgE, the fifth class of antibodies exhibits only very low serum concentrations, as a consequence of the high affinity binding of soluble IgE to the FcR ϵ receptor expressed by tissue mast cells, which play important functions in anti-helminth and anti-parasite immunity. IgEs also play a role in type 1 allergic hypersensitivity, resulting from cross-linking of cell-bound IgE immunoglobulins on mast cells by innocuous antigens (Janeway *et al*, 2005). As a consequence of different gene duplication events, different mammals express different numbers of subtypes of IgG, IgA and IgE. Humans, for example express four types of IgG and two subtypes of IgA. Human serum IgG contains approximately 65%, 25%, 6% and 4% of IgG1, IgG2, IgG3 and IgG4 subtypes, respectively (Reeves & Todd, 1996). These subtypes differ in certain effector functions: IgG4 is inefficient in complement activation, while IgG2 and IgG3 bind poorly to FcR γ receptors on phagocytes .

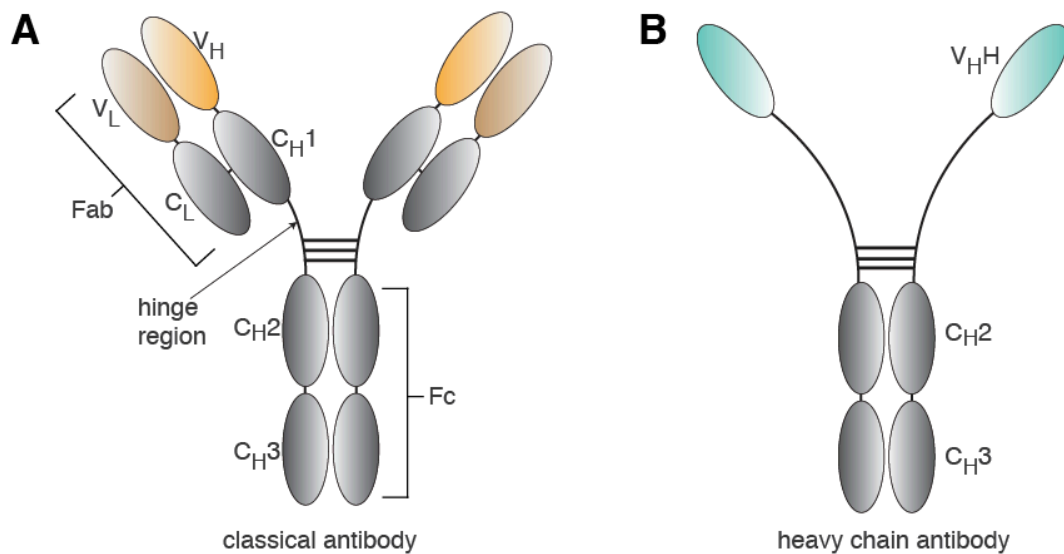


Figure 1.3. Conventional antibodies versus heavy chain antibodies. Llamas possess in addition to classical IgG1 antibodies composed of a heavy chain and a light chain (A), so called heavy chain (only) antibodies (hcAbs) of the IgG2 and IgG3 subclasses consisting solely of a heavy chain polypeptide (B). (A) Each light chain of a classical antibody comprise a variable domain (V_L) and a constant domain (C_L) whereas the heavy chain is composed of one variable domain V_H and 3 constant domains designated C_H1 – C_H3. C_H1 and C_H2 domains are linked by a proline-rich flexible hinge region. Each light chain associates with a respective heavy chain by disulfide bonds. Similar disulfide bonds in the hinge region link individual heavy chain polypeptides. A combined V_L-C_L and V_H-C_H1 is called the Fab fragment (fragment of antigen binding) whereas the C_H2-C_H3 domains comprise the Fc domain. Both V_L and V_H combine to form the antigen binding paratope of the antibody whereas effector functions are mediated by the Fc domain. (B) Llama hcAb antibodies on the other hand, lack the light chain and the C_H1 domain of the heavy chain. Antigen binding is carried out solely by the V_HH domain which is linked directly to the C_H2 domain through the hinge region.

1.3.2 Llama heavy chain antibodies and nanobodies

Lineage specific gene duplications and mutations account for the distinct IgG subclasses found in llamas and other camelids (camel, dromedary, vicuña, guanaco). Peculiar to camelids is the complete lack of light chains and of the CH1 domain by antibodies of the IgG2 and IgG3 subclasses (**Fig. 1.3**) (Hamers-Casterman *et al*, 1993; Nguyen *et al*, 2002) while camelid IgG1 antibodies display a conventional antibody structure. IgG1 comprises up to 75% of llama serum IgGs with IgG2 and IgG3 making up a combined 25% – 45%. The variable domain of the so-called heavy chain only antibodies (hcAb) is linked directly to the C_H2 domain by the hinge region. Llama IgG2 and IgG3 subclasses differ in the length of the hinge regions. IgG2 is a long hinge hcAb whereas IgG3 comprises the short hinge subtype. Distinct from the antigen binding paratope of conventional antibodies which is determined by combined variable regions of both light and heavy chains, a single variable domain of the hcAb is responsible for antigen binding. The domain is designated V_HH (variable domain of the heavy chain only antibody) to distinguish it from the V_H counterpart of conventional antibodies. V_HHs can be cloned and recombinantly expressed as the smallest antibody fragment with antigen binding properties (Muyldermans *et al*, 2001). Due to their small size, these single domain antibodies are also referred to as Nanobodies® (Nbs). Evolutionary substitution of 4 hydrophobic amino acids at the former interface to the VL domain to hydrophilic residues accounts for the high solubility and stability of V_HH domains. This permits the recombinant expression of Nbs as water soluble protein molecules (Vu *et al*, 1997).

Nbs are easily expressed in *E.coli* as periplasmic proteins or in eukaryotic cells as secretory proteins with high yields at relatively low costs (Wesolowski *et al*, 2009; Holliger & Hudson, 2005). They are thermostable and are able to withstand harsh pH conditions. Furthermore, Nbs show superior tissue penetration and quick systemic clearance compared to conventional antibodies. Nbs are versatile, easily reformatted when required, into homo- or hetero-polymeric molecules to increase avidity; into bi-paratopic formats for specific tissue targeting or to increase serum half life; or into Nb-Fc fusion proteins to reconstitute effector functions or facilitate *in vivo* recycling and increase serum half-life (Scheuplein *et al*, 2010; Tijink *et al*, 2008). Importantly, the CDR3 regions of V_HH are on average longer than in classical antibodies reaching as long as 26 amino acids (Desmyter *et al*, 1996). These long CDR3 regions can form finger-like structures that reach

into crevices on protein surfaces inaccessible to flat paratopes of conventional antibodies. Indeed, following immunization of llamas with enzymes carrying a deep active site crevice, the induced heavy chain antibodies often show a propensity to block the enzymatic activity (**Fig 1.4**) (Desmyter *et al*, 1996; De Genst *et al*, 2006; Koch-Nolte *et al*, 2007; Alzogaray *et al*, 2011). The goal of the present project was to harness this inherent propensity of nanobodies to reach functional crevices on proteins in order to generate specific antagonists of the P2X7 ion channel.

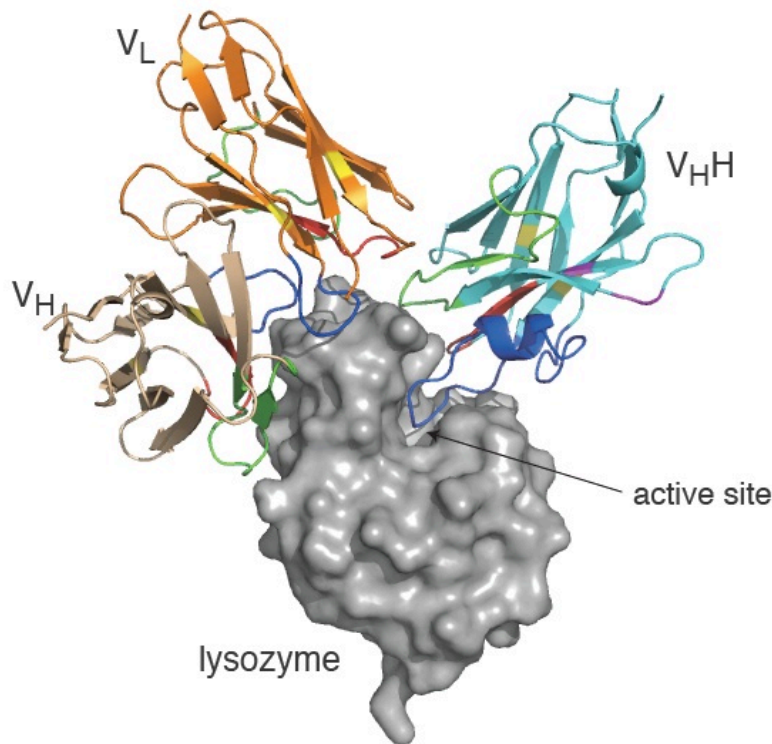


Figure 1.4. Antigen binding by scFv (single chain variable fragment (V_L-V_H), derived from conventional antibodies) versus V_HH (derived from hcAbs). While conventional antibodies tend to bind antigens by planar conformational paratopes, the CDR3 regions of V_HHs of hcAbs can form finger-like structures able to target and bind cryptic epitopes of antigens such as the active site of an enzyme as shown above for hen egg lysozyme. (Figure was generated with PyMOL using pdb files, 1MEL and 1IC4. CDR1, CDR2 and CDR3 are color-coded red, green and blue respectively. Canonical cysteines forming a conserved disulfide bridge between β strands of FR1 and FR3 are shown in yellow. Hydrophilic amino acid substitutions in FR2 accounting for high water soluble of V_HH domains are colored pink).

1.4 Phage display

With the help of the technology of phage display, antibody and antibody fragments as well as peptides directed against specific targets have been generated. Phage display permits the selection of antigen-specific molecules from a library of such molecules expressed as fusion proteins with bacteriophage coat proteins (Smith, 1985).

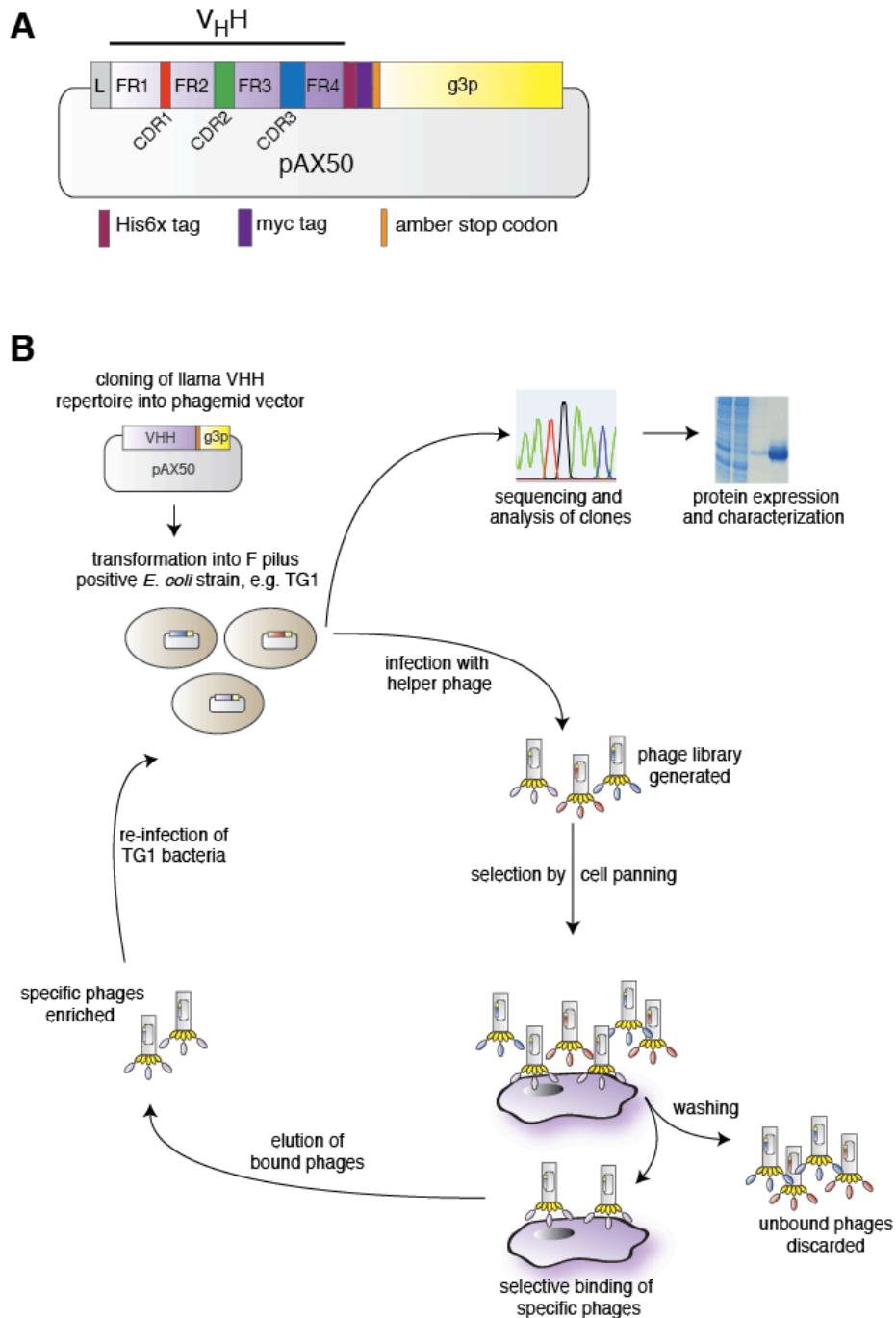


Figure 1.5 Schematic representation of a V_H-encoding phagemid (A) and the generation of a phage library and selection of V_H fragments by bio-panning using phage display technology (B). L in (A) = N-terminal leader driving secretion of the V_H into the periplasmic space

1.4.1 Bacteriophages: biology and structure

Bacteriophages (or simply, phages) are viruses which infect bacteria. The filamentous phages infect male Gram-negative bacteria expressing the F-pilus as a docking receptor for virus infection (Russel, 1991). The filamentous phages do not undergo a lytic infection. Rather, their genetic material directs the replication machinery of the infected bacterium to package and secrete phage particles each enclosed with a single-stranded phage DNA genome. Infection of the host is initiated by interaction of the phage minor coat protein g3p, with the F-pilus of the host bacterium. Subsequently, only the single stranded virus DNA is injected into the host which is converted into a double-stranded pseudo-plasmid, the replicative form. The DNA replication machinery of the host cell uses the replicative form as a template to produce multiple copies of single stranded phage DNA in a process called rolling circle replication. The single strands serve as templates for the synthesis of phage proteins which spontaneously assemble to form phage particles (Russel, 1991). The filamentous phages utilized in the technology of phage display (M13, f1 and fd strains) are single stranded viruses whose entire genome consist of 11 genes expressed in varying copies. Phage display takes advantage of the two coat proteins, g3p and g8p while display via g3p preferred (Barbas *et al*, 1991). Each filamentous phage consists of about 3 – 5 copies of the minor coat protein, g3p, and up to 2700 copies the major coat protein, g8p (Azzazy & Highsmith, 2002).

1.4.2 Generation of phage libraries

Selection of antibodies by phage display requires the generation of a phage library (Clackson *et al*, 1991). Usually, the immune repertoire of a non-immunized (naive) or antigen-immunized (immune) animal is cloned into a phagemid vector containing an antibiotic resistance gene and transformed into bacterial cells. The number of antibiotic resistant bacterial clones derived from this transformation corresponds to the size of the library. Superinfection of the harvested clones with a helper phage generates a phage library. For the molecular cloning of llama Nanobody (Nb) libraries, RNA is purified from B cells isolated from an immunized llama. The RNA is reverse transcribed into cDNA with the help of random hexamers and a reverse transcriptase. The cDNA is used as template to amplify the V_HH repertoire of the heavy chain only antibodies with the help of specific primers. The primers also insert restriction sites which permit the cloning of the V_HH repertoire into a phagemid vector such as pHEN2 or pAX50 (Barbas *et al*,

1991; Mead & Kemper, 1988; Tijink *et al*, 2008; Alzogaray *et al*, 2011; Wesolowski *et al*, 2009) The phagemid vector entails a bacterial origin of replication as well as the wildtype M13 origin of replication. The V_HHs are cloned upstream of the M13 g3p gene interjected by an amber stop codon (**Fig. 1.5A**). The amber stop codon is recognized as a translation termination site in some bacterial strains (e.g. HB2151) for the expression of V_HH fragments but translated as pyrrolysine in other strains (TG1) for the display of V_HH fragments as fusion proteins with phage g3p. The ligation products of the llama V_HH PCR amplification products and the phagemid vector are transformed into TG1 cells generating a library of bacterial clones. In order to generate the corresponding phage library, the bacteria library are cultivated and infected with helper phages (e.g. M13K07). Helper phages possess a weaker origin of replication and an impaired packaging signal sequence. As a result, when the helper phages infect bacteria expressing phagemids harboring the wildtype origin of replication, the phagemid sequence is preferentially replicated and packaged as single stranded DNA in progeny phage particles (Russel, 1991; Barbas *et al*, 1991). Moreover, the phagemid-encoded V_HH is displayed as a fusion protein with phage g3p thereby linking phage genotype (V_HH phagemid) with phenotype (V_HH displayed). The phages can be precipitated from the supernatant of the culture using polyethylene glycol (PEG) and stored or used for the selection of antigen-specific antibody fragments in a process called bio-panning (**Fig. 1.5B**) (Azzazy & Highsmith, 2002).

1.4.3 Selection by bio-panning

Selections of phages carrying antigen-specific V-domains typically involve panning the phage library on an immobilized version of the antigen of interest. The phage library is incubated with immobilized antigen and unbound phages are removed by washing. To reduce non-specific binding of phages to the matrix on which the antigen is immobilized (e.g. walls of a test tube, sepharose beads, cells), antigens and phages are usually separately incubated in a buffer containing high concentrations of carrier proteins, such as BSA or milk powder, prior to panning. Bound phages are eluted and amplified in a step called phage rescue. Phage rescue involves (i) re-infection of TG1 cells with eluted phages, (ii) cultivating infected bacteria, (ii) superinfection of bacteria with helper phage to induce packing of phage particles and (iv) precipitation of the soluble phages from the culture supernatant. Selection are typically carried out on immobilized antigens, either on ELISA plates, beads or cells (Azzazy & Highsmith, 2002). Potential disadvantages of the

immobilization on vessel walls or beads include denaturation and masking of specific epitopes. In the cases of membrane proteins, e.g. ion channels such as P2X7, selections can be performed on cells transfected to express the antigen on the cell surface. A major advantage of this technique is that the target antigen is in native conformation. A disadvantage is the potential binding of phages to other cell surface proteins and/or cellular debris. To reduce binding to other cellular component, the cell background may be changed in sequential rounds of panning, e.g. from human HEK cells to mouse lymphoma cells to reduce the chances for selection of phage specific for other antigens. Other selection methods include selection with soluble biotinylated antigens immobilized on streptavidin beads or *in vivo* selections (Pasqualini & Ruoslahti, 1996) by injecting phage libraries into animals followed by recovery of phages from specific tissues. Considering the fact that P2X7 is natively expressed as a homotrimeric multipass transembrane protein, a cell-based panning strategy was chosen for this thesis.

1.5 Autoimmune glomerulonephritis

Glomerulonephritis (GN) is a major cause of renal failure (Tam, 2006). A characteristic pathological mechanism is the glomerular sub-epithelial deposition of immune complexes which induce inflammation and activate complement cascades (Pusey & Peters, 1993). Such immune complexes may contain autoantibodies specific for glomerular auto-antigens such as the phospholipase A2 receptor (Beck *et al*, 2009), neutral endopeptidase, or aldose reductase (Debiec *et al*, 2002; Prunotto *et al*, 2010). A characteristic feature of rapid progressive glomerulonephritis (RPGN) is crescent formation (Tam, 2006). Crescents have been described to arise from damaged glomerular basement membrane (GBM) leading to the leakage of plasma proteins such as fibrin. Epithelial cells sense released fibrin and proliferate forming a crescent taking up the space of the bowman capsule, surrounding and compressing the glomerular tuft. Infiltrating leukocytes such as monocytes and macrophages also contribute to crescent formation (Becker *et al*, 2008; Jennette, 2003). In addition, there is an effacement of podocyte foot process and the disruption of the renal filtration barrier (Glassock, 2010).

Various animals models of experimentally induced nephritis have been reported. One method utilizes antibodies induced by immunization with glomerular extracts from another

species. Antisera are collected and injected into the donor of glomerular extract to induce rapidly developing acute nephritis or slowly developing chronic nephritis (Durvasula & Shankland, 2003). Atkins and colleagues showed that interleukin-1 β plays an important role in the rat model of nephrotoxic nephritis and that intrinsic renal cells were a major source of the pro-inflammatory cytokine (Tesch *et al*, 1997). In fact, treatment with an antagonist of interleukin-1 β suppressed the experimental crescent glomerulonephritis (Lan *et al*, 1993). Turner *et al* observed an increase in the glomerular expression of P2X7 in both rat and mouse models of nephrotoxic nephritis (Turner *et al*, 2007). Considering the central role of P2X7 activation in mediating release of IL-1 β , Taylor *et al* investigated disease progression in P2X7-deficient mice and the effects of treating rats with broad spectrum P2X7 inhibitors (Taylor *et al*, 2009). Deletion of the purinergic receptor resulted in a significant reduction in disease score. Furthermore, treatment with a pharmacological small molecule antagonist of P2X7 ameliorated nephritis in rats. Recently, Meyer-Schwesinger *et al* reported that injection of mice with antisera from sheep immunized with cultured mouse podocytes results in development of severe nephrotic syndrome accompanied with effacement of podocyte foot processes (Meyer-Schwesinger *et al*, 2011). As presented here, P2X7-specific Nbs were tested for their potential therapeutic effect in this anti-podocyte nephritis model in collaboration with the group of Meyer-Schwesinger at the University Medical Center, Hamburg.

2 Goals of the project

The central goal of this project was to generate P2X7-specific nanobodies (Nbs) from immunized llamas (**Fig. 2.1**). The isolated Nbs were to be functionally characterized for their ability to block or enhance nucleotide-induced activation of P2X7, i.e., P2X7-mediated shedding of CD62L and CD27, externalization of phosphatidylserine, and uptake of propidium iodide (Scheuplein *et al.*, 2009; Moon *et al.*, 2006). The Nbs were to provide new tools for investigating and modulating the functions of P2X7 *in vitro* and *in vivo* and for therapeutic applications in P2X7-mediated disease models. To test their therapeutic potential, the Nbs were to be probed for their protective role in a pilot experiment with a mouse model of antibody-induced autoimmune glomerulonephritis (Meyer-Schwesinger *et al.*, 2011).

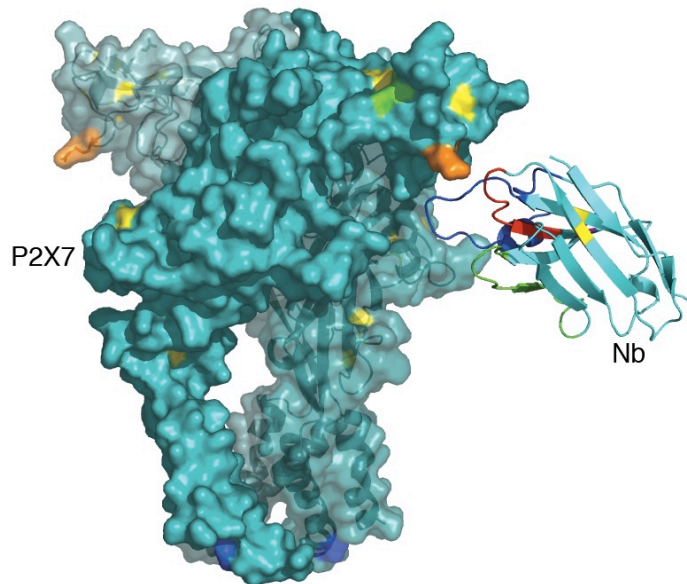


Figure 2.1. Schematic representation of the goal of this project to target and block P2X7 with Nbs. By virtue of their long CDR3 regions, Nbs can target clefts on proteins such as the ATP binding pocket of P2X7. (The figure was generated with PyMOL using pdb files 4DW1 and 1MEL).

To this end, a collaboration was initiated with Ablynx to immunize llamas with cDNA constructs encoding mouse and human P2X7 and with HEK cells transfected to stably express mouse or human P2X7 (Möller *et al.*, 2007).

3 Materials

3.1 Lab Equipment

<i>Equipment</i>	<i>Model/Type</i>	<i>Firm</i>
Flow cytometer	FACSCalibur	BD Biosciences
	FACSCanto II	BD Biosciences
Fluorescence microscope	Axiovert 200M	Zeiss
Analytical scale	Type 1412	Sartorius
Centrifuges	Rotanta 460 R	Hettich
	RC 26 Plus	Sorvall
	Biofuge pico	Heraeus
Freezer	HFC 586 Basic	Heraeus
DNA gel electrophoresis	40-0708	Peqlab biotechnology
Protein gel electrophoresis	Xcell II MiniCell	Invitrogen
Waterbath	Type 1007	<i>Gesellschaft für Labortechnik</i>
Incubator	B6060	Heraeus
Liquid nitrogen tank	K series	Taylor-Wharton
Laminator	Vacufix electronic	Petra electric
Magnetic stirrer	RCTS 26	OmniLab
Microwave	M 637 EC	Miele
Micropipettes	Research Type	Eppendorf
Neubauer cell chamber		LaborOptik
Nanodrop	2000c	Peqlab biotechnology
Photometer	Ultraspec 2000	Pharmacia
	SmartSpec3000	BioRad
PCR Thermal Cycler	T3	Biometra
Scanner	CanonScan 9800F	Canon
Sterile work bench	BSB4	GELAIR
	HeraSafe	Heraeus
Vortex		Neolab
Pipetteboy		Integra
Shaker incubators	HT INFORS	Unitron
UV table		
UV iluminator	Type TI 1	Biometra
Heat block	Thermomixer Compact	Eppendorf
Infrared lamp		Philips
Roller		Staurt
Film developer		
ELISA plate reader	Wallac 1441	Perkin-Elmer
pH meter		Mettler
Autoclave	Varioclave	H+P Labortechnik

3.2 Consumables

<i>Consumable</i>	<i>Type</i>	<i>Manufacturer</i>
Cell sieves	70 µm	Falcon
Pipette tips	various sizes	Eppendorf
	various sizes	Sarstedt
Cell culture flask	T-25, T-75, T-225	Greiner/Nunc
Erlenmeyer flask	various sizes	PP Corning Inc
Syringes and needles	various sizes	Braun/BD Biosciences
Gloves	Safeskin	Kimberly-Clark
	Vibrant	Aurelia
		Hartmann
Hyperfilm	ECL	Amersham-Pharmacia
Microcentrifuge tubes	various sizes	Eppendorf
Microplates	various sizes	Greiner
Parafilm		Pechiney plastic packaging
Sterile filtration	Steriflip, Stericup	Millipore
Falcon tubes	15 ml, 50 ml	Greiner
Serological pipettes	various sizes	BD Falcon
FACS tubes	various	BD Biosciences
Disposal bags	Plastibrand	Brand
SDS-PAGE gels	10% and 12% NuPAGE	Invitrogen

3.3 Chemicals

<i>Chemical</i>	<i>Manufacturer</i>
AEBSF	Merck
Aqua ad iniectabilia	Braun
Bacto agar	BD/Difco
Bacto soyotone	BD/Difco
Bacto tryptone	BD/Difco
Bacto yeast extract	BD/Difco
β-mecarptoethanol	Gibco
Bovine serum albumin, BSA	Merck
Carbenicillin	Serva
DMEM medium	Gibco
di-potassiumhydrogenphosphate	Merck
DNA Typing Grade Agarose	Gibco
dNTPs	Invitrogen
Ethidium bromide	Molecular probes
EDTA	Merck

Fetal calf serum, FCS	PAA
Imidazole	Merck
IPTG	Roche
jetPEI	Polyplus
Kanamycin	Roche
LB Agar	BD/Difco
LB Broth	BD/Difco
2xYT	BD/Difco
Terrific broth	USB Corp
Methanol	Walter GmbH
NuPAGE antioxidant	Invitrogen
NuPAGE sample reducing agent, 10x	Invitrogen
NuPAGE SDS-PAGE sample buffer, 4x	Invitrogen
Sodium chloride	Merck
Sodium phosphate	Merck
di-sodium phosphate	Merck
NAD ⁺	Sigma-Aldrich
ATP, sodium salt	Sigma-Aldrich
PBS	Gibco
Sucrose	Merck
TAE, DNA typing grade, 50x	Invitrogen
TMB substrate	Pierce
Tris-HCl	Sigma
Tween-20	ICI-Americas
SOC-medium	Sigma
Hepes, 1 M	Gibco
RPMI 1640	Gibco
Propidium iodide	Sigma-Aldrich
Sodium hydroxide	Merck
Potassium hydrogen carbonate	Merck
Calcium chloride	Serva
Trypsin, 10x	Invitrogen
LD nearIR	Invitrogen
L-Glutamine, 200 mM	Gibco
Sodium pyruvate, 100 mM	Gibco
MEM, non essential amino acids, 10 mM	Gibco
NuPAGE transfer buffer, 20x	Invitrogen

3.4 Affinity Chromatography matrices

<i>Matrix</i>	<i>Firm</i>
Ni-NTA agarose	Qiagen
M2 agarose	Sigma-Aldrich
AminoLink-Ab agarose	Pierce/Self-made

3.5 Media, buffers and solutions

3.5.1 Eukaryotic cell culture media

Complete DMEM, 5% FCS

- 500 ml DMEM
- 5 ml Glutamine
- 5 ml Sodium pyruvate
- 5 ml Hepes
- 5 ml MEM, non essential amino acids
- 25 ml FCS

Complete RPMI 1640, 5% FCS

- 500 ml RPMI-1640
- 5 ml Glutamine
- 5 ml Sodium pyruvate
- 5 ml Hepes
- 5 ml MEM, non essential amino acids
- 25 ml FCS

3.5.2 Bacterial culture media

LB broth

- 25 g/l in de-ionized water

2xYT

- 31 g/l in de-ionized water

Terrific broth

- 54 g/l in de-ionized water
- 4 ml Glycerol

SOC-medium

- 0.5 % Yeast extract
- 2 % Tryptone
- 10 mM NaCl
- 2.5 mM KCl
- 10 mM MgCl₂
- 10 mM MgSO₄
- 20 mM Glucose

LB Agar 30.5 g/l in de-ionized water

Carbenicillin, stock 100 mg/ml used at 100 µg/ml

Kanamycin, stock 50 mg/ml used at 50 µg/ml

All bacterial media were autoclaved before use. Respective antibiotics were added after autoclaving prior to use.

3.5.3 Eukaryotic cell lysis buffer

Triton X-100 lysis buffer 1% Triton X-100
1 mM AEBSF
in 1x PBS

ACK erythrocyte lysis buffer 155 mM NH₄Cl
10 mM KHCO₃
100 µM EDTA
pH 7.2 in de-ionized water

BD erythrocyte lysis buffer 10% v/v BD lysis buffer
in de-ionized water

3.5.4 Bacterial cell lysis buffer

TS lysis buffer 20% Sucrose w/v
30 mM Tris-HCl, pH 8
1 mM AEBSF
± 100 µg/ml Lysozyme
in de-ionized water

3.5.5 Antibody staining buffers

FCS washing and staining buffer 2% FCS in 1x PBS

BSA washing and staining buffer 0.2% BSA in 1x PBS

Annexin V binding buffer, 10x 1.4 M NaCl
25 mM CaCl₂
in 100 mM HEPES, pH 7.4
used at 1x in de-ionized water

3.5.6 SDS-PAGE and western blot buffers

MES gel running buffer	1x MES buffer (Invitrogen) in de-ionized water
Sample preparation buffer	1x NuPAGE SDS sample buffer 1x NuPAGE sample reducing buffer
Blot buffer	1x NuPAGE transfer buffer 10% Methanol 0.1% Antioxidant in de-ionized water
Membrane washing buffer	0.05% Tween-20 in PBS
Membrane blocking buffer	5% Milk powder in membrane washing buffer

3.5.7 DNA agarose gel electrophoresis buffer

TAE gel running buffer	1x TAE buffer (Invitrogen) in de-ionized buffer
Sample preparation buffer	1x DNA loading dye (Fermentes)

3.5.8 Affinity chromatography buffers

Washing buffer (Ni-NTA)	2.65 mM Na ₂ HPO ₄ 46.35 mM NaH ₂ PO ₄ 0.3 M NaCl 3 mM Imidazole pH 8 in de-ionized water
Elution buffer (Ni-NTA)	2.65 mM Na ₂ HPO ₄ 46.35 mM NaH ₂ PO ₄ 0.3 M NaCl 250 mM Imidazole pH 8 in de-ionized water
Washing buffer (M2 and AminoLink agarose)	1x PBS
Elution buffer (M2 and AminoLink agarose)	0.1 M Glycine, pH 2.7
Neutralization buffer	1 M Tris-HCl, pH 9

3.6 DNA and protein standards

<i>DNA standards</i>	<i>Manufacturer</i>
GeneRule, 1kB	Fermentas
SmartLadder	Eurogentec

<i>Protein standards</i>	<i>Manufacturer</i>
Novex Sharp pre-stained Supermark	Invitrogen
	Self-made
	100 µg/ml BSA
	75 µg/ml IgG
	10 µg/ml Lysozyme
	in 1x PBS

3.7 Enzymes

<i>Polymerases</i>	<i>Manufacturer</i>
KOD Hot Start	Novagen
Phusion	New England Biolabs

<i>Restriction enzymes</i>	<i>Manufacturer</i>
BamHI	New England Biolabs
BstEII	New England Biolabs
DpnI	New England Biolabs
MfeI	New England Biolabs
NcoI	New England Biolabs
NheI	New England Biolabs
NotI	New England Biolabs
SfiI	New England Biolabs
XbaI	New England Biolabs

3.8 Oligonucleotides and plasmids

All DNA oligonucleotides (primers) and plasmids are listed in the Appendix

3.9 Kits

<i>Kit</i>	<i>Manufacturer</i>
AminoLink® Plus Immobilization kit	Pierce

BCA™ Protein Assay kit	Pierce
QIaprep Spin Miniprep kit	Qiagen
QIaprep Spin Gel purification kit	Qiagen

3.10 Antibodies

<i>Antigen</i>	<i>Fluorochrome conjugate</i>	<i>Clone</i>	<i>Manufacturer</i>
mCD3	Pacific Blue	17A2	BioLegend
mCD4	eFluor450	RM4-5	eBioscience
mCD62L	PE	MEL-14	BD
mCD27	PE	LG.3A10	BD
mCD25	APC	PC61.5	eBioscience
mCD161c	PE-Cy7	PK136	eBioscience
mP2X7	Alexa Fluor 647	HANO44	AG Nolte
hP2X7	Alexa Fluor 647	L4	AG Nolte
	Alexa Fluor 647	1c113Fc	AG Nolte
	Alexa Fluor 647	3c23Fc	AG Nolte
hCD4	APC/Cy7	RPA-T4	BioLegend
hCD8	Pacific Blue	RPA-T8	BioLegend
hCD62L	FITC	DREG-56	BD
mIgG	PE		Dianova
	Alexa Fluor 647		Molecular Probes
C-myc Tag	FITC	9E10	Serotec
	Alexa Fluor 647	9E10	CellSignaling
Annexin V	FITC		BD
	APC		BD

3.11 Helperphages

M13KO7	Amersham Biosciences
VCSM13	Stratagene

3.12 Cell lines

Cell line	Source
DC27.10	Ag Fleischer
DC27.10 NOD	Ag Nolte {Bannas:2005ip}
RPMI 8226	Ag Trepel

HEK	Ag Nolte
CHO	Ag Nolte
Yac-1	Ag Nolte
HEK hP2X7	Ag Nolte
HEK mP2X7	Ag Nolte
Yac-1 hP2X7	Ag Nolte
CHO hP2X7	Ag Nolte

3.13 *E. coli* strains

Strain	Source
HB2151	Amersham
TG1	Stratagene
XL-2 Blue	Stratagene
XL-10 Gold	Stratagene

3.14 Mouse strains

C57bl/6 wt	UKE, Hamburg
Balb/c wt	UKE, Hamburg

4 Methods

4.1 Methods in molecular biology

4.1.1 Transformation of bacteria

Transformation of chemically competent bacteria

Chemically competent bacteria strains were transformed by heat shock. 100 µl of competent bacteria cells were thawed on ice for 30 min (all bacteria strains were stored at -80°C). 1, 2 or 5 µl of plasmid miniprep, mutagenesis or ligation reactions, respectively, were added to competent cells followed by a further 30 min incubation on ice. The cells were then heat-shocked at 42°C for 30 seconds and immediately put on ice for further 2 min. 900 µl respectively of pre-warmed SOC medium (also 42°C) were added and the cell suspension incubated at 37°C and 450 rpm in a heat block for 60 min. Required volumes of the cultivated cells were plated out on agar plates containing respective antibiotics and incubated overnight at 37°C.

Transformation of electro-competent bacteria

Electro-competent bacteria strains were transformed per electric shock. 170 µl of electro-competent TG1 bacteria cells (Lucigen) were thawed on ice for 30 min and further incubated with 30 µl of desalted ligation reaction on ice for 30 min in cuvettes. Each 40 µl of the cell mix were then pulsed with 1800 V for 4 - 5 ms (program EC1, MicroPulser, Biorad). Cells were recuperated at 37°C and 250 rpm for 60 min in 1 ml SOC medium and plated out accordingly.

4.1.2 Cultivation of bacterial culture

Bacterial cultures were cultivated in LB, Terrific broth (supplemented with 0.4% glycerol) or 2xYT media. Single clones transformed with the respective plasmids were picked and used to inoculate respective media volumes containing 100 µg/ml (ampicillin or carbenicillin) or 50 µg/ml (kanamycin) antibiotics. Pre-cultures were cultivated overnight in 5 ml volumes of inoculated media at 37°C and 230 rpm. Main cultures of respective volumes were cultivated during a single day at same conditions. Cultures were induced with IPTG where required at 0.5 mM final concentration upon reaching OD₆₀₀ values of 0.5 and cultivated for a further five hours after induction. Cells were harvested by centrifugation at 4600 rpm for 15 min (Hettich) and culture supernatants discarded.

4.1.3 Cryopreservation of bacteria

For longterm storage of bacteria, glycerol stocks were made. Aliquots of bacterial culture were centrifuged and the cell pellet resuspended in 20% glycerol in respective media. The suspension was stored at -80°C or shock-frozen in liquid nitrogen and stored in liquid nitrogen (-195°C).

4.1.4 Preparation of plasmid DNA

For small and large scale preparation of bacterial plasmid DNA, 5 ml or 100 ml respectively of LB medium containing antibiotics were inoculated with a single colony and cultivated overnight (~18 h) at 37°C and 230 rpm. Plasmid DNA was extracted using Qiaprep® Spin Miniprep or Maxiprep kits (Qiagen, Hilden) following the manufacturer's protocol.

4.1.5 Quantification of DNA and RNA

The concentration of double-stranded DNA (plasmids, PCR and restriction digestion fragments) and RNA was determined spectrophotometrically by absorbance at 260 nm using the conversion factor: $A_{260} = 1 = 50 \mu\text{g/ml}$ for DNA and $A_{260} = 1 = 40 \mu\text{g/ml}$ for RNA. The ratio of A_{260}/A_{280} was used as a marker for purity. Preparations with an A_{260}/A_{280} value of 1.8 – 2.0 for DNA and 2.0 – 2.2 for RNA were considered pure.

4.1.6 Restriction digestion of DNA

Restriction digestion of double-stranded DNA fragments for purposes of cloning or analysis was carried out with respective restriction enzymes in buffers and temperature conditions recommended by the manufacturer. Incubations were carried out in PCR cycler in 20 μl or 40 μl reaction volumes for 1 – 5 h. The website of New England Biolabs was resourceful in the choice of buffers for restriction digestion analyses with two enzymes.

4.1.7 Dephosphorylation of DNA fragments

Enzyme-digested plasmid vector DNA fragments used for cloning were dephosphorylated to reduce level of re-ligation of vector. To completed restriction digestion reactions, 2.2 μl or 4.2 μl (for reactions in 20 μl and 40 μl respectively) of antarctic phosphatase buffer (Invitrogen, 10x) and 1 μl of the phosphatase were added. Dephosphorylation was carried

out by incubation at 37°C for 2 h followed by an t enzyme inactivation step involving a 20 min incubation at 65°C.

4.1.8 Agarose gel electrophoresis of DNA and RNA fragments

DNA fragments were size-fractionated per agarose gel electrophoresis (Sambrook & Russel, 2001). Depending on the size of the fragments as well as the purpose of the analysis, gels, with 1% - 2% agarose were made in TAE buffer with 0.5 µg/ml ethidium bromide. Samples were prepared with loading buffer (Invitrogen) and gels routinely ran at 70 – 90 V. DNA bands were visualized by UV-illuminator and photographed for documentation or excised and fragments eluted for ligation reactions.

4.1.9 Extraction of DNA fragments from agarose gel

The elution of DNA fragments from agarose gels was carried out with the QIAquick gel extraction kit (QIAGEN) following the manufacturer's protocol. DNA fragments were eluted with 15 – 50 µl de-ionized water depending on estimated amount of DNA based on agarose gel.

4.1.10 Ligation of DNA fragments

Ligation reactions were carried out with the T4 ligase (Invitrogen) in buffer recommended by manufacturer in a reaction volume of 10 µl or 20 µl. Generally, 50 ng or 100 ng of vector was ligated with respective amounts of insert in a 1:3, vector:insert ratio. Ligation reactions were routinely carried out at 16°C overnight (~16h).

4.1.11 Polymerase chain reaction (PCR)

Polymerase chain reaction (PCR) is a method by which DNA fragments are amplified in a reaction where temperatures are cyclically raised and lowered. A typical PCR reaction consists of a template DNA, complementary oligonucleotides (primers), dNTPs and a polymerase in a suitable buffer with required salts. During the reaction, the template DNA is copied and amplified by the polymerase by incorporating dNTPs to one end of the template-complementary primer in the 5'- 3' direction in several cycles. Routinely, PCR cycles consist of denaturation, annealing and elongation steps. Double-stranded DNA is denatured to single strands at a high temperature (usually 90 - 95°C) permitting annealing of the primer in the annealing step (usually at 50 - 65°C) which is then used as starting

point for extension and copying of the template DNA by the polymerase in the elongation step (usually at 69 - 72°C). The cycle is then repeated as many times as required with each newly synthesized strand becoming part of the template pool in subsequent cycles. PCR reactions were used for amplification and mutagenesis of DNA fragment, incorporation of restriction sites, DNA sequencing and genotyping. In this project, the following PCR reactions were utilized:

Amplification of V_{HH} and V_H fragments from cDNA

cDNA	10 µl	94°C	2'	25x
ABL051 + ABL052 (4:1)	1 µl	94°C	30''	
ABL003	1 µl	52°C	1'	
dNTPs (10 µM)	1 µl	72°C	2'	
Buffer (10x)	5 µl	72°C	7'	
Expand High Fidelity enzyme	0.75 µl	4°C	pause	
H ₂ O	31.25 µl			
	<u>Σ = 50 µl</u>			

Nested PCR for the amplification of V_{HH} fragments and cloning

DNA (from amplification reaction: 5 ng		94°C	2'	10x
ABL050	1 µl	94°C	30''	
ABL003	1 µl	55°C	1'	
dNTPs (10 µM)	1 µl	72°C	2' 30''	
Buffer (10x)	5 µl	72°C	7'	
Expand High Fidelity enzyme	0.5 µl	4°C	pause	
H ₂ O	ad			
	<u>Σ = 50 µl</u>			

Amplification of V_{HH} fragment for cloning of dimers and Fc fusion proteins

Template	2 ng	95°C	2'	30x
Primer for	1 µl	95°C	30''	
Primer rev	1 µl	58°C	10''	
dNTPs (2 µM)	5 µl	70°C	30''	
Buffer (10x)	5 µl	70°C	7'	
MgSO ₄ (25 mM)	2 µl	4°C	pause	
KOD HOT Start	1 µl			
H ₂ O	ad			
	<u>Σ = 50 µl</u>			

Site directed mutagenesis of pCDNA6 human P2X7

Template	30 ng	95°C	2'	18x
Primer for	1 µl	95°C	30''	
Primer rev	1 µl	55°C	1'	
dNTPs (2 µM)	5 µl	68°C	7'	
Buffer (10x)	5 µl	68°C	10'	
MgSO4 (25 mM)	2 µl	4°C	pause	
KOD HOT Start	1 µl			
H ₂ O	ad			
	<hr/>			
	Σ = 50 µl			

4.1.12 DNA sequencing

All DNA sequencing was performed using the services of SeqLab. 700 ng of plasmid DNA were submitted with 20 pmol of respective primer in a total volume of 7 µl adjusted with de-ionized water when required.

4.1.13 Preparation of RNA from peripheral llama blood lymphocytes

Total RNA isolated from peripheral blood lymphocytes were prepared and provided by Ablynx.

4.1.14 Reverse transcription of RNA to cDNA

Total RNA isolated from peripheral blood lymphocytes was used for the preparation of complementary DNA (cDNA) per reverse transcription. RNA was incubated with random hexamers (Invitrogen) and dNTPs as follows:

RNA	11 µg	65°C	5'
Random hexamers (50 µM)	2 µl	4°C	pause
dNTPs (10 mM)	2 µl		
H ₂ O	10 µl		
	<hr/>		
	Σ = 20 µl		

To the above reaction was added the reverse transcriptase (SuperScript III, Invitrogen) in buffer recommended by manufacturer for cDNA synthesis. Eight identical reactions per llama were set up.

RNA + hexamers reaction	20 μ l	50°C	50'
Buffer (10x)	4 μ l	85°C	5'
MgCl ₂ (25 mM)	8 μ l	4°C	pause
DTT (100 mM)	4 μ l		
RNaseOUT (40 U/ml)	2 μ l		
SuperScript III	2 μ l		
	<hr/>		
	$\Sigma = 40 \mu$ l		

4.1.15 Construction of anti-P2X7 VHH library

Complementary DNA (cDNA) synthesized as described in 4.1.14 were pooled and used for the amplification of antibody fragments. Using the primer combination of ABL051 (V_HH) + ABL052 (V_H) as forward primers and ABL003 (anneals to C_H2 domain) as reverse primers (see 4.1.11 for PCR reaction mix and program), a 700 bp and a 1000 bp fragment corresponding to amplicons from IgG2 and IgG3 heavy chain antibodies or IgG1 conventional antibodies respectively were attained. 8 reactions per animal were set up and pooled. The 700 bp fragments were excised and purified from a 1.5% preparative agarose gel and subjected to a further Nested PCR (see 4.1.11 for PCR reaction mix and program) with a primer pair of ABL050 and ABL003 (primer ABL050 anneals to V_HH fragment and entails the restriction sites SfiI and MfeI in tandem). 15 reactions per animal were carried out. Reactions for each llama were pooled and a 5 μ l aliquot analyzed per 1.5% agarose gel electrophoresis and the rest desalted via Qiaquick PCR purification. Purified PCR products were first digested with SfiI overnight, desalted and subsequently digested with BstEII for 3 h. Digested materials were size fractionated by 2% agarose gel electrophoresis. V_HH fragments (~ 400 bp) were excised and purified. A similarly digested vector (pAX50, provided by Ablynx) and V_HH insert fragments were ligated at 16°C overnight, desalted by Qiaquick PCR purification and eluted with 30 μ l elution buffer. Each 170 μ l aliquot of electrocompetent TG1 cells were pre-incubated with 30 μ l of eluted ligation reaction on ice for 30 min. Five 40 μ l aliquots of the reaction mix were each pulsed with electric shock (see **section 4.1.1**) and recuperated with 1 ml SOC medium for 1h at 37°C and 250 rpm (total of 5 ml). To determine size of libraries, aliquots of recuperated bacterial culture were titrated in 2xYT Amp-100 Glu-2% medium and 5 μ l of each dilution step plated on LB agar Amp-100 Glu-2% plates. The remainder of transformation reactions were further cultivated in 2xYT Amp-100 Glu-2% medium until OD₆₀₀ \approx 2 was achieved and cryopreserved as glycerol stocks at -80°C (see **section 4.1.3**).

SfiI digestion

Nested PCR puri	180 μ l	50°C	overnight (~16h)
Buffer 3 (10x)	21 μ l		
BSA (100x)	2.1 μ l		
SfiI (20 U/ μ l)	5 μ l		
H ₂ O	1.9 μ l		
	<hr/>		
	$\Sigma = 210 \mu$ l		

BstEII digestion

SfiI digested mat	60 μ l	60°C	3h
Buffer 2 (10x)	8 μ l		
BSA (100x)	0.8 μ l		
BstEII (10 U/ μ l)	4 μ l		
H ₂ O	7.2 μ l		
	<hr/>		
	$\Sigma = 80 \mu$ l		

Ligation of pAX50-V_{HH}

Vector (pAX50)	1 μ g	16°C	overnight (~16h)
Insert (VHH)	500 ng		
Buffer (10x)	15 μ l		
Ligase	3.3 μ l		
H ₂ O	107 μ l		
	<hr/>		
	$\Sigma = 150 \mu$ l		

4.1.16 Phage rescue (generation of V_{HH} phage library)

To generate anti-P2X7 V_{HH} phage libraries, an aliquot (30 μ l of glycerol stock) of pAX50 V_{HH}-transformed bacteria culture were cultivated in 10 ml of 2xYT medium Carb-100 Glu-2% until OD₆₀₀ \approx 0.5 was reached (see **section 4.1.2**). 5 ml of the culture was super-infected at a multiplicity of infection index of 10 with M13KO7 helper phage and incubated at 37°C 150 rpm for 30 min. The bacterial culture was pellet by centrifugation at 4000 rpm for 5 min (Hettich) and resuspended in 50 ml 2xYT Carb-100 Kana-50 and cultivated overnight at 25°C and 230 rpm for phage production. Phages were subsequently precipitated from supernatant and stored at 4°C as phage library (see **section 4.1.17**)

4.1.17 Phage precipitation

Phages were precipitated from supernatants of cultivated infected pAX50-transformed TG1 cells (see **sections 4.1.16** and **4.1.18**). Helper-phage infected TG1 cells cultivated

overnight were pelleted per centrifugation at 4600 rpm for 10 min at 4°C. 40 ml of phage-containing supernatants were transferred into chilled 50 ml Falcon tubes containing 10 ml of PEG/NaCl (20% PEG 6000 in 2.5 M NaCl), mixed thoroughly and incubated for 30 min on ice to precipitate phages. Precipitated phages were pelleted by centrifugation at 4600 rpm for 10 min at 4°C. Supernatants were discarded completely by decantation. Phage pellet was resuspended in 1 ml PBS and transferred to a 1.5 ml Eppendorf tube and centrifuged at 13000 rpm for 1 min to remove non-soluble debris. Supernatant was transferred to a chilled 1.5 ml Eppendorf tube pre-layered with 250 µl PEG/NaCl for a second phage precipitation step. After incubating on ice for 10 min, precipitated phages were pelleted by centrifugation at 13000 rpm for 10 min. Supernatants were discarded and phage pellet resuspended in 1 ml PBS. To remove non-soluble debris, phages in PBS were centrifuged at 13000 rpm for 1 min and phage-containing supernatant transferred to a fresh 1.5 ml Eppendorf tube. The centrifugation and transfer step (13000 rpm, 1 min) were repeated until no further debris pellet was observed. Soluble phages in PBS were stored at 4°C.

4.2 Methods in cell biology

4.2.1 Cell culture of eukaryotic cells

Adherent cell lines (HEK and CHO) were cultivated in filter-capped T-25, T-75 or T-225 flasks (Nunc) in complete DMEM medium. The cultures were subcultivated (splitting) 1:5 – 1:20 every 2 or 3 days into new flasks. Cells were washed once with PBS and detached by incubation with trypsin for 1 – 3 min (1, 2 and 4 ml for T-25, T-75 and T-225 flasks respectively). Trypsin was inactivated by addition of DMEM at least three times the volume of trypsin. The cell suspensions were either immediately subcultivated or centrifuged at 1200 rpm for 8 min to sediment cells. Supernatants were removed by decantation and the cells resuspended and subcultivated. Cells were cultured in 4 ml and 10 or 30 ml complete DMEM in T-25, T-75 or T-225 flasks respectively. Non-adherent suspension cell lines (Yac-1, DC27.10 and RPMI 8226) were cultivated in 10 cm and 20 cm uncoated petri dishes in complete RPMI medium. Cells were subcultivated at 1:5 – 1:60 every 2 or 3 days into new petri dishes. Cells were resuspended in media and respective volumes or dilutions transferred to fresh petri dishes. Cell cultures were grown in a steam-saturated incubator maintained at 37°C and 5% CO₂.

4.2.2 Determination of cell number using Neubauer chamber

To determine cell numbers, cell suspensions were diluted respectively and 10 μ l loaded in a Neubauer (LaborOptik) cell counting chamber. When required cells were diluted in trypan blue solution to distinguish dead cells. Cells in major quadrants were counted under the microscope and the cell numbers from 4 major quadrants averaged. Since the volume of each major quadrant is 0.1 μ l (0.1 mm x 1 mm x 1mm), the cell number per ml was thus calculated as: mean cell number in major quadrants x 10000 x dilution factor.

4.2.3 Transfection of eukaryotic cells

Eukaryotic cells were transfected using jetPEI following the manufacturer's protocol. For analysis of cell surface proteins, cells were harvested 20 – 48 h post transfection and cell surface proteins stained. For the expression of Fc fusion proteins, transfected cells were subcultured into 500 ml incubation bottles. 24 h post transfection supernatants were harvested 5 days post transfection and proteins purified by affinity chromatography.

4.2.4 Preparation of HEK cell lysates

HEK cell lysates from P2X7-transfected cells were made for immunoprecipitation analysis and western blot analyses. Harvested cells were counted and washed with respective volumes of PBS. Each 2×10^7 cells were resuspended in 500 μ l 1% Triton X-100, 1 mM AEBSF in PBS. Cell suspensions were incubated on ice for 20 min and centrifuged at 800 g for 10 min at 4°C. Supernatants were transferred into fresh tubes stored at 4°C or used directly for western blot or immunoprecipitation.

4.2.5 Enrichment of P2X7-specific HEK cells per Easy-Sep

To increase the proportion of human P2X7 high expressors in stably transfected HEK cells, a PE-based Easy-Sep enrichment was carried out. 1×10^7 cells were pre-incubated with 500 ng of anti-hP2X7 mAb L4 at room temperature for 20 min in a FACS tube and washed once with 500 μ l in complete DMEM medium to remove excess antibodies. Cells were then incubated with 100 μ l of 1:100 diluted, sterile-filtered PE-conjugated anti-mIgG in complete DMEM medium. Following a 20 min incubation at room temperature, cells were washed once and resuspended in 10 μ l Easy-Sep PE cocktail in 200 μ l complete DMEM and incubated at room temperature for 10 min after which 5 μ l of Easy-Sep magnetic beads were added. Following a further 15 min incubation at room temperature, 2.3 ml of

complete DMEM was added and the FACS tube placed in an Easy-Sep magnetic block. After a 5 min incubation, unbound cells were discarded by decantation in one swing. As a washing step, FACS tube was removed from magnetic block and another 2.3 ml complete DMEM added and discarded as described above. In total, 3 washing steps were carried out. Finally, remaining bound cells were transferred to culture flask in complete DMEM medium containing blasticidin (100 µg/ml) and an aliquot analyzed by flow cytometry to assess extent of enrichment.

4.2.6 Panning of phages on cells and phage rescue

To select nanobodies directed against P2X7 in native conformation, panning of phage library was carried out on cells. Selection of anti-mP2X7 nanobodies was carried out by Ablynx using mP2X7-transfected CHO cells in round 1 and Yac-1 cells endogenously expressing P2X7 in round 2. Selection of anti-hP2X7 nanobodies was carried out personally as follows: each first round of selection was carried out with 2.5×10^7 Yac-1 cells transfected to stably express human P2X7 followed by a similar selection in round 2 on 2.5×10^7 hP2X7-transfected HEK cells. 200 µl of phage library (see 4.1.16 and 4.1.17) were added to cells in 1.8 ml blocking buffer (2% FCS and 4% milk powder in PBS) to a final volume of 2 ml in an Eppendorf tube and the whole incubated on ice with rolling for 2h. Subsequently, cells were pelleted by centrifugation at 1600 rpm for 5 min. For selection of nanobodies with binding epitopes distinct from 1c81 and 1c113 (see results), Yac-1 hP2X7 cells used in the first round, were pre-incubated in blocking solution supplemented with 700 ng each of 1c81 and 1c113 nanobodies. Cells were then incubated with phages as above. Subsequently, cells were centrifuged and supernatant containing unbound phages discarded by decantation. Cells were washed to remove further non-specific phages. Each wash was followed by a centrifugation step at 1600 rpm for 5 min at 4°C and supernatant discarded. Cells were washed twice \times 10 ml blocking solution and transferred to fresh Falcon tubes for a further 3x \times 10 ml blocking solution washing steps. Subsequently, cells were washed 3x \times 10 ml with PBS in the same Falcon tubes. Cells were then transferred to fresh 1.5 ml Eppendorf tubes for a further 2x \times 1 ml washes with PBS. To elute cell-bound phages, cell pellet was resuspended in 500 µl 1x trypsin and incubated at room temperature for 15 min. Cells were then centrifuged at 13000 rpm for 1 min. The supernatant containing eluted phages were transferred to a fresh tube pre-layered with 50 µl of 100 mM AEBSF to inactivate trypsin.

To rescue (amplify) eluted phages, 300 μ l of eluted phages were added to 2.5 ml of TG1 culture at $OD_{600} \approx 0.5$ and incubated at 37°C, 150 rpm for 30 min. Infected TG1 culture were precipitated by centrifugation at 4000 rpm for 10 min at 4°C. Supernatant was discarded and bacterial pellet resuspended in 300 μ l 2xYT medium and plated out on LB Agar Carb-100 Glu-2% plates and incubated at 30°C overnight. Bacterial colonies were scrapped off the culture plates with 10 ml of 2xYT Carb-100 Glu-2% and cell suspension incubated at room temperature for 10 min with rolling. 10 ml of fresh 2xYT Carb-100 Glu-2% were inoculated with cell suspension at starting $OD_{600} = 0.05$ and rest of cell suspension were centrifuged at 4600 rpm for 10 min and stored at 1 ml glycerol stock (see **section 4.1.3**). Inoculated culture was cultivated until $OD_{600} \approx 0.5$ was reached and 5 ml used for phage rescue and precipitation as described in 4.1.16 and 4.1.17. 200 μ l of soluble phages were taken for the second round of cell panning.

4.2.7 Flow cytometry (FACS)

Flow cytometry (also FACS, fluorescence-activated cell sorting) is a method used for the simultaneous analysis of multiple cell parameters of individual cells within a population. Flow cytometry permits the differentiation between cells based on size, complexity and expression of cell surface or intracellular molecules; up to several thousands of cells per second can be analyzed. A standard modern flow cytometer comprises of a fluidics system, lasers as source of light, optics, detectors and electronics. Cells passing through the cytometer are focussed to a flow of single cells by hydrodynamic forces built up by the fluidics system. This permits the analysis of each cell individually. The fluidics present the stream of single cells through the beam of a laser. As cells pass through the laser beam, they scatter light in all directions. Light scattered in low angle directions i.e. almost in the same direction as the light beam is referred to as forward scatter, whereas light scattering in larger angles is called sideward scatter. Scattered light are collected by detectors. Forward scatter parameters reflect the size of a cell whereas sideward scattering are indicative of the extent of granularity or complexity of a cell. In addition to size and complexity, fluorochrome-conjugated antibodies and other molecules are used to detect the expression of specific molecules by cells or to determine the state of cells. Fluorochromes emit fluorescence when excited with light of suitable wavelength. A number of mirrors, filters and detectors transmit and record the emitted fluorescence. The level of expression of specific molecules can be determined, retrospectively, from the intensity of fluorescence

emitted. In this project, FACS Calibur and FACS CantoII cytometers (BD Biosciences) were used. Analysis of FACS data were carried out using the FlowJo software (Tree Star Inc)

4.2.8 Preparation of leukocytes from peripheral blood (mouse and human)

To prepare peripheral blood leukocytes, 50 μ l or 100 μ l of mouse or human blood were stained with respective antibodies for 30 min at room temperature in FACS tubes (see **section 4.2.11**). Erythrocytes were subsequently lysed by incubation with 1 ml or 2 ml of 1x BD Lysis buffer at room temperature for 10 minutes. Cells were centrifuged at 1600 rpm for 5 min at 4°C and supernatant discarded. Cells were washed once with 1 ml of washing buffer with FCS (**section 3.5**). In cases of staining with fluorochrome-conjugated Annexin V, cells were washed with 1 ml Annexin V staining buffer after lysis of erythrocytes and stained (see **section 4.2.11**).

4.2.9 Preparation of splenocytes

Mice were anesthetized with isoflurane/O₂ and sacrificed by cervical dislocation. Spleens were removed and transferred to 10 ml ice-cold PBS washing buffer, 0.2% BSA (see section 3.5) in 15-ml Falcon tubes. Spleens were crushed and pressed through a cell strainer (BD) with 70 μ m mesh using the plunger of a 5 ml syringe in a 10 cm petri dish. The suspension was centrifuged at 1600 rpm for 5 min at 4°C to pellet cells. Cell pellets were resuspended in 5 ml of ACK lysis buffer and incubated on ice for 5 min for the lysis of erythrocytes. Cells were then centrifuged to remove lysis buffer and washed once with 10 ml of washing buffer to remove excess of lysis buffer. Splenocytes were resuspended in 5 ml washing buffer.

4.2.10 Preparation of liver leukocytes

Mice were anesthetized with isoflurane/O₂ and sacrificed by cervical dislocation, fixated at all four paws with needles with abdomen facing up and dissected to expose liver and heart. Liver lobes were cut and liver perfused with 10 ml of washing buffer by intracardial injection in the left heart ventricle. Livers were removed and transferred to 30 ml ice-cold PBS washing buffer, 0.2% BSA (see **section 3.5**) in 50-ml Falcon tubes. Livers were crushed through a metal sieve with 100 μ m mesh using the plunger of a 10 ml syringe in a

10 cm petri dish. Cell suspensions in 30 ml washing buffer were centrifuged at 1600 rpm for 5 min at 4°C to pellet cells.

Liver lymphocytes were separated by gradient centrifugation. To this end, liver cell suspensions were resuspended in 40% Percoll in unsupplemented RPMI medium and carefully layered on 3 ml of 70% Percoll (also in unsupplemented RPMI medium). Cells were centrifuged at 1600 rpm at 12°C for 20 min at lowest acceleration and deceleration in a Hettich centrifuge. The lymphocyte layer of cells were removed and transferred to fresh 15 ml Falcon tubes. Cells were washed once with 10 ml of 0.2% BSA washing buffer. Cell pellets were resuspended in 5 ml of ACK lysis buffer and incubated on ice for 5 min for lysis of erythrocytes. Lysis buffer was removed by centrifugation and cells washed once with 10 ml of washing buffer. Liver leukocytes were resuspended in 400 µl washing buffer.

4.2.11 Staining of cell surface proteins

Cell lines

Approximately $10^5 - 10^6$ cells were incubated with respective fluorochrome-conjugated antibodies (amounts as suggested by manufacturer or based on antibody titration results) for 30 min on ice or 20 min at room temperature in 100 µl FCS washing buffer in a 96-well plate. Cells were centrifuged at 1600 rpm for 5 min at 4°C and supernatant containing excess unbound antibodies discarded in one swing. Cells were subsequently washed once with 150 µl of washing buffer and resuspended in 200 – 400 µl buffer for FACS analysis. In cases of 2-step staining, cells were first incubated with 100 – 500 ng of unconjugated antibody in 100 µl for 30 min on ice or for 20 min at room temperature. Cells were centrifuged and supernatant discarded and further washed once as described above. Bound antibodies were detected with respective species-specific fluorochrome-conjugated secondary antibodies.

Peripheral blood

To stain leukocytes in mouse or human peripheral blood, 50 µl (mouse) or 100 µl (human) of heparinized full blood were incubated with a master mix of respective fluorochrome-conjugated antibodies for 30 – 60 min on ice in FACS tubes. Erythrocytes were lysed as described in **section 4.2.8** cells washed and analyzed by flow cytometry. When detection of exposed phosphatidylserine with Annexin V was carried out, cells were stained with all

other fluorochrome-conjugated antibodies as described above, erythrocytes lysed and cells washed with 1 ml Annexin binding buffer (see **section 4.2.8**). Staining of phosphatidylserine was carried out with fluorochrome-conjugated Annexin V in 200 μ l binding buffer. Following an incubation on ice for 30 - 60 min, 2 ml of Annexin V binding buffer was added to cells for washing and the whole centrifuged at 1600 rpm for 5 min at 4°C. Cells were resuspended in 300 μ l Annexin V binding buffer and analyzed by FACS.

Mouse splenocytes and liver leukocytes

Approximately 10^6 splenocytes or 10^5 liver leukocytes in 100 μ l washing buffer were transferred to V-bottom 96-well plates and pelleted by centrifugation at 1600 rpm for 5 min at 4°C. Cells were resuspended in 50 μ l of BSA washing buffer supplemented with 2% rat serum and 40 μ g/ml of anti-CD16/CD32 (clone 2.4G2) and incubated on ice for 10 min as Fc-block (Fc-block reduces non-specific staining by fluorochrome-conjugated antibodies by saturating free binding sites and Fc receptors CD16 and CD32). A master mix of respective fluorochrome-conjugated antibodies in 50 μ l washing buffer was added to cells to a final volume of 100 μ l and incubated on ice for 30 min. Cells were centrifuged at 1600 rpm for 5 min at 4°C and supernatant of excess unbound antibodies discard by decantation in one swing. Cells were further washed once with 100 μ l of washing buffer and resuspended in 100 - 300 μ l washing buffer for FACS analysis. In cases of detection with fluorochrome-conjugated Annexin V, cells were washed once in 100 μ l of Annexin V binding buffer prior to incubation with Fc block. Fc block and fluorochrome-conjugated antibodies as well as washing and FACS analysis were carried out as described above albeit in Annexin V binding buffer. The following antibody panels were used:

Antibody panels for staining of splenocytes

	<i>Panel 1</i>	<i>Panel 2</i>	<i>Panel 3</i>	<i>Panel 4</i>
<i>FITC</i>	anti-myc	Annexin V	anti-myc	Annexin V
<i>PE</i>	CD27	CD27	CD27	CD27
<i>APC</i>	CD25	CD25	CD25	CD25
<i>V450</i>	CD4	CD3e	CD3e	CD4
<i>APC-Cy7</i>	Live/dead	Live/dead	Live/dead	Live/dead
<i>PerCP</i>		CD4	CD4	

Antibody panels for staining of liver leukocytes

	<i>Panel 1</i>	<i>Panel 2</i>	<i>Panel 3</i>	<i>Panel 4</i>
<i>FITC</i>	Annexin V	Annexin V	anti-myc	Annexin V
<i>PE</i>	CD27	CD27	CD27	CD27
<i>APC</i>	anti-myc	CD25	CD25	anti-myc
<i>V450</i>	CD3e	CD3e	CD3e	CD3e
<i>APC-Cy7</i>	Live/dead	Live/dead	Live/dead	Live/dead
<i>PE-Cy7</i>	NK1.1	NK1.1	NK1.1	NK1.1

4.2.12 P2X7-mediated shedding of cell surface proteins and exposition of phosphatidylserine – blockade by Nanobodies

Yac-1 cell line

For screening of nanobodies for blockade of P2X7-mediated shedding of CD62L, 5×10^5 Yac-1 cells in a 96-well plate were pre-incubated with 2 μg of respective nanobodies in 75 μl of complete RPMI medium at room temperature for 15 min. 75 μl of a 40 μM NAD or 200 μM ATP stock was added and the whole incubated at 37°C for 20 min in an incubator. Cells were centrifuged at 1600 rpm for 5 min and supernatants discarded in one swing. Cells were washed once with 150 μl complete RPMI medium. Cells were stained with anti-mCD62L PE (MEL-14) as described in **section 4.2.11** and analyzed by FACS.

For dose response analyses of anti-mP2X7 nanobodies in the blockade of P2X7-mediated CD62L shedding in Yac-1 cells, nanobodies were titrated in a 96-well plate as follows: nanobody stocks of 30 μg in 60 μl in complete RPMI medium were made. 20 μl from the stock was transferred to 40 μl of layered complete RPMI medium and mixed thoroughly. 20 μl from the first dilution step was further transferred to the next 40 μl layered medium and the dilution series carried out for 7 steps. Each step comprised a 1:3 dilution. 20 μl of each step was removed and transferred to another 96-well plate resulting in two identical plates. 5×10^5 Yac-1 cells in 115 μl complete RPMI medium were added to each respective well with titrated nanobodies and the whole incubated at room temperature for 15 min. 15 μl of a 200 μM NAD or 1 mM ATP stock was added resulting in final NAD and ATP concentrations of 20 μM and 100 μM respectively in reaction volumes of 150 μl . In the case of P2X7 synergistic nanobodies, final concentrations of 2 μM and 30 μM of NAD or ATP respectively were used. Cells were incubated at 37°C for 20 min in an incubator and centrifuged at 1600 rpm for 5 min at 4°C. Supernatants were discarded in one swing; cells

were washed once with 150 μ l complete RPMI medium and stained with PE-conjugated anti-CD62L (MEL-14) as described in **section 4.2.11** and analyzed by FACS.

For dose response analyses of ligands (NAD and ATP), 5×10^5 Yac-1 cells were pre-incubated with 5 μ g of respective nanobodies in 150 μ l complete RPMI medium. 15 μ l of titrated NAD or ATP stocks were added (1:11) and the whole incubated at 37°C for 20 min in an incubator. Titrated NAD stocks were made as follows: 500 μ l of 5.94 mM NAD in RPMI medium was made as main stock. 200 μ l of the stock was transferred to 400 μ l of layered complete RPMI medium and mixed thoroughly. 200 μ l from the first dilution step was further transferred to the next 400 μ l layered medium and the dilution series carried out for 7 steps. Similarly a 500 μ l ATP stock of 29.7 mM was made and titrated as described above for NAD. Each step comprised a 1:3 dilution step. Cells were centrifuged at 1600 rpm for 5 min at 4°C and supernatants discarded in one swing. Cells were washed once with 150 μ l complete RPMI medium and stained with anti-mCD62L PE (MEL-14) and analyzed by FACS.

Transfected HEK cells

HEK cells at 60% confluence in a T-75 cell culture flask were transfected with 4 μ g pCDNA6 hP2X7 Y155 T348 and 4 μ g pCMVSPORT6 mCD62L or with 4 μ g pCMVSPORT6 mCD62L only in a T-25 flask as described in 4.2.3. 24 h post transfection, cells were harvested by trypsinization as described in 4.2.1 and resuspended in fresh complete DMEM. 5×10^5 HEK cells in 100 μ l complete DMEM medium were pelleted by centrifugation at 1600 rpm for 5 min at 4°C in V-bottom 96-well plates. Cell pellets were resuspended in 120 μ l of ATP in complete DMEM (0.25 mM - 4 mM). Cells were incubated at 37°C for 60 min in a waterbath. In P2X7 blockade assays, pelleted HEK cells were pre-incubated with 2 μ g of respective nanobody Fc fusion proteins in 80 μ l of complete DMEM medium for 15 min at room temperature. 40 μ l of a 6 mM or 12 mM ATP stock in complete DMEM medium were added to a final ATP concentration of 2 mM or 4 mM respectively. Cells were incubated at 37°C for 60 min in a waterbath and subsequently centrifuged at 1600 rpm for 5 min at 4°C and supernatant discarded in one swing. Cells were washed with 150 μ l of complete DMEM and stained with anti-CD62L PE (MEL-14) and anti-hP2X7 Alexa Fluor 647 (L4) as described in **section 4.2.11**.

With respect to dose-response assays in the blockade of hP2X7, HEK cells at 50% confluence in a T-225 culture flask were co-transfected with 15 µg pCDNA6 hP2X7 Y155 T348, 15 µg pCMVSPORT6 mCD62L and 5 µg eGFP. 24 h post transfection cells were harvested and resuspended in fresh DMEM. Nanobodies and mAb were titrated in a 96-well plate as follows: 1 µg antibody in 90 µl complete DMEM medium was made as stock. 30 µl of the stock (0.3 µg antibody) was transferred to 60 µl of layered medium, mixed thoroughly and 30 µl (0.1 µg antibody) transferred to the next well containing 60 µl medium, each step comprising a 1:3 dilution. The dilution series was carried out for 7 dilution steps. 30 µl of each step was added to 10⁵ transfected HEK cells in 50 µl medium to a volume of 80 µl. 40 µl of a 12 mM ATP stock in complete DMEM medium was added to the suspension to a final ATP concentration of 4 mM in 120 µl final reaction volume. Cells were incubated at 37°C for 60 min in a waterbath to induced P2X7 activation and subsequently centrifuged at 1600 rpm for 5 min at 4°C and supernatant discarded in one swing. Cells were washed with 150 µl of complete DMEM and stained with anti-CD62L PE (MEL-14) and anti-hP2X7 Alexa Fluor 647 (L4).

Human peripheral blood

100 µl aliquots of full blood from 3 donors were pre-incubated with 0.5 µg of 1067Fc, 1c113Fc, 1c81Fc, 3c23Fc or 1 µg of mAb L4 for 30 min at room temperature in FACS tubes. 100 µl of a 8 mM ATP stock in complete RPMI medium was added to each reaction to a final ATP concentration of 4 mM. Cells were incubated at 37°C for 30 min in a waterbath. 2 ml of Annexin V binding buffer was added and the whole centrifuged at 1600 rpm for 5 min at 4°C. Supernatants were discarded and cells stained with a master mix of fluorochrome-conjugated antibodies in 200 µl Annexin V binding buffer: CD62L FITC (DREG-56; Annexin V APC; CD4 APC/Cy7 (RPA-T4) and CD8 Pacific Blue (RPA-T8).

Mouse splenocytes and liver leukocytes

For *in vitro* CD62L shedding analyses in primary cells, 5 x 10⁵ splenocytes from a wildtype Balb/c mouse in 75 µl complete RPMI medium was pre-incubated with 1 µg of respective nanobodies in a 96-well plate. 75 µl of a 100 µM NAD or 400 µM ATP stock in complete RPMI medium were added to final NAD and ATP concentration of 50 µM and 200 µM respectively. Cells were incubated at 37°C for 20 min in a waterbath and subsequently centrifuged at 1600 rpm for 5 min at 4°C. Supernatants were discarded and

cells washed with 150 µl washing buffer, 0.2% BSA. Cells were stained for mCD62L PE (MEL-14) and CD3e APC (17A2).

Regarding *ex vivo* CD27 shedding experiments, approximately 10^6 splenocytes or 10^5 liver leukocytes from wildtype B6 mice injected with nanobodies (see **section 4.4.2**) in washing buffer were pelleted in V-bottom 96-well plates. Cells were resuspended in 100 µl of 30 µM NAD or 250 µM ATP in complete RPMI medium or medium without exogenous nucleotides and incubated at 37°C for 15 min in a waterbath. Cells were centrifuged at 1600 rpm for 5 min at 4°C and supernatants discarded in one swing and stained as described in 4.2.11. Cell-bound nanobodies were detected via anti-myc staining.

4.2.13 P2X7-mediated apoptosis assays

To investigate the blockade of ATP-mediated apoptosis by nanobodies 5×10^5 RPMI 8226 cells were pre-incubated with 900 ng of respective antibodies in 150 µl of complete RPMI cells in FACS tubes for 15 min at room temperature. Subsequently, 150 µl of a 4 mM ATP stock in complete RPMI medium was added to a final ATP concentration of 2 mM. Cells were incubated at 37°C for 60 min in a waterbath and FACS tubes immediately incubated on ice. 100 µl each of the cell suspension from each reaction were removed and transferred to a separate 96-well plate and further incubated overnight i.e. 24 h in an incubator. Cells were centrifuged at 1600 rpm for 5 min and supernatants discarded in one swing. Cells were washed once in 150 µl Annexin V binding buffer and stained with Annexin V APC and propidium iodide as described in **section 4.2.11** and analyzed by FACS.

4.2.14 Screening for P2X7-specific Nanobody clones

After panning phages on transfected cells, TG1 cells were infected with eluted phages (see **section 4.2.6**) and plated out on agar plates supplemented with 2% glucose and 100 µg/ml carbenicillin and incubated overnight at 37°C. Random bacterial clones were picked and sequenced and sorted into families of Nanobodies (Nbs) according to CDR3 sequence. To screen the selected clones for P2X7-specificity, 5 ml bacterial cultures were inoculated and periplasma lysates (PPLs) prepared as described in **sections 4.1.2** and **4.3.1**. Nbs in crude PPLs were screened for binding to P2X7. To this end, 10 µl of PPL was pre-incubated with 500 ng anti-myc FITC (9E10) in 90 µl PBS with 2% FCS for 30 min at 4°C to generate bivalent Nb-mAb molecules. To distinguish specific clones from clones which bind to cell

surface antigens other than P2X7, pre-incubate was added to a mixture of stably transfected HEK m/hP2X7 cells and untransfected HEK cells and further incubated for 30 min at 4°C. Cells were washed as described in **section 4.2.11** (cell lines) and analyzed by FACS. Screened Nb clones were defined as follow: (i) single negative cell population shows a non-binder; (ii) double population dot plot depicts a P2X7-specific binder which discriminates between P2X7-transfected and untransfected HEK cells and; (iii) single positive population shows a Nb clone which binds a cell surface antigen on HEK cells other than P2X7.

4.3 Methods in protein biochemistry

4.3.1 Preparation of bacterial periplasma lysates

Periplasma lysates were prepared from cultures of TG1 cells transformed with pAX100 (monomers) or pAX138 (dimers) constructs encoding anti-mP2X7 nanobodies. Similar lysates were prepared from HB2151 cultures transformed with pAX50 (monomers) or pHEN2 (dimers) encoding anti-hP2X7 nanobodies. Respective main cultures were prepared as described in **section 4.1.2**. Bacteria cultures were harvested by centrifugation at 4600 rpm for 15 min (Hettich Rotanta 460R). Supernatants were decanted and bacteria lysed. Cell pellets were resuspended in 5 ml TS lysis buffer per gram wet pellet weight and incubated on ice for 20 min. Lysates were centrifuged at 15000 rpm for 30 min at 4°C (Sorvall). The supernatants containing nanobodies were sterile centrifuged and purified by specific affinity chromatography

4.3.2 Protein purification by affinity chromatography

Immobilized metal affinity chromatography (Nickel-NTA)

His6x-tagged nanobodies were purified by immobilized metal affinity chromatography using Ni-NTA columns. Bacterial periplasma lysates (PPL) were loaded on 1 ml Ni-NTA matrix columns and flowthrough collected. Columns were washed once with 20 ml washing buffer. Column-bound proteins were eluted with elution buffer in 1 ml elution fractions and collected in 1.5 ml Eppendorf tubes. 10 µl of each from PPL, flowthrough, wash and elution fractions were size-fractionated by SDS-PAGE.

M2 anti-FLAG affinity chromatography

FLAG-tagged (DYKDDDDK) nanobody Fc fusion proteins were purified by M2 anti-FLAG column affinity chromatography. Supernatants of transfected HEK cell cultures (4.2.3) were harvested and centrifuged at 1600 rpm for 5 min and sterile centrifuged. Supernatants were loaded on respective 2 ml M2-coupled agarose columns and flowthrough collected. Columns were washed with 20 ml of PBS and eluted with 2.5 ml fractions of elution buffer. Each 2.5 ml elution fraction was collected and neutralized in 250 μ l of neutralization buffer.

Hano43/Hano44-coupled AminoLink affinity immunoprecipitation

Recombinant P2X7 in native conformation was immunoprecipitated with anti-mP2X7 mAbs HANO43/HANO44-coupled AminoLink agarose matrix. Lysates of HEK cells transfected to stably express mP2X7 were made as described in **section 4.2.4**. To each 10 ml of lysate (10^8 cells) were added 100 μ l of the matrix and the suspension incubated at 4°C overnight with rolling. The matrix was precipitated by centrifugation at 1600 rpm for 5 min. Supernatant was removed and matrix washed (the lysis buffer was used as washing buffer). P2X7-bound agarose matrix pellet was resuspended in 5 ml of lysis buffer and centrifuged as above and supernatant removed. Subsequently pellet was resuspended in 5 ml lysis buffer, incubated for 5 min at room temperature with rolling and centrifuged to remove buffer. This step was repeated twice. The matrix was resuspended in 500 μ l of lysis buffer and transferred to 1.5 ml Eppendorf tubes. A 50 μ l aliquot (i.e. 10 μ l matrix) was removed and analyzed by SDS-PAGE to estimate amount of P2X7 precipitated. The aliquot was transferred to a separate tube and centrifuged at 2500 rpm for 5 min and supernatant removed. The matrix was resuspended in 10 μ l of 2x SDS-PAGE sample buffer and sample analyzed by SDS-PAGE.

4.3.3 Sodium dodecyl sulfate polyacrylamide gel electrophoresis (SDS-PAGE)

SDS-PAGE is a method by which proteins are size fractionated with the help of an electric field. The proteins are mixed with sample buffer containing the anionic detergent, SDS, that denatures the proteins and confers a net negative to all proteins in the mix. Protein analysis by SDS-PAGE was carried out with the NuPAGE® Novex® system (Invitrogen). Routinely, samples were size-fractionated on 12% precast bis-tris gels with MES running buffer (Invitrogen). All SDS-PAGE in this work were done under reducing conditions. To

this end samples were prepared with NuPAGE® LDS sample buffer (Invitrogen) and 10% NuPAGE® sample reducing agent (Invitrogen) and incubated at 70°C for 15 min. The samples were centrifuged for 1 min at 13000 rpm and loaded on gels. The electrophoresis was routinely carried out at 200 V, 110 mA for 40 min.

4.3.4 Coomassie blue staining

Visualization of protein bands in SDS-PAGE gels was carried out by coomassie blue staining. Coomassie brilliant blue is a non-polar anionic dye which binds to proteins non-specifically. The Novex® colloidal blue staining kit was used following the manufacturer's protocol. Proteins were typically stained overnight (~16 h). Non-specific staining of the gel was removed by washing the gel in de-ionized water with active-coal filled destaining bags (Amersco). Destained gels were soaked in Novex® Gel-Dry drying solution and mounted, sandwiched between two transparent cellophane films to dry. Dried gels were scanned and documented.

4.3.5 Desalting of protein elution fractions

Elution fractions of proteins from affinity column chromatography were desalted to change storage buffer to PBS. The gel filtration based PD-10 desalting columns (GE Healthcare) were used following manufacturer's protocol. When required, protein fractions were concentrated using Amicon Ultra Centrifugal filter columns (Millipore) with suitable molecular weight cut-off.

4.3.6 Quantification of proteins

Protein fractions were quantified using the BCA™ protein assay kit (Pierce) and following the manufacturer's protocol. The method is based on the ability of peptides to reduce Cu^{2+} to Cu^+ in a weak alkaline solution. In a second step, 1 mole of Cu^+ reacts with 2 moles of bicinchonic acid (BCA) to form a water soluble purple complex. The purple complex of Cu^+ /BCA exhibits a strong linear absorbance with increasing protein concentration. Absorbance was measured at a wavelength of 562 nm with a photometer. For quantification, a 2 mg/ml BSA standard was used to plot a titration curve from which other concentrations were determined.

4.4 Methods in animal experiments

4.4.1 Immunization of llamas

Llama immunizations were carried out by Ablynx using the services of Eurogentec by a DNA prime-protein boost strategy (Möller *et al*, 2007). Eight llamas in 3 groups were immunized. Llamas 407, 414 and 417 (group 1) were immunized per gene gun (Biorad) on shaved left and right flanks with cDNA constructs of mouse P2X7 (mP2X7) adsorbed on gold particles (1 μm , 12 shots each with 1 μg DNA/mg gold) and boosted with the same, 3 times in 2-week intervals. Llamas 405 and 418 (group 2) were immunized with cDNA constructs of mouse and human P2X7 (hP2X7) and boosted with the same, similar to group 1. Three and 9 days post final DNA immunization, 100 ml peripheral blood aliquots were collected. Total RNA was prepared from blood lymphocytes, the V_HH repertoire was amplified by RT-PCR and cloned into the pAX50 phagemid vector, generating phage libraries PBL1 and PBL2. Llamas were further boosted once with 2×10^7 HEK cells transfected to stably express P2X7 (group 1 with HEK mP2X7 only; group 2 with HEK mP2X7 and HEK hP2X7). Four and 8 days post boost immunizations, peripheral blood was collected and immune libraries PBL3 and PBL4 generated. Following a further boost with matrix-bound precipitated recombinant mP2X7, phage libraries PBL5 and PBL6 were generated. Llamas 413, 415 and 416 (group 3) were immunized with HEK mP2X7 cells only and boosted 3 times in 2 week intervals. Peripheral blood samples were collected and respective libraries generated (PBL1 and PBL2)

4.4.2 Injection of mice with anti-P2X7 nanobodies

For *in vivo* P2X7 blockade experiments, mice were injected with nanobodies intravenously into tail vein. The mice were sacrificed after 2 or 24 h and the *in vivo* blockade of P2X7 by injected nanobodies assayed by nucleotide-mediated CD27 shedding and PS-flashing. Respective amounts of nanobodies were injected in a volume of 100 μl or 200 μl PBS intravenously or in 500 μl PBS intraperitoneally in a volume of 500 μl PBS.

4.4.3 Induction of anti-podocyte nephritis in mice

To induce antibody-mediated experimental autoimmune nephritis in mice, B6 mice were injected with anti-podocyte serum (Meyer-Schwesinger *et al*, 2011). Mice were injection intravenously with 300 μl sheep anti-podocyte immune serum (APN) or with the same volume of sheep pre-immune serum (PI) as control (**Fig. 4.1**). Five or six mice per group

were injected with 50 µg of half-life extended Nbs (HLE-Nbs) Dum-ALB-Dum (control), 13A7-13A7-ALB (P2X7 antagonist) or with 14D5-14D5-ALB (P2X7 synergist) 2 h prior to injection with APN and injected with 25 µg of respective HLE-Nbs on days 3, 6, 9 and 12. Three mice per group received PI and PBS or PI and HLE-Nb 14D5-14D5-ALB injected at the same intervals as described above for APN groups. HLE-Nbs were injected intraperitoneally in 1 ml PBS and mice placed in metabolic cages for 4 – 6 h for urine collection. Disease course was monitored by proteinuria using qualitative urine sticks. The experiment was ended on day 15 and mice sacrificed. Albumin content in urine were quantified by standard ELISA (Meyer-Schwesinger *et al*, 2011) whereas urine creatinine, serum creatinine, triglycerides and cholesterol were determined in the central diagnostic labs at UKE, Hamburg.

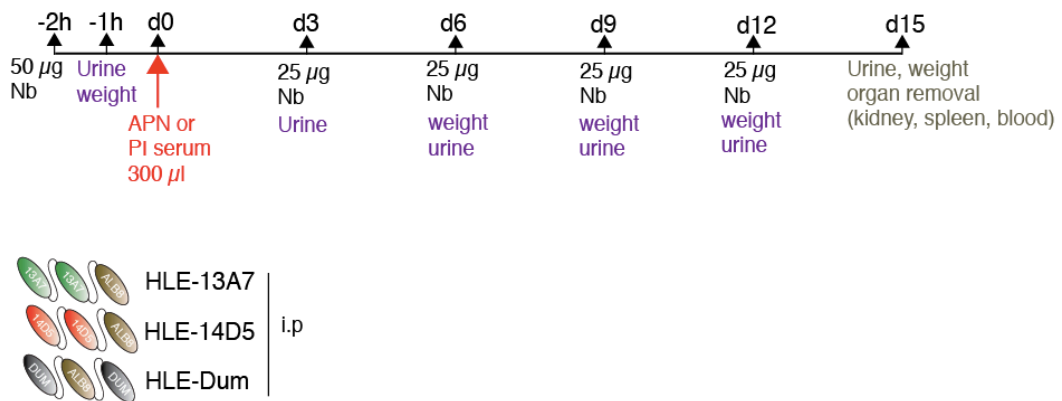


Figure 4.1. Timeline for the induction and monitoring of anti-podocyte nephritis in mice and the probing of effect of Nbs in the disease model. (APN = anti-podocyte nephritis serum; PI = pre-immune serum; HLE-13A7 = 13A7-13A7-ALB, HLE-14D5 = 14D5-14D5-ALB, HLE-Dum = Dum-ALB-Dum; i.p. intraperitoneal)

5 Results

The results section is divided into three parts. In chapter 5.1, the immunization of llamas, generation of libraries and selection of Nanobodies (Nbs) are presented. Moreover, initial screenings of the selected Nbs for binding to P2X7 are shown. Characterization of anti-human P2X7 Nbs is presented in chapter 5.2. All three selected families of Nbs block P2X7-mediated shedding of cell surface proteins in both transfected cells as well as primary T cells, albeit with different potencies. Furthermore, two of three selected Nbs blocked P2X7-mediated cell death in a human myeloma cell line. In chapter 5.3, an extensive characterization of anti-mouse P2X7 Nbs is presented. Here too, it is demonstrated that several selected Nbs block P2X7-mediated shedding of CD62L and CD27 as well the exposition of phosphatidylserine both *in vitro* and *in vivo*. Moreover, other selected Nbs potentiate activation of P2X7 by reducing ligand threshold concentrations. The Nbs also show therapeutic or exacerbation effect in a mouse model of kidney inflammation.

5.1 Cloning, selection, reformatting and expression of anti-P2X7 Nbs

This chapter describes the immunization of eight llamas with P2X7-encoding expression vectors, P2X7-transfected HEK cells, and purified P2X7 and an analysis of the P2X7-specific antibody response. Thereafter, the PCR-amplification of the llama Nanobody (Nb) immune repertoire from cDNA of peripheral blood leukocytes and the generation of phage display libraries are demonstrated. Panning of phage on cells expressing P2X7 yielded 31 Nb families, 18 of which were confirmed to bind specifically to cells transfected with mouse P2X7 (mP2X7) and 3 to cells transfected with human P2X7 (hP2X7). Five Nbs were selected for reformatting and expression as recombinant monovalent and bivalent Nbs and as Nb-Fc fusion proteins in prokaryotic and eukaryotic expression systems. Finally, the potential cross-reactivity of these five Nb-Fc fusion proteins with mouse, rat and human orthologs of P2X7 was analyzed by flow cytometry of transiently transfected HEK cells.

5.1.1 Immunized llamas show P2X7-specific antibody response

To induce an antibody response against mouse and human P2X7, eight llamas were immunized according to the scheme shown in **Fig. 5.1A**. Llamas in group 1 (407, 414 and

417) and group 2 (405 and 418) were immunized with a DNA-prime and protein-boost strategy previously used to generate Nbs against a cell surface enzyme (Koch-Nolte *et al*, 2007). Llamas were primed with four ballistic DNA immunizations of cDNA constructs of mP2X7 only (group 1) or a cocktail of mP2X7 and hP2X7 (group two) adsorbed on 1- μ m gold particles. Following a single boost with HEK cells stably transfected with mP2X7 and hP2X7 (**Fig. 5.1B**), llamas were further immunized with mP2X7 immunoprecipitated with mP2X7-specific monoclonal antibodies Hano43 and Hano44 immobilized on AminoLink agarose beads (**Fig. 5.1C**). Llamas in group 3 were immunized four times with mP2X7-transfected HEK cells.

The induction of an anti-P2X7 humoral immune was verified in sera obtained from immunized llamas, eight (groups 1 and 2) or ten (group 2) days after the final boost with P2X7-transfected cells. Untransfected HEK cells were incubated with 1:200 dilutions of llama immune sera to adsorb potential HEK cell-specific antibodies. Unbound serum antibodies were subsequently incubated with HEK cells transfected to stably express mP2X7 or with a separate aliquot of untransfected HEK cells. Cell-bound llama antibodies were detected by flow cytometry after a two-step staining protocol with mouse anti-llama IgG primary antibody followed by a PE-conjugated donkey anti-mouse IgG (**Fig. 5.2**). As a control for non-specific binding by the secondary and tertiary antibodies, transfected HEK cells were incubated in PBS without llama antibodies prior to the same antibody detection steps.

The results indicate a successful induction of anti-mP2X7 antibody response in each group of immunized llamas (**Fig. 5.2**). For the llamas immunized with the cDNA-prime protein-boost strategy for mouse P2X7 (group 1, llamas 407, 414 and 417), anti-mouse P2X7 antibodies could be detected for llamas 414 and 417 but not for llama 407. Both llamas subjected to the immunization with a cocktail of mouse and human P2X7 with the cDNA-prime protein-boost strategy (group 2, llamas 405 and 418) showed a strong anti-mP2X7 response. Similarly, all llamas immunized only with transfected HEK cells (group 3, llamas 413, 415 and 416) showed detectable mP2X7-specific antibody responses albeit weaker than that observed in both groups 1 and 2. The strongest antibody responses were detected in the sera of llamas immunized with the cDNA-prime protein-boost strategy (llama 414 from group one and both llamas of group two).

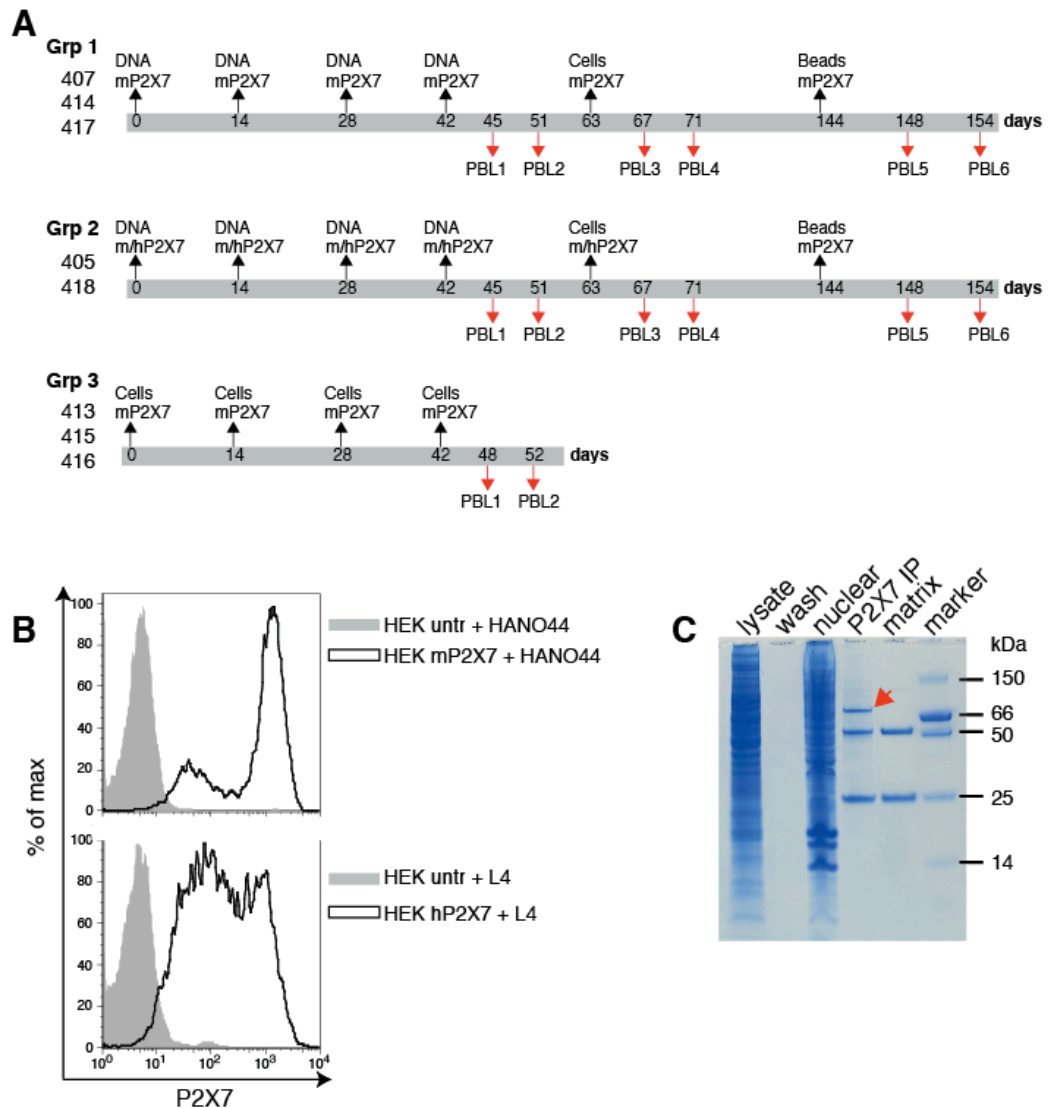


Figure 5.1. Immunization scheme and sample preparation for immunization. (A) Two groups of llamas were immunized with a DNA-prime and protein-boost strategy (Koch-Nolte *et al.*, 2007). After four ballistic DNA immunizations, animals were boosted with HEK cells stably transfected with mP2X7 and hP2X7 and recombinant mP2X7 adsorbed on beads. Cocktails of cDNA constructs for mP2X7 and hP2X7 were adsorbed on 1- μ m gold particles. Llamas received 12 shots each with 1 μ g DNA/mg gold per immunization, a boost with HEK cells stably expressing mP2X7 (2×10^7 , pretreated for 15 min with 1mM ATP) or hP2X7 (3×10^7), and a final boost with mouse P2X7 immunoprecipitated with Hano43 and Hano44 immobilized on AminoLink agarose beads (5 μ g / 50 μ l beads). A third group of llamas was immunized with HEK cells transfected to stably express mP2X7 (2×10^7 cells per immunization). Phage libraries were generated from blood samples collected at the end of each phase of immunization (PBL1 - PBL6). (B) FACS analyses of P2X7 expression levels on stably transfected HEK cells used for immunization with Alexa Fluor 647-conjugated mAbs Hano44 (anti-mP2X7) (Möller *et al.*, 2007) and L4 (anti-hP2X7) (Buell *et al.*, 1998). Untransfected cells (HEK unrtr) stained with the same antibodies were used as controls (gray histograms). (C) SDS-PAGE analysis of bead-bound recombinant mP2X7 used for immunization. Mouse P2X7 (~72 kDa, red arrow) was precipitated from lysates of HEK cells stably transfected with mP2X7 using mAb Hano44 immobilized on agarose beads (AminoLink, Pierce) (lysate = cell lysate of 2×10^7 HEK mP2X7 cells; wash = 10 μ l of first wash fraction; nuclear = nuclear lysate 2×10^7 HEK mP2X7 cells; P2X7 IP = immunoprecipitate of mP2X7 from 2×10^7 HEK mP2X7 cells on 15 μ l Hano44-AminoLink agarose beads (marked with red arrowhead); matrix = 15 μ l Hano44-AminoLink agarose beads only; marker = super marker).

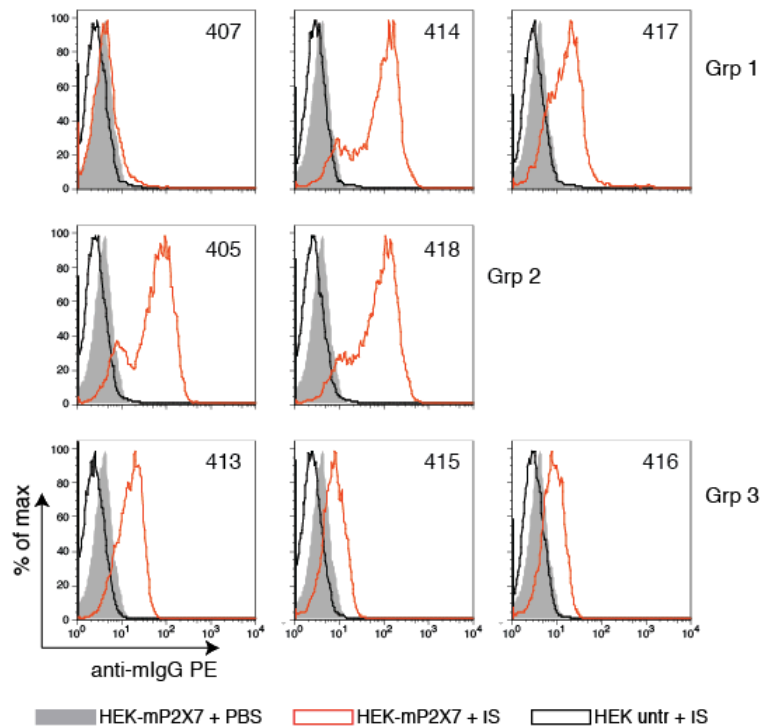


Figure 5.2. Monitoring the induction of anti-P2X7 antibody response in immunized llamas by FACS.

Llamas were immunized by a DNA prime-and-protein boost strategy (groups one and two) or immunized solely with transfected cells (group 3). Blood samples were collected on day 71 (groups one and two) or day 52 (group 3) from llamas and sera prepared. 1:200 dilutions of immune sera (IS) were pre-absorbed on untransfected HEK cells and unbound sera used to stain HEK cells transfected to stably express mP2X7 (HEK-mP2X7) and untransfected HEK cells (HEK untr). Bound anti-P2X7 llama antibodies were detected with a sequential mouse anti-llama and donkey anti-mouse PE staining. As a control HEK-mP2X7 cells incubated with PBS were stained similar to cells incubated with immune sera.

5.1.2 Cloning of PCR-amplified V_HH coding regions yields immune libraries

To generate phage libraries for the selection of anti-P2X7 Nbs, the V_HH repertoires of immunized llamas were cloned from peripheral blood lymphocytes obtained 3-10 days after the third (PBL1, PBL2), fourth (PBL3, PBL4) or fifth boost (PBL5, PBL6) as illustrated in **Fig. 5.1A**. RNA prepared from peripheral blood lymphocytes (from 50 ml blood samples) was reverse transcribed into cDNA and cDNAs obtained following each immunization phase combined (e.g. PBL5+PBL6). The V_HH coding regions were PCR-amplified from the cDNAs using a two-step amplification strategy (**Fig. 5.3**).

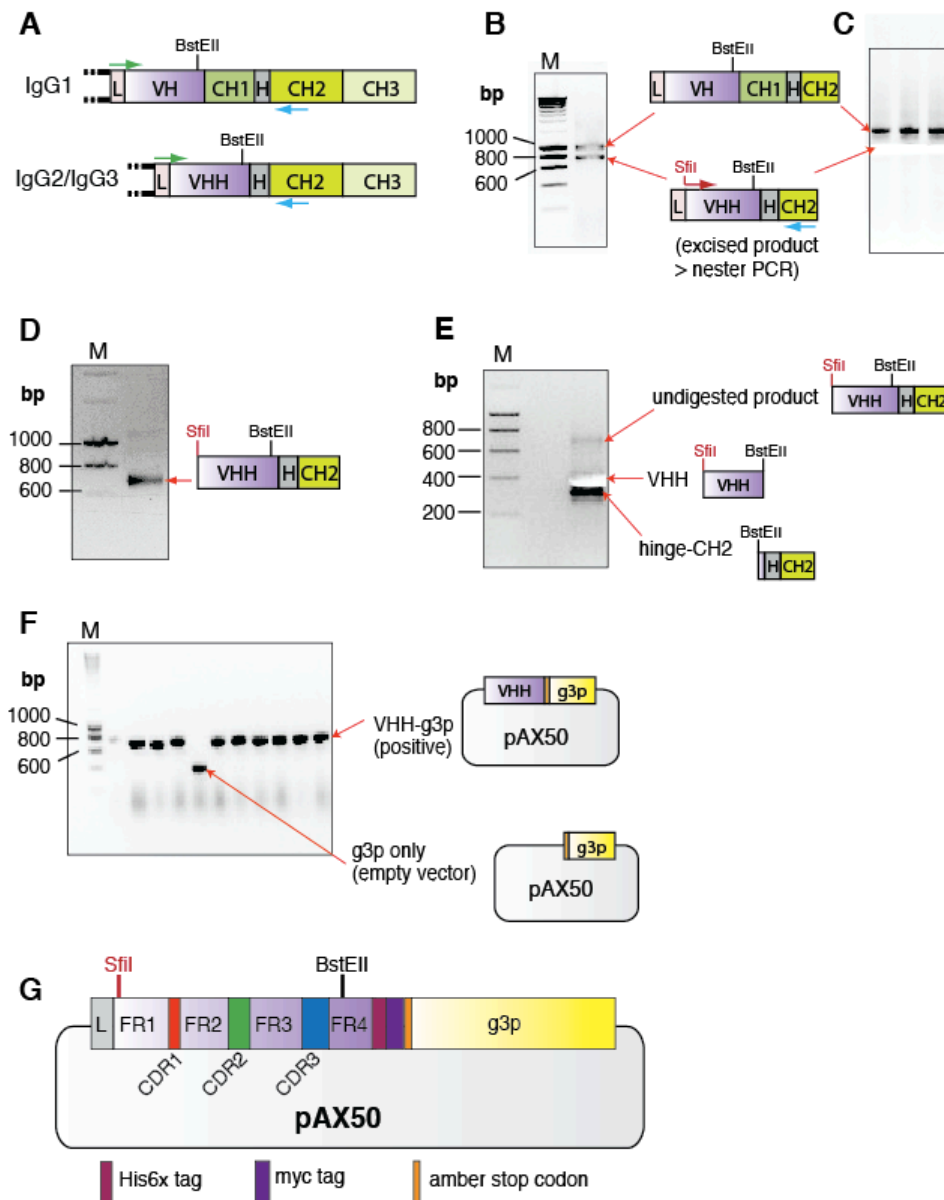


Figure 5.3. Cloning and generation of anti-P2X7 V_HH phage library. (A) Schematic representation of llama IgG1 and IgG2/IgG3 loci. (B) The antibody repertoire of P2X7-immunized llamas was amplified from pools of PBL cDNAs obtained from the same phase of immunization (e.g. PBL5+PBL6) using a combination of degenerate forward primers complementary to most known V_HH and VH families (ABL051, ALB052) and a common reverse primer which anneals to a region in the middle of the C_H2 domain conserved in the three llama IgG subclasses (ABL003). (C) The 700 bp band corresponding to the V_HH, hinge and part of C_H2 fragment was excised from agarose gels and purified. (D) A nested PCR using forward primer ABL050 with 5'-SfiI site and ABL003 was used to amplify V_HH fragments. (E) Restriction digestion of PCR material with SfiI and BstEII (which cuts in a natural site in FR4 region) gave products of 400 bp (corresponding to V_HH) and 300 bp (corresponding to hinge and part of C_H2). V_HH fragments were ligated into a similarly digested pAX50 phagemid vector and transformed into TG1 cells to generate a library. (F) A colony PCR using LMB3 and M13R was carried out to test for presence of inserts of the appropriate size. Insert frequency was 82 – 100%. The above figure demonstrate the cloning and generation of llama libraries PBL5+6 of llama 405. All other libraries were generated similarly. (G) Representation of pAX50 vector with V_HH and g3p genes interspersed by hexahistidine tag (His6x), myc tag and ambers stop codon (TAG). A bacterial leader sequence (L) directs translated V_HH into bacterial periplasma. (M = smart ladder)

Using primer combinations of ABL051 and ABL052 (forward) versus ABL003 (reverse), both heavy chain antibody as well as classical antibody repertoires of llamas were successfully amplified (**Figs. 5.3A** and **5.3B**, shown for llama 405 PBL5+6). DNA fragments resolved by agarose gel electrophoresis and corresponding to the heavy chain antibody repertoire (~700 bp) were excised and purified (**Fig. 5.3C**). The purified material was subjected to a nested PCR amplification step therewith inserting and SfiI restriction site at the N-terminus (**Fig. 5.3D**). Nested PCR products were digested with SfiI and BstEII taking advantage of the naturally occurring BstEII site found in FR4 of over 90% of all llama V_HH domains. Digested materials were size-fractionated by agarose gel electrophoresis and bands corresponding to SfiI-V_HH-BstEII fragments (~400 bp) were excised and purified (**Fig. 5.3E**). Restriction digested material was ligated into the pAX50 phagemid vector and transformed into TG1 cells to generate Nb libraries.

Sizes of the generated libraries (number of independent clones) were determined by plating out dilution series of transformed cells. To determine the efficiency of insert cloning, 23 random clones were picked and subjected to colony PCR and analyzed by agarose gel electrophoresis (**Figs. 5.3F** and **5.3G** and **Table 5.1**). Libraries with sizes of $1.8 \times 10^7 - 3.8 \times 10^8$ were obtained, with percentages of phagemids carrying inserts of 82 – 100%. Corresponding phage libraries were generated by superinfection of cultivated bacterial library with helper phage as described in sections **4.1.16** and **4.1.17**. Similar library sizes were obtained for all llamas from all phases of immunization.

Table 5.1. Titers of libraries generated from P2X7-immunized llamas

Library	Llamas	Immunization type	Library size (titre)	Insert %
PBL1+2	413, 415, 416	cell	$1.8 \times 10^8 - 2.3 \times 10^8$	92 - 100
PBL1+2	407, 414, 417, 405, 418	DNA	$8 \times 10^7 - 3.8 \times 10^8$	92 - 100
PBL3+4	407, 414, 417, 405, 418	DNA + cell boost	$1.8 \times 10^7 - 2.5 \times 10^8$	83 - 100
PBL5+6	414, 417, 405, 418	DNA + cells + P2X7 IP boost	$9 \times 10^7 - 2.5 \times 10^8$	82 - 91

5.1.3 Panning of phage libraries on P2X7-expressing cells yields 18 families of mP2X7-specific and 3 families of hP2X7-specific Nbs

To select P2X7-specific Nbs from the generated libraries, phages were subjected to two rounds of panning on Yac-1 lymphoma cells endogenously expressing mouse P2X7 or on cells transfected to stably express mouse or human versions of the purine receptor (CHO mP2X7, HEK hP2X7 and or Yac-1 hP2X7). Selections for anti-mP2X7 Nbs were

performed at Ablynx with cells provided by our group, whereas selections for anti-hP2X7 Nbs were carried out by myself at the Institute of Immunology in Hamburg.

Selections of anti-mP2X7 Nbs were carried out with phage libraries PBL1+2 from all llamas and with PBL3+4 from llamas of groups 1 and 2 immunized by the cDNA-prime and protein-boost strategy. Anti-mP2X7 Nbs were selected by panning phages on mP2X7-transfected CHO cells in round one (R1). Cell-bound phages were eluted by trypsinization and amplified in *E.coli*. Phages from R1 were panned on Yac-1 cells endogenously expressing mP2X7 in round two (R2). Eluted phages from R2 were used to re-infect TG1 cells and plated out on agar plates. Clones were picked for sequencing and preparation of periplasma lysates (PPL). The successful sequencing of 285 clones revealed 23 distinct families of Nbs (**Table 5.2**).

Selections for anti-hP2X7 Nbs were similarly carried out in two rounds using phage libraries PBL5+6 from llamas 405 and 418 immunized with a cocktail of mouse and human P2X7 constructs. Two selections were performed each comprising R1 selections on hP2X7-transfected Yac-1 cells and R2 selections on hP2X7-transfected HEK cells. Prior to cell panning in selection two, however, P2X7 binding sites of the two confirmed clones obtained in selection one were masked by pre-incubating cells with purified Nbs 1c81 and 1c113 to minimize re-selection of the same Nbs. For both selections, 92 clones from R2 outputs were successfully sequenced. Sequencing of the 92 clones revealed 8 distinct families of Nbs (**Table 5.3**).

In order to determine whether the isolated clones specifically bind mouse or human P2X7, a screening assay was developed to distinguish P2X7-specific binders from non-binders and from binders to other cell surface antigens. 10 μ l aliquots of periplasma lysates (PPL) (containing an estimate of 20-100 ng of monovalent myc-tagged Nbs) were pre-incubated with 500 ng of anti-myc FITC to permit formation of bivalent Nb-anti-myc mAb molecules. The pre-incubate was added to a mixture of untransfected HEK cells and P2X7-transfected cells. Following a 20-min incubation on ice, cells were washed and analyzed by FACS (**Figs. 5.4 and 5.5**).

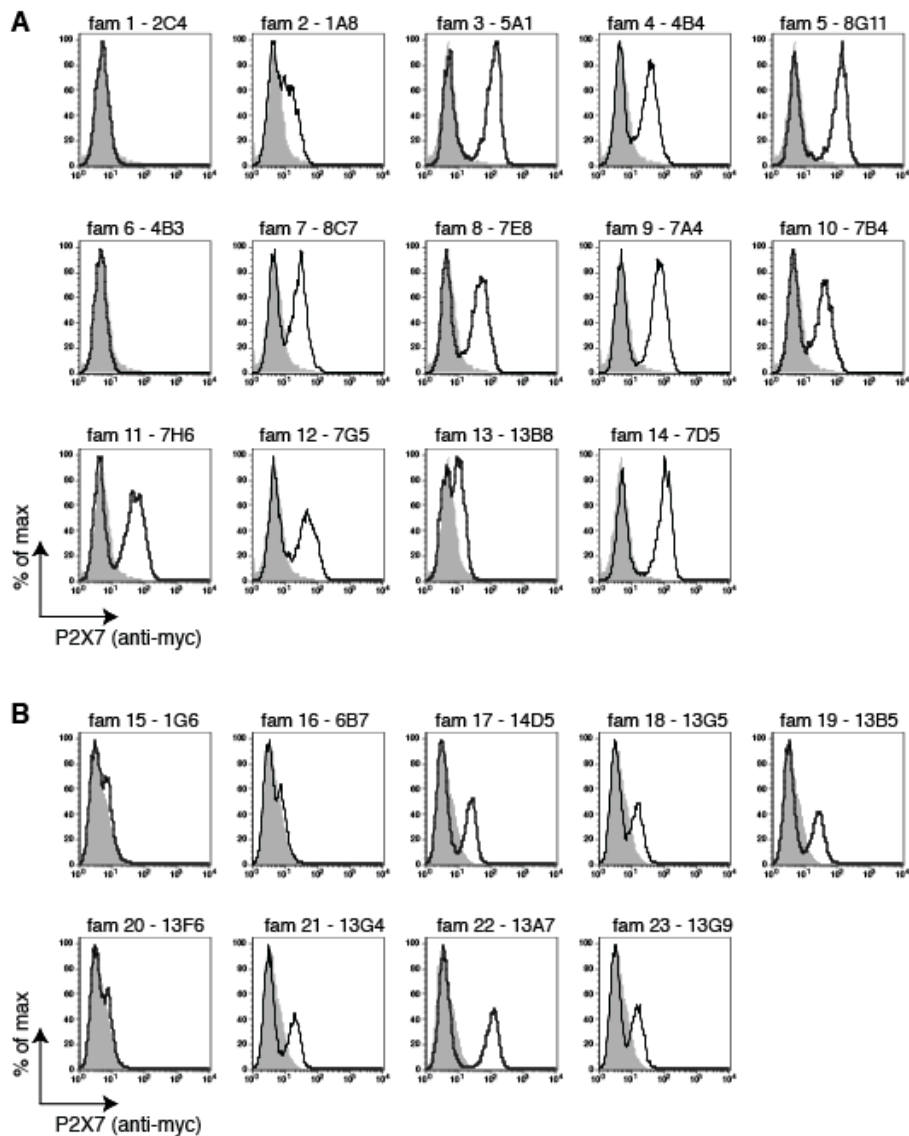


Figure 5.4. FACS screening of selected VHHs for specific binding to mouse P2X7-transfected cells. (A, B) Nbs selected on mP2X7-expressing cells were screened in two batches (A and B) for binding to HEK cells stably transfected with mP2X7 and lack of binding to untransfected cells using a 1:1 mixture of these cells. This permits distinction of mP2X7-specific binders from non-binders (lack of binding either both cell types) as well as from binders specific for other cell surface antigens (showing non-selective binding to both cell types). 10 μ l aliquots of periplasma lysates (PPL) were pre-incubated with 500 ng of anti-myc FITC before addition to the mixture of untransfected HEK cells and mP2X7-transfected cells. Following a 20-min incubation on ice, cells were washed and analyzed by FACS. PPL from *E. coli* transformed with an empty pAX50 vector was used as negative control (gray histograms).

Anti-mP2X7 Nbs were screened in two batches (Figs. 5.4A and 5.4B). As a control, periplasma lysate from bacterial culture transformed with an empty vector was used (gray histograms). Eighteen of twenty-three selected clones showed binding to mP2X7-transfected HEK cells but not to untransfected cells. Two clones (families 1 and 6) did not show any detectable binding whereas three clones showed only very low, possibly unspecific binding (families 15, 16, and 20).

Table 5.2. Families of isolated Nb clones selected against mouse P2X7

Family	Llama	Nb	# of Hits R1	# of Hits R2	# of mut. vs. parent	Immun. phase	CDR3	IFI name
1	414	2C4	30x			PBL3+4	GHFTVDSGKVLLRTDISS	-18
		2A6	1x		1	PBL3+4	GHFTVDSGKVLLRTDISS	
		4D5		1x	1	PBL3+4	GHFTVDSGKVLLRTDISS	
		4G6		1x	1	PBL3+4	GHFTVDSGKVLLRTDVSS	
2	417	1A8	5x			PBL1+2	GHFVYNDGAISLNTARGSGF	-20
		1C9	1x		1	PBL1+2	GHFVYNDGAISLNTARGSGF	
3	413	5A1	5x			PBL1+2	GTSVYHYQY	-9
		5B1	11x		2	PBL1+2	GTSVYHYQY	
		5F1	21x		1	PBL1+2	GTSVYHYQY	
		7E2		2x	2	PBL1+2	GTSVYHYQY	
		7F1		1x	2	PBL1+2	GTSVYHYQY	
		7F3		1x	2	PBL1+2	GTSVYHYQY	
		11G1	2x		2	PBL1+2	GTSVYHYQY	
4	414	4B4		5x		PBL3+4	FLGPNWYSYDGRPSSYDF	-18
		4G4		1x	3	PBL3+4	FLGPNWYSYDGRPSSYDF	
5	418	8G11		5x		PBL3+4	VIELGVLEPRDY	-12
		6A11	27x		2	PBL3+4	RIELGVLEPRDY	
		6H10	13x		8	PBL3+4	RIELGVLEPRDY	
		8E6		1x	3	PBL1+2	RIELGVLEPRDY	
		8F5		1x	6	PBL1+2	RIELGVLEPRDY	
		8B4		2x	2	PBL1+2	RIELGVLEPRDY	
		14G4		1x	6	PBL1+2	RIELGILEPRDY	
		8H5		1x	6	PBL1+2	RIELGVLVPRDY	
		14F10		1x	7	PBL3+4	RIELGPLVPRDY	
		8A11		2x	7	PBL3+4	RIELGPLVPRDY	
		8H6		3x	6	PBL1+2	TIELGVLEPRDY	
		8G12		7x	7	PBL3+4	TIELGVLEPRDY	
		14F6		2x	3	PBL1+2	TIELGVLEPRDY	
		8B12		6x	6	PBL3+4	TIELGVLEPRDY	
		14G11		2x	7	PBL3+4	TIELGVLVPRDY	
6	407	4B3		1x		PBL3+4	DYASLCTIETGYGSLYDY	+18
		8C7		50x		PBL3+4	SPVLSIVLDTRGLEY	
		8E7		17x	1	PBL3+4	SPVLSIVLDTRGLEY	
		6D7	2x		2	PBL3+4	SPVLSIVLDTRGLEY	
		7E8		9x		PBL1+2	STSGSAYLPYRVYQYDS	
7	405	7D6		3x	2	PBL1+2	STSGSVYLPYRVYQYDS	-15
		7F5		1x	1	PBL1+2	STSGSAYLPYRVHQYDS	
		7A4		7x		PBL1+2	SITSYVSTWQHDYDY	
8	415	13E8		7x	7	PBL1+2	SISSYSSRWQDDYDY	-15
		7B4		1x		PBL1+2	GLEYMSTIRYTYEY	
9	415	7H6		3x		PBL1+2	DSYIIGAGVRDY	-12

Family	Llama	Nb	# of Hits R1	# of Hits R2	# of mut. vs. parent	Immun. phase	CDR3	IFI name
12	415	7G5		2x		PBL1+2	ECQRWAYPNRIGA	+13
		13F4		1x	1	PBL1+2	ECQRWAYPNRIGA	
13	416	7D8		4x		PBL1+2	GWGRVITVQHMCADRSIFTS	+20
		13B8		1x	7	PBL1+2	GWGRVMTVQHMCADRSIFTS	
14	415	7D5		1x		PBL1+2	AWKYDRASYDFPEAYDY	-17
15	414	1G6	1x			PBL1+2	GYRGGYLG YRLTLEGSYDV	-20
16	405	6B7	1x			PBL3+4	SGSLLDVTSEAVYTD	-15
17	418	14D5		1x		PBL1+2	RVRDY	-6
18	415	13G5		2x		PBL1+2	SRRAYLPAKVGEYDF	-15
19	415	13B5		1x		PBL1+2	EELGDGLGYLAYRYDY	-16
20	415	13F6		1x		PBL1+2	PRGV	-4
21	415	13G4		2x		PBL1+2	TLTWLGIHEYEYNT	-14
22	416	13A7		1x		PBL1+2	GPLTKRRQCVPGFDFSMDF	+18
		13E9		1x	12	PBL1+2	GPLTRRRQCVPGFDFSMDF	
23	416	13G9		1x		PBL1+2	KANYESPSRETSYAY	-15

Table 5.3. Families of isolated Nb clones selected against human P2X7

Family	Llama	Nb	# of Hits R2	# of mut. vs. parent	Immun. phase	CDR3	IFI name	
a	405	1c81	34x			PBL5+6	HSETRGGTRYFDRPSLYNY	-19
		3c22	4x	1		PBL5+6	HSETRDGTRTFDRPSLYNY	
		3c29	1x	1		PBL5+6	HSETRGGTRYFDRPSLYNY	
b	418	1c113	39x			PBL5+6	RLRFEVSSNY	-10
c	418	1c121	1x			PBL5+6	EKPLGGA	-7
d	418	1c126	1x			PBL5+6	KRRFPIWRDY	-10
e	405	3c23	1x			PBL5+6	ADETLGAVPNFRLHEKYEYDY	-21
		3c28	2x	1		PBL5+6	ADETLGAVPNFRLHEKYEYDY	
f	405	3c31	1x			PBL5+6	DPVRRGWGCRDHYKY	+15
g	418	3c34	3x			PBL5+6	ILSGKKT	-7
		3c36	1x	30		PBL5+6	ILSGKKT	
		3c40	1x	25		PBL5+6	ILAGKKS	
h	418	3c39	3x			PBL5+6	YTQAHYY	-7

Similar analyses were performed for clones selected on human-P2X7 transfected cells. The results for clones obtained in selection one and in selection two are shown in **Fig. 5.5A** and **Fig. 5.5B**, respectively. Three families of Nbs were found to bind specifically to hP2X7-transfected but not to untransfected cells (families a, b, and e). Four families of Nbs did not show any detectable binding to hP2X7 transfected cells (families c, d, f, and g) and one family (h) showed binding to both, untransfected and hP2X7 transfected cells.

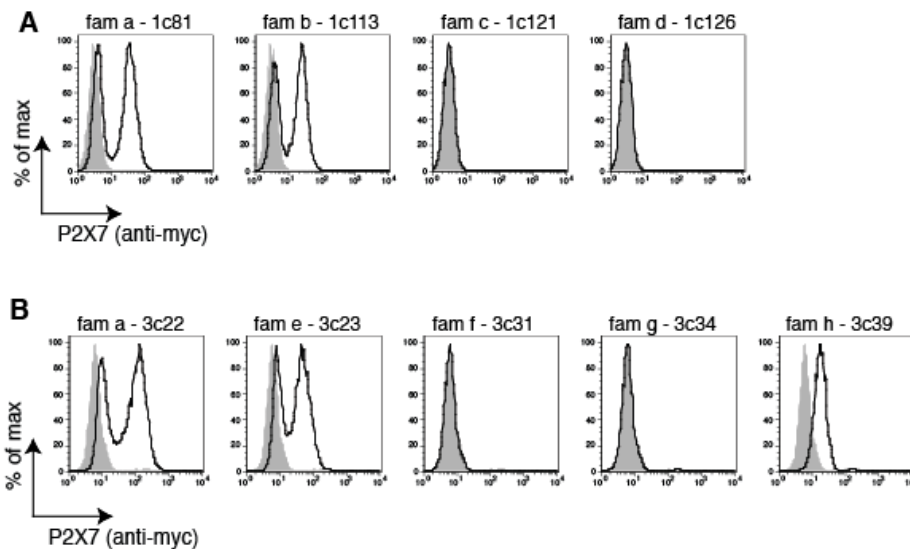


Figure 5.5. FACS screening of selected VHs for specific binding to human P2X7 transfected HEK cells. (A, B) Anti-P2X7 Nb selection one (A) and selection two (B) were screened for binding to hP2X7. To exclude non-binders as well as clones which bind other cell surface antigens, a mixture of untransfected and hP2X7-transfected HEK cells were used. 3 - 10 μ l aliquots of periplasma lysates (PPL) were pre-incubated with 500 – 1000 ng of anti-myc FITC. The pre-incubate was added to a mixture of untransfected HEK cells and hP2X7-transfected cells. Following a 20-min incubation on ice, cells were washed and analyzed by FACS. PPL from a mP2X7-specific Nb was used as negative control (gray histograms).

5.1.4 Reformatting, expression and purification of Nanobodies in monomeric, dimeric, bi-specific and Nb-Fc fusion formats

Three mouse P2X7-specific Nbs (13A7, 8G11 and 14D5) and three human P2X7-specific Nbs (1c81, 1c113, 3c23) were further reformatted to increase affinity, to boost functional potency, and to extend half-life *in vivo*. Homomeric dimers of anti-mP2X7 Nbs (13A7-13A7, 8G11-8G11 and 14D5-14D5) were cloned by Ablynx, who also provided bi-specific, half-life extended Nb molecules (HLE-Nbs) constructed by linkage of Nb dimers to an albumin-specific Nb (13A7-13A7-ALB, 8G11-8G11-ALB and 14D5-14D5-ALB). Homomeric and heteromeric dimers of anti-hP2X7 Nbs were constructed by myself at the Institute of Immunology in Hamburg. V_HH gene fragments were amplified by PCR, so as to insert a 35-amino acid i.e., 7x GS (GGGGS) linker between adjacent VHs using long flanking primers (SfiI-Nb1-20GS-BamHI-15GS-Nb2-NotI), followed by digestion with SfiI and NotI and ligation into the pHEN2 phagemid in frame with the vector-encoded C-terminal His6x and c-myc tags. Anti-mP2X7 and anti-hP2X7 Nbs were also recloned as fusion proteins to the Fc domain of mouse IgG1 by PCR amplification with primers flanked by suitable restriction enzyme sites (5' BglII, and 3' XhoI), followed by digestion

and ligation into the eukaryotic expression vector, pME (providing an N-terminal FLAG-tag) (Scheuplein *et al*, 2010).

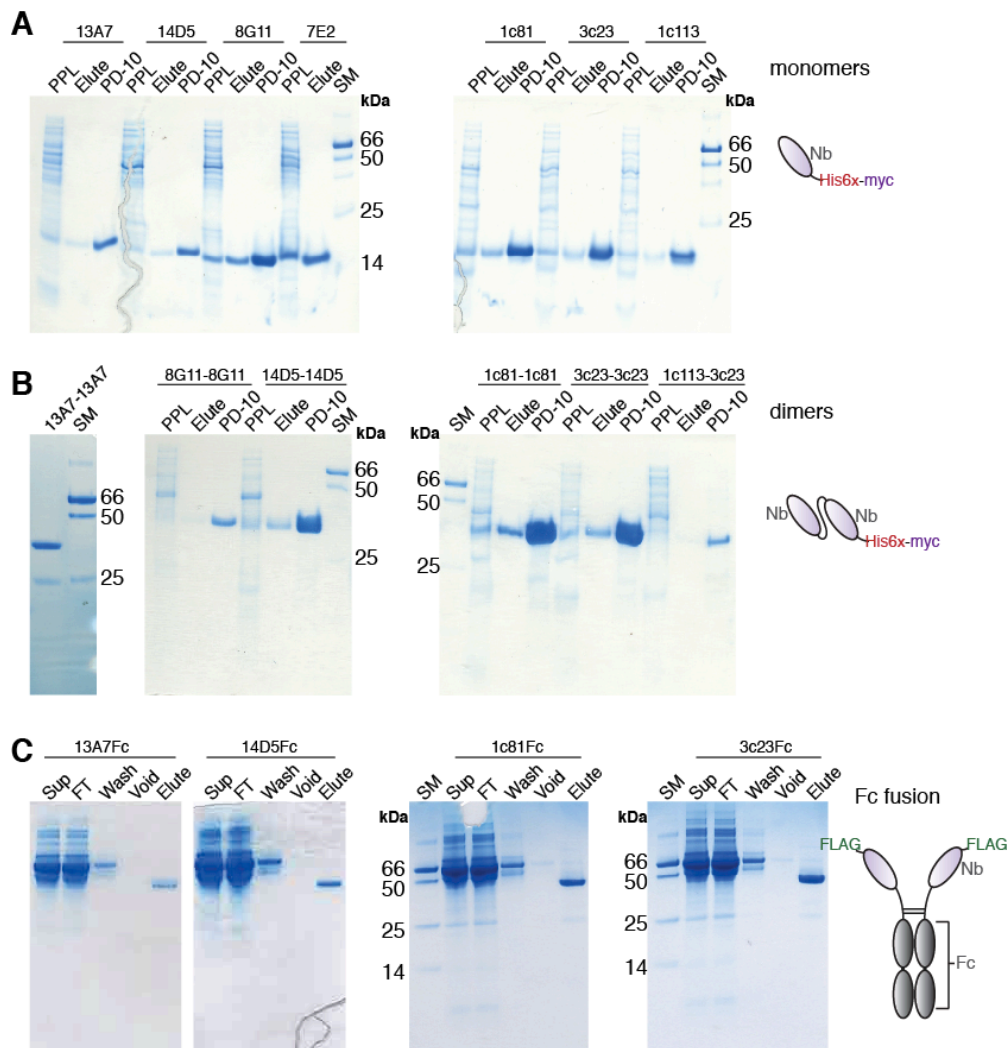


Figure 5.6. Expression and purification of Nbs in monomeric, dimeric and Nb-Fc fusion protein formats. (A) Monomeric Nbs were expressed as soluble His6x-tagged proteins in 50 ml cultures of transformed HB2151 *E. coli* and purified from periplasma lysates (PPL, 5 ml per gram *E. coli* pellet) by immobilized metal affinity chromatography (PPL = lanes were loaded with 10 μ l of 5 ml periplasma lysates obtained from 50 ml bacterial culture; Elute = lanes loaded with 10 μ l of a 2.5 ml elution fraction derived from 5 ml PPL; PD-10 = lanes loaded with 10 μ l of per PD-10 column desalted elution fractions subsequently concentrated to 500 μ l of pure Nbs in PBS). (B) Dimeric Nbs were also expressed as soluble His6x-tagged proteins in 150 ml cultures of transformed HB2151 *E. coli* (except for Nb 14D5-14D5 which was expressed in a 100 ml culture) and purified from periplasma lysates (PPL, 5 ml per gram *E. coli* pellet) by immobilized metal affinity chromatography (PPL = lanes were loaded with 10 μ l of 10 – 15 ml periplasma lysates obtained from 100 – 150 ml bacterial culture; Elute = lanes loaded with 10 μ l of a 2.5 ml elution fraction derived from 10 – 15 ml PPL; PD-10 = lanes loaded with 10 μ l of per PD-10 column desalted elution fractions subsequently concentrated to 250 μ l of pure dimeric Nbs in PBS). (C) N-terminally FLAG-tagged Nb-Fc fusion proteins were expressed in transiently transfected HEK cells. Five days after transfection, Nb-Fc fusion proteins were purified from 500 ml HEK cell supernatants by affinity chromatography on M2-anti-FLAG immobilized on agarose beads. Elution fractions were desalted by gel filtration using PD-10 columns and concentrated using centrifugation filters (Sup = lanes loaded with 10 μ l of HEK cell supernatant; FT = lanes were loaded with 10 μ l of flowthrough of unbound proteins; Wash = lanes loaded with 10 μ l of 20 ml wash fraction; Void = 10 μ l of a 1 ml first elution fraction; Elute = lanes loaded with 10 μ l of 2.5 ml elution fraction). In all cases SM = 10 μ l of super marker.

Monomeric and dimeric Nbs were expressed as soluble His6x-tagged proteins in HB2151 *E. coli* and purified from periplasma lysates by immobilized metal affinity chromatography. Purification was monitored by SDS-PAGE (**Figs. 5.6A** and **5.6B**). A yield of 0.4 – 6 mg purified protein per litre of *E.coli* culture was achieved for monomeric Nbs whereas dimeric Nbs were purified with yields of 0.1 – 3 mg/l. Bivalent Nb-Fc fusion constructs were expressed as N-terminally FLAG-tagged proteins in transiently transfected HEK cells. Five days after transfection, Nb-Fc fusion proteins were purified from cell supernatants by affinity chromatography on M2-anti-FLAG immobilized on agarose beads. Purified Nb-Fc proteins were obtained with yields of 0.2 mg – 1.6 mg per liter of HEK cell culture supernatant (**Fig. 5.6C**). In all cases, elution fractions were desalted by gel filtration using PD-10 columns and purified proteins were concentrated when necessary using centrifugation filters with suitable molecular weight cut-offs (3000 MW for monomeric VHHs and 10.000 MW for other proteins).

5.1.5 Nb 1c81 recognizes mouse, rat and human P2X7, four other Nbs show selective reactivity with mouse or human P2X7

In order to analyze the potential cross-reactivity of the selected Nbs with mouse, rat or human orthologs of P2X7, FACS analyses were performed with the reformatted Nb-Fc fusion proteins described in the previous section. HEK cells were co-transfected with expression constructs for GFP and either mP2X7, rP2X7 or hP2X7. Twenty-four hours post transfection, harvested cells were incubated with 100 µl of HEK cell or hybridoma supernatants of Nb-Fc fusion proteins (see **section 5.1.4**) or mAb L4, respectively. Cells were washed and cell-bound Nb-Fc proteins or mAbs detected by staining with Alexa Fluor 647-conjugated anti-mouse IgG and data collected by flow cytometry (**Fig. 5.7**).

The results show that Nbs 14D5 and 13A7 bind specifically to mP2X7 but not to the rat or human orthologs. Nbs 3c23 and 1c113 recognize hP2X7, but not mP2X7 or rP2X7, whereas Nb 1c81 specifically reacts with cells transfected with either mP2X7, rP2X7 or hP2X7. By comparison, monoclonal antibody, L4 (Buell *et al*, 1998) binds rP2X7 and hP2X7 but not mP2X7 whilst a control Nb, 1067 (anti-hCD38) did not react with P2X7.

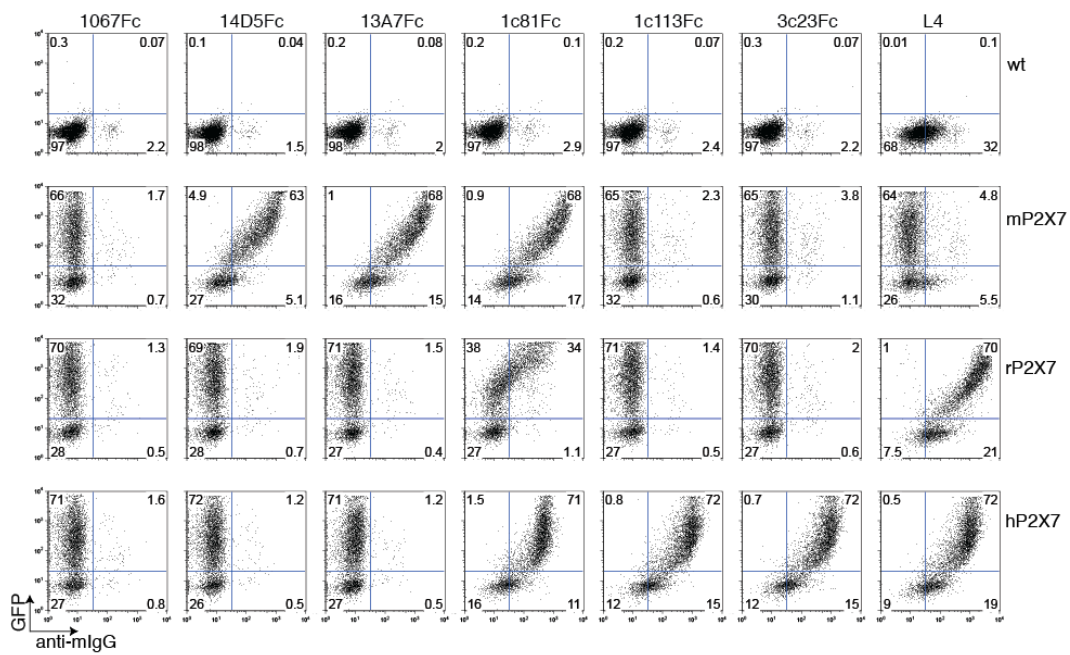


Figure 5.7. FACS analyses of the potential crossreactivity of selected Nb-Fc fusion proteins with mouse, rat and human orthologues of P2X7. HEK cells were co-transfected with expression constructs for GFP and either mP2X7, rP2X7, or hP2X7. 24 h post transfection, cells were harvested by trypsinization and incubated with 100 μ l of respective Nb-Fc fusion proteins HEK cell supernatant or mAb L4 hybridoma supernatant (Buell *et al.*, 1998) as indicated. Cells were washed and bound antibodies detected with anti-mouse IgG Alexa Fluor 647. As controls, untransfected HEK cells (wt) were subjected to the same staining procedures. 1067 is a Nb specific for human CD38 (Unger, 2012). This figure is representative of two independent experiments with similar results.

5.2 Molecular and functional characterization of hP2X7-specific

Nanobodies

As described in the first chapter of the results, three different families of Nbs were selected from llamas 408 and 415 by panning on cells expressing human P2X7 (hP2X7). Nbs 1c113 (b) and 3c23 (e) were confirmed to specifically recognize hP2X7 but not mouse or rat P2X7, while Nb 1c81 (a) was shown to recognize the P2X7 orthologs from human, rat and mouse. These three Nbs were expressed as His6x-tagged monomers and bivalent Nb-Fc fusion proteins in *E. coli* and HEK cells respectively. This chapter of the results section describes the further molecular and functional characterization of these Nbs with respect to their relative binding epitopes on P2X7, their utility for detecting low levels of P2X7 on the surface of human leukocytes, and their inhibitory potencies of P2X7 on lymphoma cell lines and primary leukocytes – as evidenced by ATP-induced shedding of CD62L, externalization of phosphatidylserine, and uptake of propidium iodide. The Nbs were compared in these analyses to the human P2X7-specific L4 monoclonal antibody developed at GlaxoSmithKline and previously reported to exhibit capacity to inhibit activation of P2X7.

5.2.1 Cross-blockade binding analyses show that Nbs 1c81 and 1c113 share an overlapping binding site with the anti-hP2X7 mAb L4

In order to determine whether the selected Nbs recognize distinct or overlapping epitopes, cross-blocking analyses were performed with unconjugated and Alexa Fluor 647 (AF674)-conjugated Nb-Fc fusion proteins and mAb L4 (**Fig. 5.8**). HEK cells transfected to stably express high levels of hP2X7 were pre-incubated with saturating levels of either unconjugated anti-hP2X7 mAb, L4 (Buell *et al*, 1998), or anti-hP2X7 Nb-Fc fusion proteins 1c81Fc, 1c113Fc or 3c23Fc, a control Nb-Fc (1067Fc, anti-hCD38 (Unger, 2012)), or medium only (vehicle). Without washing, cells were then stained with AF647-conjugated Nb-Fc 1c113Fc, 3c23Fc, or mAb L4 in amounts 10 times less than unconjugated antibodies.

As expected, the control Nb-Fc 1067Fc did not inhibit staining by the AF647-conjugated P2X7-specific Nb-Fc proteins or mAb, whereas staining was effectively blocked by pre-incubation with an excess of the unconjugated version of the fluorochrome-conjugated Nb-Fc or mAb used for staining. Staining with AF647-conjugated 1c113Fc (1c113Fc AF647)

was also completely blocked by unlabeled 1c81Fc and mAb L4 but not by 3c23Fc. Concurrently, 3c23Fc AF647 staining was completely abrogated by unconjugated 3c23Fc but was unaffected by the other antibodies. Finally, whereas binding of mAb L4 AF647 was unaffected by 3c23Fc, staining was abrogated in the presence of unconjugated 1c113Fc and partially blocked by 1c81Fc (**Fig. 5.8**).

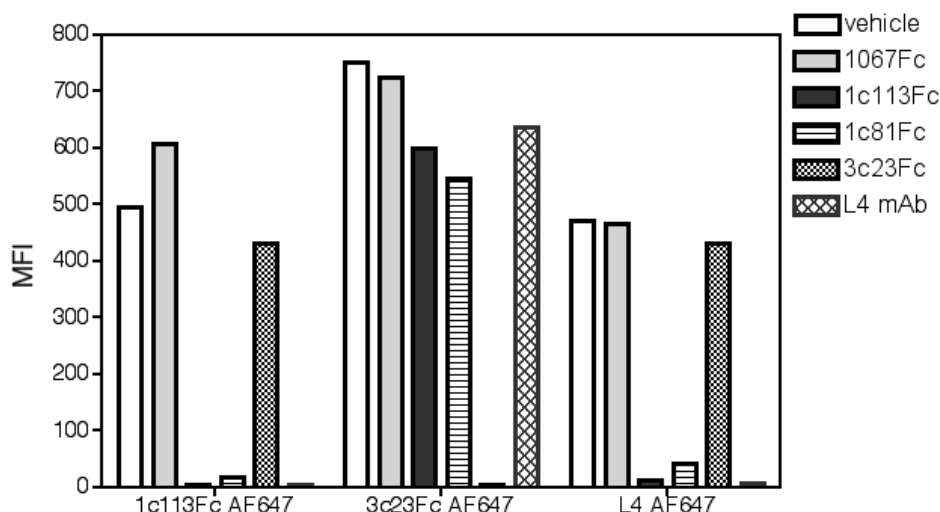


Figure 5.8. Analyses of the capacity of unconjugated anti-hP2X7 mAbs and Nb-Fc fusion proteins to block staining of P2X7-transfected HEK cells with fluorochrome-conjugated mAb L4 or Nb-Fc proteins, 1c113Fc or 3c23Fc. 5×10^5 HEK cells stably transfected with hP2X7 were incubated with $3 \mu\text{g}$ of respective unconjugated antibodies in $95 \mu\text{l}$ of DMEM containing 5% FCS for 15 min at room temperature. Without washing, $1 \mu\text{l}$ ($\sim 250 \text{ ng}$) of Alexa Fluor 647 (AF647)-conjugated 1c113Fc, 3c23Fc or mAb L4 was added and incubation was continued at 4°C for 20 min. Cells were washed and analyzed by flow cytometry (FACS Calibur, BD). MFI, mean fluorescence intensity. AF647-conjugates of Nb-Fc or mAb used for staining are indicated below the panel whereas unconjugated Nb-Fc and mAb used for blocking are indicated on the top right. (Vehicle = medium without blocking Abs). This figure is representative of 2 cumulative and independent experiments with similar results.

5.2.2. Combination of epitope-independent Nbs permits visualization of P2X7 on human peripheral blood lymphocytes and monocytes

Detection of the surface expression of P2X7 on primary lymphocytes is limited by the availability of suitable tools and the inherent low expression of the purine receptor on lymphocyte subsets (Buell *et al*, 1998). Having shown that 3c23Fc does not interfere with binding of 1c113Fc and *vice versa*, it was tested whether a combination of these two fluorochrome-labelled Nb-Fc fusion proteins would improve detection of P2X7 on lymphocyte and monocyte populations in human peripheral blood. To this end, comparative stainings of PBLs from a single donor were performed with AF647-conjugated Nb-Fc proteins 1c113Fc, 3c23Fc, or a combination of the two Nb-Fc fusion

proteins versus mAb L4 (**Fig. 5.9**). In order to verify the specificity of the observed staining, blocking analyses were performed with a 10-fold excess of a combination of the same unlabeled Nb-Fc fusion proteins used for staining, or a control Nb-Fc, 1067Fc.

The results demonstrate that the combination of Nb-Fc fusion proteins with independent epitopes yields improved detection sensitivity as compared to staining with mAb L4 alone (MFI of 21 vs. 11 for CD4⁺ cells and MFI of 17 vs. 10 for CD4⁻ cells with similar background staining i.e., unblocked vs. blocked) (**Fig. 5.9**)

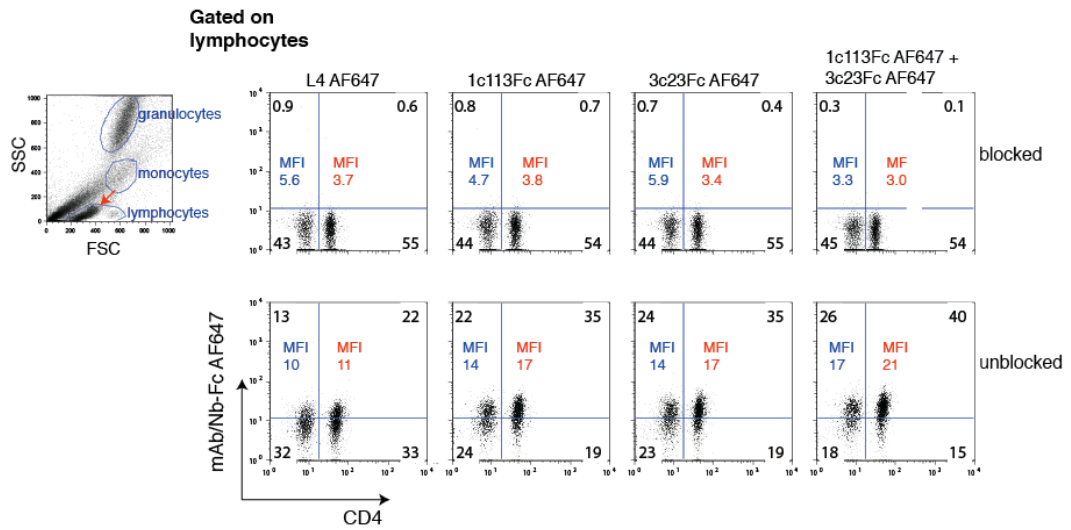


Figure 5.9. Improved staining of P2X7 on primary leukocytes with a combination of hP2X7-specific Nb-Fc proteins, 1c113Fc and 3c23Fc. (A) 100 μ l blood aliquots from a single donor were pre-incubated with a combination of 3 μ g each of 1c113Fc and 3c23Fc ("blocked"). Parallel aliquots were incubated with 3 μ g of 1067Fc only ("unblocked"). After a 30-min incubation at room temperature, a mastermix of conjugated antibodies was added: 1c113Fc A647 (~250 ng); 3c23Fc A647 (~250 ng); and anti-CD4 Pacific Blue (RPA-T4). Cells were incubated on ice for 30 min for antibody staining. Erythrocytes were lysed by 10 min room temperature incubation with 2 ml BD Lysis solution. Cells were washed once with 3 ml complete RPMI and analyzed by flow cytometry (FACS Calibur, BD). Lymphocytes were gated based on low forward scatter (FSC) vs sideward scatter (SSC) property (arrowhead). Black numbers indicate the percentage of cells in the respective quadrant. MFI values in blue and red indicate the mean fluorescent intensity of CD4⁻ and CD4⁺ lymphocytes, respectively.

In order to validate the utility of combining 1c113Fc and 3c23Fc for detecting P2X7 on leukocytes from different donors, aliquots of blood from three donors were stained by the same procedure as above (**Fig. 5.10**). Monocytes, granulocytes, and lymphocytes were gated by forward scatter versus side scatter (FSC vs. SSC) properties. CD4⁺ T cells, CD8⁺ T cells and CD4⁻/CD8⁻ lymphocytes (corresponding mainly to B cells) were delineated on the basis of CD4 and CD8 expression. Results are shown in a concatenate representation. The extent of specific staining was calculated as the fold increase in MFI of unblocked (-) versus blocked (+) staining (**Table 5.4**).

The results show specific staining of cell surface P2X7 in monocytes and all lymphocyte subsets, but not in granulocytes. The level of P2X7 expression can be ordered qualitatively as monocytes > CD4 > CD8 > CD4⁻/CD8⁻. Thus combining Nb-Fc fusion proteins of Nbs 1c113 and 3c23 is validated as a useful experimental approach in visualizing low expression of P2X7 on primary T cells.

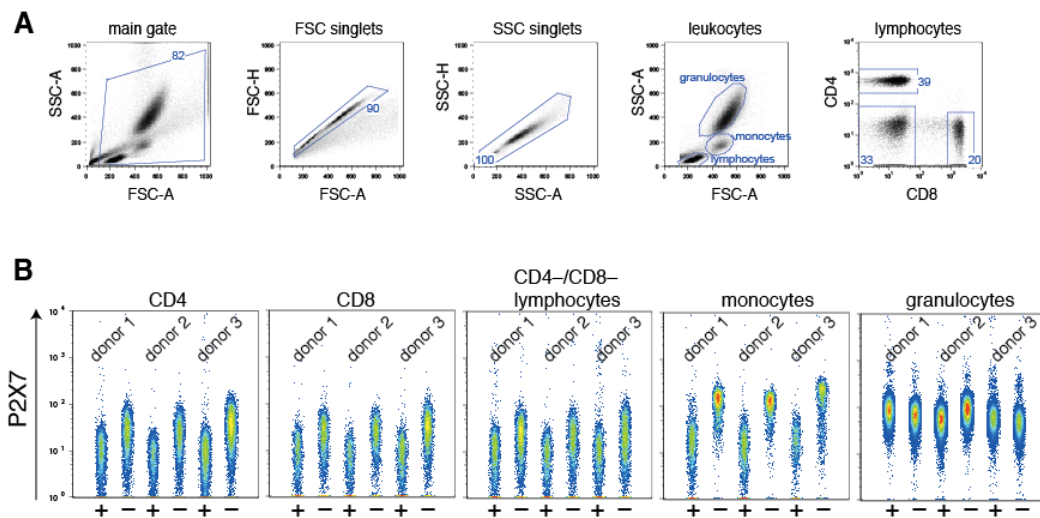


Figure 5.10. FACS analyses of P2X7 expression on peripheral blood leukocytes from three different donors. Stainings were performed as in **Figure 5.9**, but in the presence of an additional anti-CD8 AF488 mAb (RPA-T8). **(A)** Gating of granulocytes, monocytes, and lymphocytes was based on FSC versus SSC properties as indicated. Lymphocytes were further gated on as CD4⁺ T cells, CD8⁺ T cells and CD4⁻/CD8⁻ lymphocytes based on expression of subset-specific molecules. **(B)** Expression of P2X7 is shown in a concatenate representation. Pre-incubation with unconjugated blocking Nb-Fc proteins (1c113Fc + 3c23Fc) and nonblocking Nb-Fc (1067Fc) is indicated by (+) and (-), respectively, below the panels.

Table 5.4. Relative staining intensities of P2X7 on subpopulations of human peripheral blood leukocytes. Mean fluorescence intensities were determined for each population of cells shown in **Figure 5.10**. Quotients of the MFIs of unblocked (-) versus blocked (+) quotients were calculated.

	Quotient MFI AF647 unblocked/blocked		
	donor 1	donor 2	donor 3
CD4 T cells	3.1	4.2	4.5
CD8 T cells	2.7	4.5	6.4
CD4 ⁻ /CD8 ⁻ lymphocytes	2.1	1.3	1.1
monocytes	5.1	6.3	5.3
granulocytes	0.78	1.7	0.8

5.2.3 Fc-fusion proteins of Nanobodies 1c81 and 3c23 inhibit ATP-induced shedding of CD62L by hP2X7 and CD62L co-transfected HEK cells

It has previously been shown that treatment of HEK cells co-transfected with mouse P2X7 and CD62L (L-selectin) with ATP results in the P2X7-dependent shedding of CD62L (via P2X7-dependent activation of an endogenous metalloprotease) (Schwarz *et al*, 2012). To determine whether the selected Nbs could inhibit activation of human P2X7, similar CD62L shedding analyses were carried out with HEK cells 24 hours after co-transfection with CD62L and human P2X7 (Fig. 5.11). For these analyses, an allelic variant of human P2X7 previously shown to exhibit higher ATP sensitivity than most other P2X7 variants was used (Y155 T348) (Stokes *et al*, 2010). Cells were harvested and shedding of CD62L induced by incubation with relatively high concentrations of ATP (0.25 – 4 mM).

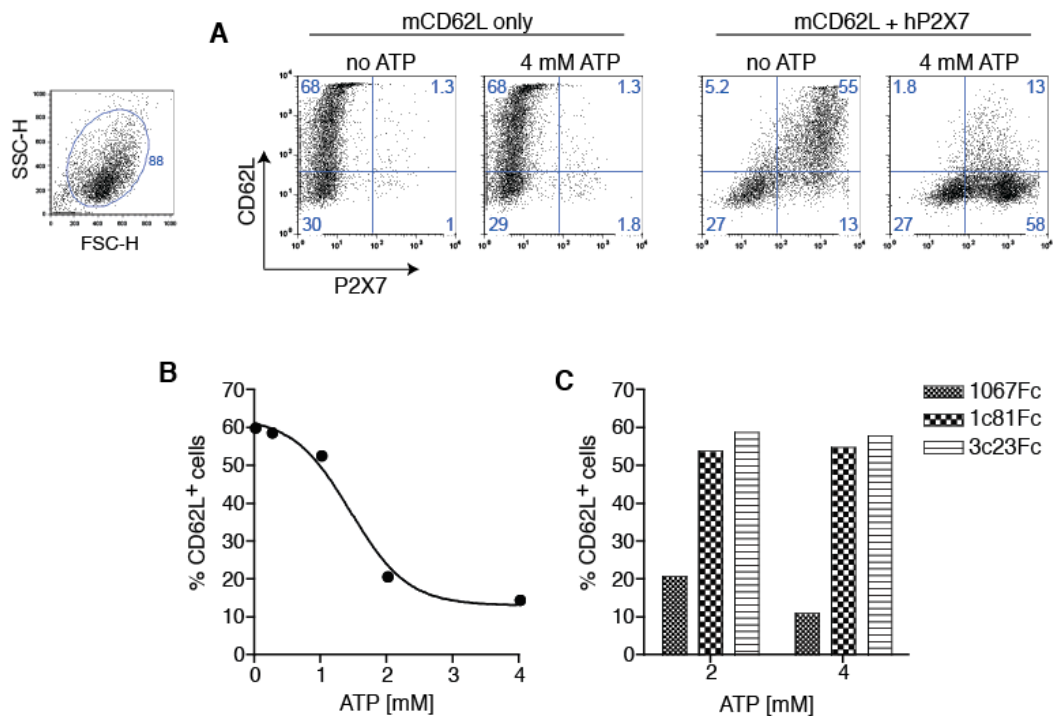


Figure 5.11. Analyses of the inhibition of ATP-induced shedding of CD62L in hP2X7 co-transfected HEK cells by Nb-Fc fusion proteins of Nbs 1c81 and 3c23. HEK cells were transfected with cDNA constructs for CD62L only, or co-transfected with constructs for CD62L and hP2X7 and harvested 24 h after transfection. (A) Cells were incubated for 60 min at 37°C in DMEM medium containing 5% FCS and 4 mM ATP. (B) In an ATP dose response assay, P2X7 and CD62L co-transfected cells were incubated with 0.25, 1, 2 or 4 mM ATP for 60 min at 37°C. (C) In a blocking assay, aliquots of cells were pre-incubated with 2 µg of Nb-Fc fusion proteins 1c81Fc or 3c23Fc or with a control Nb-Fc (anti-hCD38 1067Fc) for 15 min at room temperature in 100 µl DMEM 5% FCS, prior to a 90-min incubation with 2 mM or 4mM ATP. (Final concentration of Nb-Fc fusion proteins was 0.2 µM). Cells were washed once with 150 µl of medium and stained for 20 min at 4°C to detect cell surface CD62L (MEL-14 PE) and P2X7 (L4 AF647). After a further wash, cells were analyzed by flow cytometry (FACS Calibur, BD).

In HEK cells transfected with CD62L only, incubation with 4 mM ATP did not cause a loss of cell surface levels of CD62L (**Fig. 5.11A**). In contrast, treatment of HEK cells co-transfected with CD62L and hP2X7 with ATP induced shedding of CD62L in a dose-dependent manner (EC-50 1.5 mM; **Fig. 5.11B**). Pre-incubation of the cells with Nb-Fc fusion constructs 1c81Fc or 3c23Fc inhibited subsequent shedding of CD62L in response to high concentrations of ATP. The control Nb-Fc fusion protein 1067Fc (anti-hCD38) did not inhibit shedding (**Fig. 5.11C**).

5.2.4 In a dose-response assay, Nbs 1c81 and 3c23 inhibit shedding of CD62L in transfected HEK cells more efficiently than mAb L4

The mouse mAb L4 has been reported to inhibit P2X7 activation on human monocytes (Buell *et al*, 1998). In order to compare the blocking potencies of monovalent Nbs, bivalent Nb-Fc fusion proteins, and bivalent mAb L4, comparative dose-response assays were performed with transfected HEK cells (**Fig. 5.12**). To this end, HEK cells were co-transfected with GFP, CD62L and hP2X7. Twenty-four hours after transfection, cells were harvested by gentle trypsinization and incubated for 15 min at RT with the indicated amounts of Nb, Nb-Fc fusion protein, or mAb L4. Cells were further incubated for 60 min at 37°C in the absence or presence of 4 mM ATP before staining for cell surface CD62L and analyses by FACS. Gating positive cells permitted delineation and analyses of CD62L co-transfected cells (**Fig. 5.12A**).

The results show complete blockade of CD62L shedding by a saturating dose of Nbs 1c81 and 3c23 and corresponding Nb-Fc, a partial blockade by a saturating dose of Nb 1c113, 1c113Fc and mAb L4 while and no blockade by a control Nb (2145) and Nb-Fc fusion protein (1067Fc) was observed (**Fig. 5.12B**). Titration analyses revealed that the bivalent Nb-Fc fusion proteins have 4 – 50 fold improved molar inhibition potencies over their single domain counterparts. The anti-hP2X7 Nbs could be ordered as 3c23Fc > 3c23 > 1c81Fc > 1c113Fc > 1c81 > 1c113 in order of potency to inhibit CD62L shedding by transfected HEK cells.

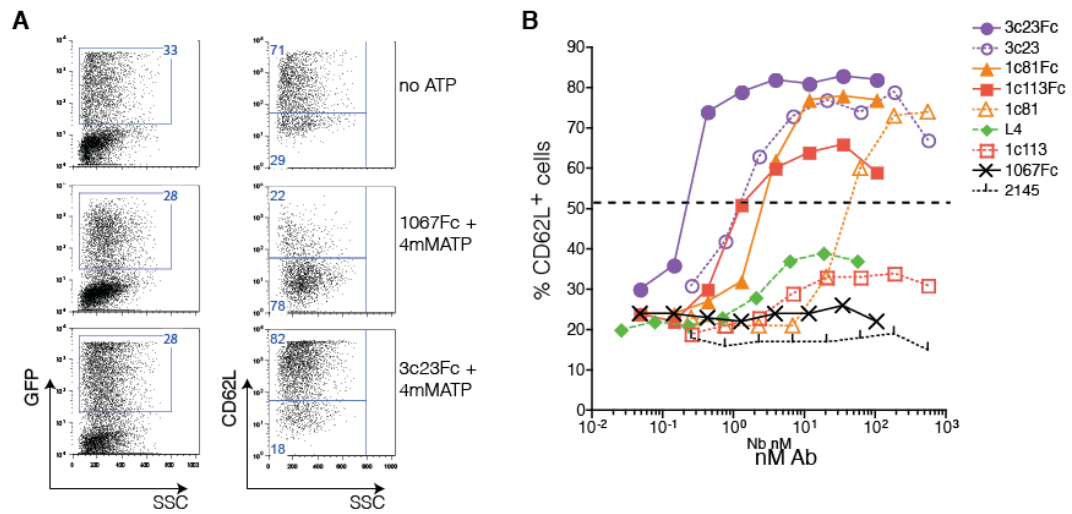


Figure 5.12. Analyses of the inhibition of ATP-induced shedding of CD62L in hP2X7 co-transfected HEK cells by monomeric Nbs, bivalent Nb-Fc and mAb L4. HEK cells were co-transfected with cDNA constructs for GFP, CD62L and hP2X7. Twenty-four hours after transfection, cells were harvested and pre-incubated for 15 min at RT in 80 μ l of DMEM medium with titrated amounts of Nbs, Nb-Fc fusion proteins, or mAb L4 (titrated in eight 1:3 dilution steps from 8.3 μ g/ml to 3.8 ng/ml corresponding to 556 – 0.25 nM for monomers, 105 – 0.05 nM for Nb-Fc and 56 – 0.03 nM for mAb L4) before addition of ATP to a final concentration of 4 mM. Cells were incubated further for 60 min at 37°C and then stained for CD62L (MEL-14 PE) before analysis by flow cytometry (FACS Calibur, BD). (A) Gating on GFP positive cells permitted delineation of transfected cells. (B) Extent of inhibition of ATP-induced shedding of CD62L is represented as percentage of CD62L⁺ cells after gating on GFP⁺ cells. IC₅₀ values were calculated at half-maximal percentage CD62L⁺ cells following treatment with ATP (marked with dotted line (see Table 5.5)).

Table 5.5. Calculated IC₅₀ values of anti-hP2X7 antibodies in the blockade of CD62L shedding in transfected HEK cells. IC₅₀ values were calculated from curves in Figure 5.12 with 52% of CD62L⁺ cells marked as point of half maximal blockade (dotted line). IC₅₀ values could not be estimated for curves with maximal inhibition below threshold.

	3c23Fc	3c23	1c81Fc	1c113Fc	1c81	L4	1c113
IC ₅₀ [nM]	0.3	1.2	2.5	1.5	45	> 56	> 556

5.2.5 Nb-Fc fusion proteins of Nanobodies 3c23 and 1c81 inhibit ATP-mediated externalization of phosphatidylserine by RPMI 8226 myeloma cells

RPMI 8226 is a human B cell myeloma cell line which endogenously expresses P2X7 (Fig. 5.13A). This cell line responds to ATP treatment with the externalization of phosphatidylserine (PS) (Farrell *et al*, 2010). FACS analyses confirmed an ATP-dose dependent externalization of PS by RPMI 8226 cells (EC₅₀ 1.8 mM) (Fig. 5.13B).

To test whether the selected Nbs could block the ATP-mediated PS-externalization by RPMI 8226 cells, the cells were pre-incubated with the mAb L4, anti-hP2X7 Nb-Fc, 1c113Fc, 1c81Fc, 3c23Fc or with a control Nb-Fc, 1067Fc for 15 min at RT and then further incubated for 60 min at 37°C with 4 mM ATP. The extent of P2X7 activation was

assayed by visualization of externalized phosphatidylserine with fluorochrome-labeled Annexin V (**Fig. 5.13C**). The results show complete blockade of ATP-induced PS-externalization by 1c81Fc and 3c23Fc, whereas 1c113Fc and the mAb L4 both only partially prevented PS-externalization. As expected, the control Nb-Fc fusion protein 1067Fc did not prevent ATP-induced externalization of PS.

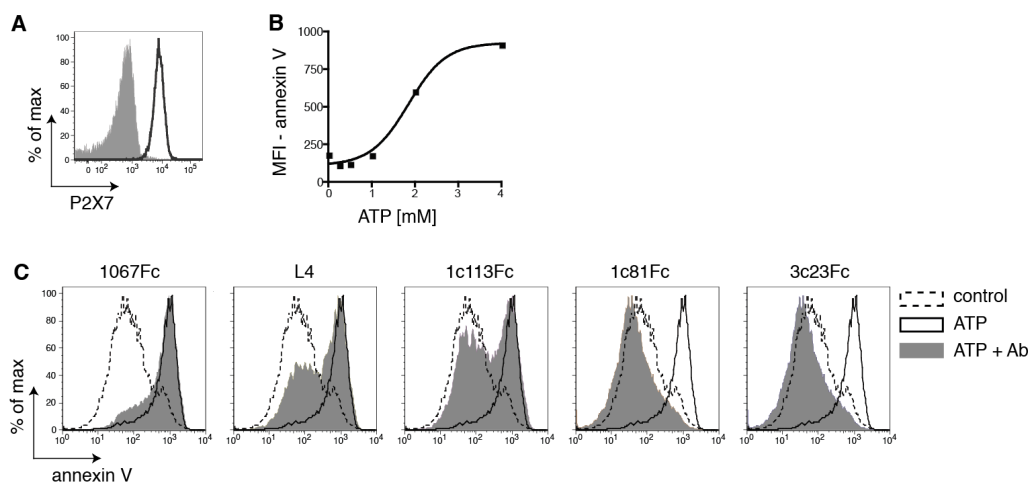


Figure 5.13. Analyses of the inhibition of ATP-mediated externalization of phosphatidylserine by RPMI 8226 cells with anti-hP2X7 Nbs. (A) P2X7 expression on RPMI 8226 cells was detected by staining 2×10^5 cells with a cocktail of AF647-conjugated 1c113Fc and 3c23Fc as in **Figure 5.9**. Grey histograms = cells pre-incubated with excess unconjugated 1c113Fc and 3c23Fc (blocked); open histograms = cells pre-incubated with excess control 1067Fc (unblocked). (B) Cells were incubated for 60 min at 37°C with the indicated concentrations of ATP before staining for externalized phosphatidylserine (PS) with APC-conjugated Annexin V. (C) RPMI 8226 cells were pre-incubated with 0.5 μ g of 1067Fc, 1c113Fc, 1c81Fc, 3c23Fc or mAb L4 for 15 min at room temperature (grey histograms) or without antibodies (solid open histograms), before addition of ATP to a final concentration of 4 mM. Cells were further incubated at 37°C for 60 min and washed once with Annexin V staining buffer prior to staining with APC-conjugated Annexin V. Cells were analyzed by flow cytometry (FACS Canto II, BD). A control sample of cells was incubated at 37°C without exogenous ATP.

5.2.6 Nb-Fc fusion proteins of Nbs 1c81 and 3c23 prevent P2X7-mediated cell death of RPMI 8226 cells

Farrell *et al* demonstrated that prolonged activation of P2X7 on RPMI 8226 cells by ATP results in cell death, as detected by irreversible uptake of propidium iodide (Farrell *et al*, 2010). Having demonstrated that Nb-Fc 1c81Fc and 3c23Fc inhibit P2X7-mediated PS-externalization (**Fig. 5.13**), it was next investigated whether these Nbs would also prevent cell death induced by overnight exposure to ATP. To this end, RPMI 8226 cells were pre-incubated with saturating amounts of the respective antibodies (3 μ g/ml) for 10 minutes prior to treatment with 2 mM ATP for 60 min or 24 h. Cells were subsequently washed and

stained with APC-conjugated Annexin V and propidium iodide to assess externalization of phosphatidylserine and cell death (**Fig. 5.14**).

During the 60-min incubation with 2 mM ATP, mAb L4 and Nb 1c113Fc, both partially prevented exposition of phosphatidylserine as compared to the controls (no Ab or control Nb-Fc, 1067Fc) (**Fig. 5.14**, upper panels; see also **Fig. 5.13**). This partial blockade did not suffice to prevent cell death during an overnight incubation with ATP (**Fig. 5.14**, lower panels). In contrast, Nb-Fc fusion proteins Nbs 1c81 and 3c23 both completely blocked P2X7-mediated exposition of phosphatidylserine and cell death irrespective of the duration of ATP treatment (**Fig. 5.14** upper and lower panels).

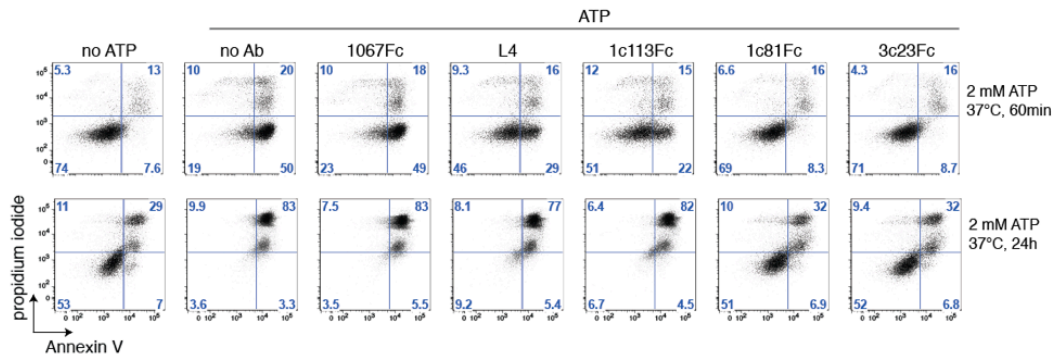
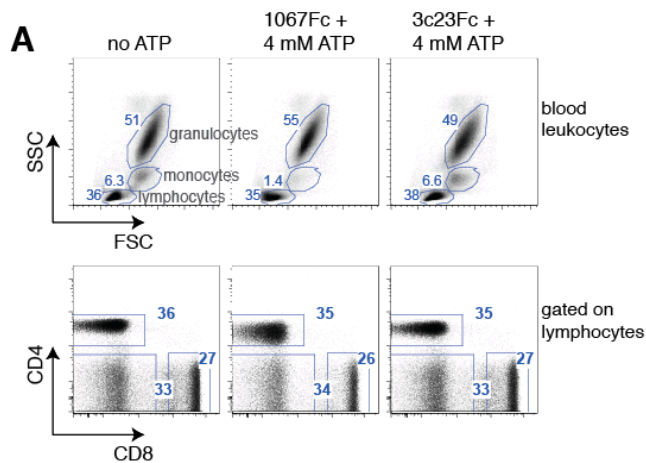


Figure 5.14. Analyses of the inhibition of ATP-mediated cell death by RPMI 8226 cells with anti-hP2X7 Nbs. RPMI 8226 cells (5×10^5 cells in 150 μ l medium) were pre-incubated with 900 ng of respective Nb-Fc fusion proteins or mAb L4 for 10 min at room temperature. 150 μ l ATP of a 4 mM stock solution was added also to final ATP concentration of 2 mM (1:2 dilution) and final antibody concentration of 3 μ g/ml. Cells were incubated at 37°C for 60 min or 24 h. Cells were washed once in Annexin V binding buffer and were then stained for exposition of phosphatidylserine with APC-conjugated Annexin V and cell death with propidium iodide. Data collection was carried out by flow cytometry (FACS Canto II, BD).

5.2.7. Nb-Fc fusion proteins of Nbs 1c81 and 3c23 block ATP-induced externalization of PS and shedding of CD62L by primary human T cells

Having demonstrated that Nbs 1c81 and 3c23 effectively block ATP-induced externalization of PS by RPMI 8226 myeloma cells that endogenously express P2X7, we next investigated whether these Nbs could also block ATP-induced externalization of PS and shedding of CD62L by primary human CD4⁺ T cells and CD8⁺ T cells. The endogenous expression of P2X7 by primary human T cells was previously demonstrated (see **Fig. 5.10**). To this end, aliquots of peripheral blood from the same donors as in **Figure 5.10** were pre-incubated for 30 min at RT with respective Nb-Fc fusion proteins or with mAb L4 prior to treatment with 4 mM ATP for 30 min at 37°C. Subsequently, cells were stained for loss of cell surface CD62L and externalization of PS (detected with Annexin V) as readouts for P2X7 activation (**Figs. 5.15-5.16**).

The results show that CD4⁺ and CD8⁺ T cells from the three donors responded to ATP treatment with shedding of CD62L and externalization of PS, albeit to different degrees (**Figs. 5.15-5.16**). Whereas only a small fraction of CD4⁺ and CD8⁺ cells from donor 1 (16%, 11%) and donor 2 (23%, 33%) responded to ATP, the majority of CD4⁺ and CD8⁺ cells from donor 3 (59%, 63%) responded to P2X7 activation with shedding of CD62L and externalization of PS. In degree of P2X7 sensitivity, the donors thus can be ordered as donor 3 > donor 2 > donor 1. Both mAb L4 and 1c113Fc partially blocked CD62L shedding and exposition of PS. Consistent with previous results, Nb-Fc fusion proteins 1c81Fc and 3c23Fc completely prevented the ATP-induced, P2X7-mediated shedding of CD62L and externalization of phosphatidylserine.



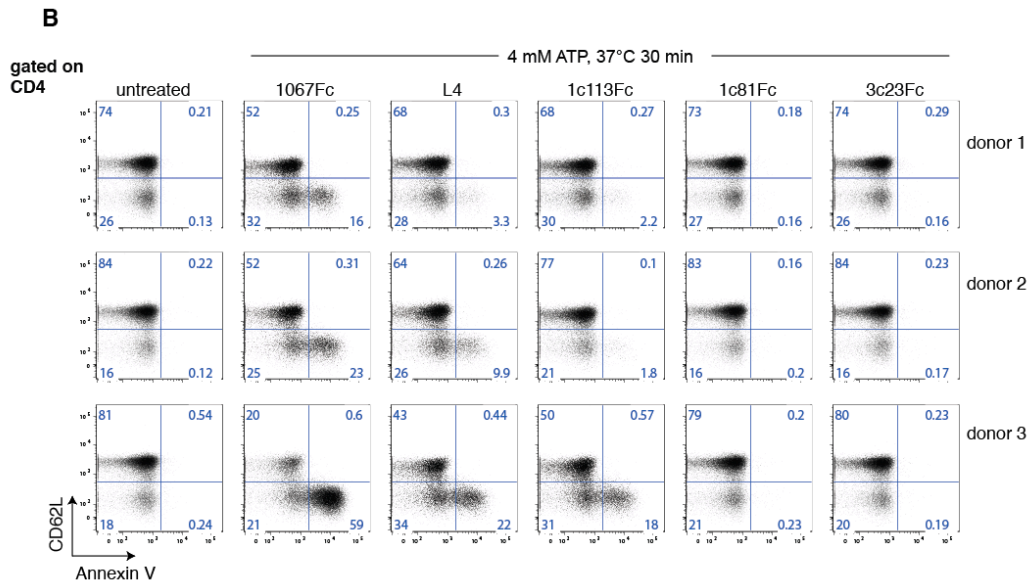


Figure 5.15. FACS analyses of the inhibition of ATP-mediated shedding of CD62L and externalization of phosphatidylserine by primary human CD4⁺ T cells with anti-hP2X7 Nbs. 100 μ l aliquots of full blood from three donors were pre-incubated with 0.5 μ g of 1067Fc, 1c113Fc, 1c81Fc, 3c23Fc or 1 μ g of mAb L4 for 30 min at RT, before addition of 100 μ l RPMI medium (untreated control) of an 8 mM ATP stock solution in RPMI medium. Cells were incubated at 37°C for 30 min, washed once with Annexin V staining buffer, and stained with anti-CD62L FITC (DREG-56), Annexin V-APC, anti-CD4 APC/Cy7 (RPA-T4), and anti-CD8 Pacific Blue (RPA-T8) for 60 min at RT. Erythrocytes were lysed by a 10 min incubation in 2 ml 1x BD Lysis solution. Cells were washed once with 1.5 ml Annexin V staining buffer and analyzed by flow cytometry (FACS CantoII, BD). (A) Lymphocytes were gated sequentially on the basis of low FSC versus SSC and CD4⁺ and CD8⁺ T cells demarcated by subset-specific cell surface markers. PS-flashing (Annexin V) vs. CD62L shedding by CD4⁺ T cells (B) are shown. Blood samples were from the same donors as those analyzed in **Figure 5.10**.

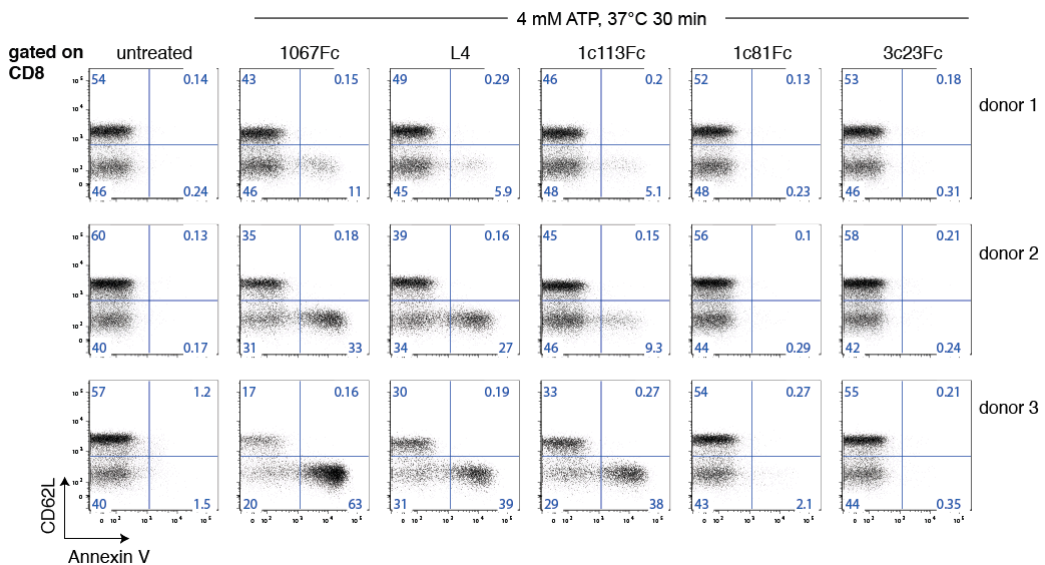


Figure 5.16. FACS analyses of the inhibition of ATP-mediated shedding of CD62L and externalization of phosphatidylserine by primary human CD8⁺ T cells with anti-hP2X7 Nbs. PS-flashing (Annexin V) vs. CD62L shedding by these T cells are shown. Samples are the same as in **Figure 15** above.

5.3 Biochemical and functional characterization of mouse P2X7-specific Nbs

In this section, the detailed characterization of anti-mP2X7 Nbs is presented. Five Nb families were shown to inhibit P2X7-mediated shedding of CD62L by Yac-1 cells and mouse splenocytes. Titration analyses show that Nbs 13A7 and 8G11 were the most potent inhibitors of activation of P2X7 by ATP and by NAD⁺-dependent ADP-ribosylation. Three other Nb families were shown to potentiate the ligand-gated activation of P2X7 by reducing threshold concentrations of NAD⁺ and ATP required for P2X7 activation. Titration analyses revealed Nb 14D5 as the most potent positive modulator of P2X7. *Ex vivo* analyses of cells obtained from spleen and liver of mice that had received a systemic injection of dimeric or half-life extended Nbs (HLE-Nbs) showed that the Nbs effectively targeted and modulated P2X7 activation *in vivo*. Finally, the results of a pilot study investigating the potential therapeutic effect of anti-mP2X7 Nbs in a mouse model of antibody induced glomerulonephritis are presented.

5.3.1 At saturating doses, several mP2X7-specific Nbs inhibit P2X7 mediated shedding of CD62L by Yac-1 lymphoma cells

In order to determine whether the selected anti-mP2X7 Nbs could affect nucleotide-induced activation of P2X7, the mouse T-lymphoma cell line, Yac-1, was utilized (**Fig. 5.17**). P2X7 activation in Yac-1 cells by NAD⁺-dependent ADP-ribosylation or by ATP induces shedding of the endogenously expressed L-selectin (Scheuplein, 2005). The EC₅₀ for NAD⁺-induced shedding of CD62L in Yac-1 cells was approximately 5 μM whereas the EC₅₀ for ATP-induced shedding of CD62L was approximately 100 μM. NAD⁺-induced shedding of CD62L is mediated by ecto-ADP-ribosyltransferase ART2.2 which activates P2X7 by ADP-ribosylation at R125 (Adriouch *et al*, 2008). ATP-induced shedding of CD62L is mediated directly by gating of P2X7 via the soluble ligand ATP and does not require ART2.2. Consistently, pre-incubation of Yac-1 cells with a saturating dose of the ART2.2 blocking Nb s+16a (Koch-Nolte *et al*, 2007) completely prevents NAD⁺ induced shedding of CD62L but does not effect ATP-induced shedding of CD62L (**Fig. 5.17**).

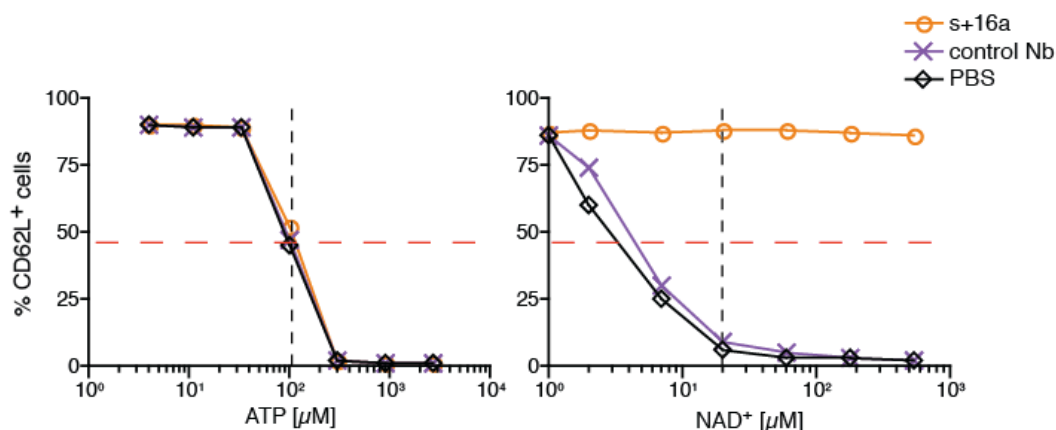


Figure 5.17. Dose responses of NAD⁺ and ATP-induced shedding of CD62L by Yac-1 cells. Yac-1 cells were incubated with 2 μM of either the ART2.2 inhibitor Nb, s+16a (Koch-Nolte *et al.*, 2007) or a control Nb or the absence of Nb in complete RPMI 5% FCS prior to treatment with serially (1:3) titrated ATP (3 – 2700 μM) or NAD⁺ (1 – 540 μM). CD62L shedding was induced by incubation of cells at 37°C for 20 min. Cells were washed once and stained for the detection of surface CD62L (MEL-14 PE). Data collection was carried out by flow cytometry (FACS Calibur, BD). Estimated EC₅₀ of both ATP (100 μM) and NAD⁺ (5 μM) are indicated with horizontal dashed red lines. Dashed vertical lines indicate respective threshold (ATP, 100 μM) 4-fold of threshold (NAD⁺, 20 μM) concentrations of nucleotides used in subsequent experiments with Yac-1 cells. This figure is representative of two experiments with similar results.

In order to assess whether any of the mP2X7-specific Nbs could similarly inhibit nucleotide induced shedding of CD62L, Yac-1 cells were pre-incubated with purified anti-P2X7 or control Nbs followed by treatment with ATP (100 μM) or NAD⁺ (20 μM) for 20 minutes at 37°C before staining with anti-CD62L MEL-14 PE and FACS analyses. The concentrations of nucleotides used in this screening experiment were chosen to lie at the EC₅₀ (ATP) and approximately four fold above the EC₅₀ (NAD⁺) for shedding of CD62L by these cells (see **Fig. 5.17**). The ART2.2-blocking Nb, s+16a was used as a control for blockade of NAD⁺-induced shedding of CD62L (Koch-Nolte *et al.*, 2007). At least one representative member of each family of Nbs was tested (**Fig. 5.18**). Screening was carried out in two experiments (**Fig. 5.18A** and **Figs. 5.18B-C**).

The results show that Nbs 13B5 (19), 7H6 (11), 13G9 (23) (**Fig. 5.18A**), 8F5 (5), 8G11 (5), 8G12 (5) (**Fig. 5.18B**) and 13A7 (22) (**Fig. 5.18C**) inhibit both NAD⁺- and ATP-mediated shedding of CD62L. Partial blockade of CD62L shedding by Nb 8E7 but not other Nbs was confirmed in follow-up experiments (not shown). Nbs 14D5 (17) (**Fig. 5.18A**), 4B4 (4) and 7D6 (8) (**Fig. 5.18C**) appeared to enhance NAD⁺- and ATP-induced shedding of CD62L (Nb families in brackets).

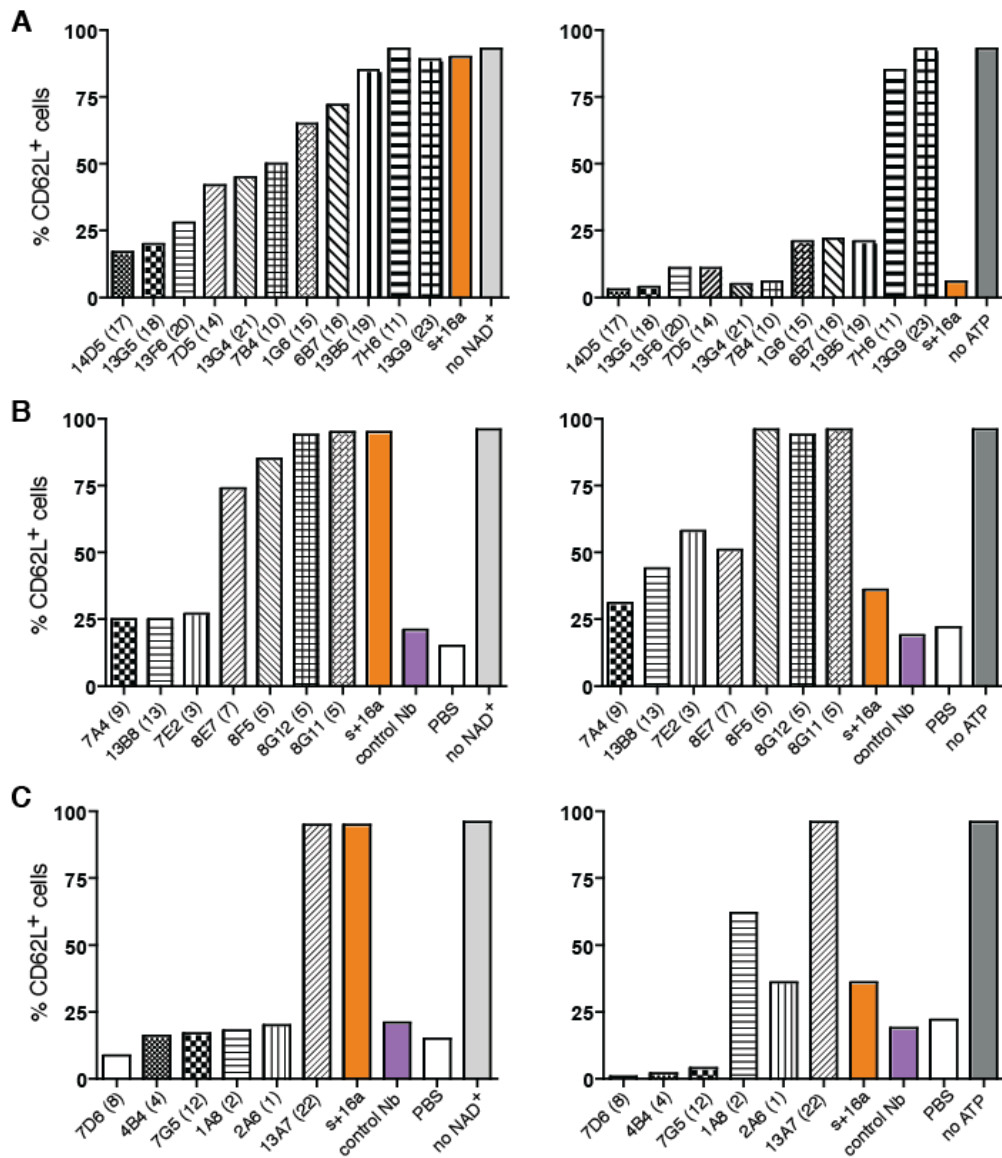


Figure 5.18. FACS assay to determine capacity of anti-mP2X7 Nbs to block or potentiate P2X7-mediated shedding of CD62L in Yac-1 cells. 5 x 10⁵ Yac-1 cells were pre-incubated with 10 μ g (A) or 5 μ g (B and C) of respective Nbs in 135 μ l RPMI medium for 15 min at room temperature before addition of 15 μ l of a 1 mM ATP or 200 μ M NAD⁺ stock solution to final ATP and NAD⁺ concentrations of 100 μ M and 20 μ M respectively. Final Nb concentrations were 4.4 μ M in (A) and 2.2 μ M in both (B) and (C). Cells were incubated at 37°C for 20 min to induce CD62L shedding, washed once with 150 μ l medium and stained for cell surface CD62L (MEL-14 PE). Data collection was carried out by flow cytometry (FACS Calibur, BD). Nb s+16a inhibits NAD⁺- but not ATP-induced P2X7 activation (Koch-Nolte *et al.*, 2007) whereas a control Nb does not affect P2X7 activation. Each corresponding Nb family is indicated in parentheses.

5.3.2 Dose-response analyses reveal a rank order of inhibitory potencies of five families of anti-mP2X7 Nbs

To compare the potency of Nbs to block activation of P2X7, dose-response analyses were carried out with seven Nbs derived from four families selected on the basis of the results presented in Fig. 5.18. For this purpose, Yac-1 cells were pre-incubated with titrated

amounts of Nbs prior to incubation with 20 μM NAD^+ or 100 μM ATP for 20 min at 37°C (Fig. 5.19). Nbs were titrated down from 4.4 μM to 6 nM in 1:3 dilution steps. Dose-response analyses were carried out in two separate experiments (Figs. 5.19A-B).

The results indicate a complete blockade of CD62L shedding at saturating levels of Nbs by anti-mP2X7 Nbs 13A7 (22), 8G11 (5), 8G12 (5), 13G9 (23) and 7H6 (11), but only a partial blockade by saturating amounts of Nbs 8F5 (5) and 13B5 (19). Titration of Nbs revealed blocking potencies in ascending order of 8F5 < 13B5 < 7H6 < 8G12 = 13G9 < 8G11 < 13A7. IC_{50} values were estimated for the Nbs based on the half maximal percentage of CD62L positive cells (red dashed line, Fig. 5.19; Table 5.6). As expected, the ART2-specific Nb, s+16a, blocked the NAD^+ - but not ATP-mediated shedding of CD62L, whereas the control Nb showed no effect (Fig. 5.19A).

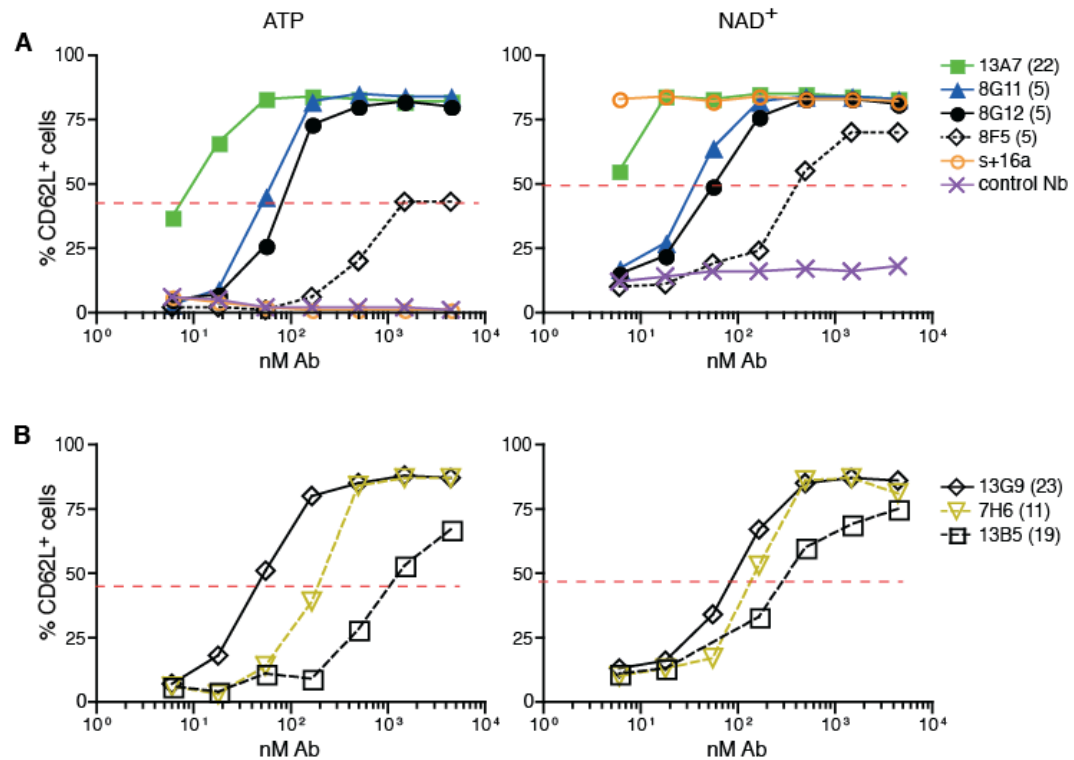


Figure 5.19. Analyses of inhibitory effects of titrated amounts of Nbs on shedding of CD62L induced by ATP and NAD^+ . Nbs were titrated in 20 μl PBS containing 0.2% BSA. 5×10^5 Yac-1 cells in 115 μl RPMI medium containing 5% FCS were added to each Nb aliquot and incubated at room temperature for 15 min. Without washing, 15 μl of a 1 mM ATP or of a 200 μM NAD^+ stock solution was added to final ATP and NAD^+ concentration of 100 μM or 20 μM respectively. Nbs were titrated down from 4.4 μM to 6 nM in 1:3 dilution steps. Cells were incubated at 37°C for 20 min to induce CD62L shedding, washed and stained for cell surface expression of CD62L (MEL-14 PE). Data collection was carried out by flow cytometry (FACS Calibur, BD). (s+16a inhibits NAD^+ - but not ATP-induced P2X7 activation (Koch-Nolte *et al*, 2007); control Nb does not affect P2X7 activation). Nbs were tested in two experiments (A and B). Estimated IC_{50} values (red dashed line) are shown in Table 5.6. This figure is representative of two experiments with similar results.

Table 5.6. Estimated IC₅₀ values of anti-mP2X7 Nbs to inhibit shedding of CD62L by Yac-1 cells. IC₅₀ values were estimated from curves in **Figure 5.19** with half maximal blockade marked at dashed red line. Nanobodies were ranked in decreasing order of potency.

	IC ₅₀ [nM]						
	13A7 (22)	8G11 (5)	13G9 (23)	8G12 (5)	7H6 (11)	13B5 (21)	8F5 (5)
ATP [100 μM]	8	50	50	80	200	1000	1500
NAD ⁺ [20 μM]	< 6	30	80	60	150	300	400

5.3.3 Titrations ATP and NAD⁺ at fixed Nb concentration reveal rank order of inhibitory and enhancing potencies of anti-mP2X7 Nbs

Having confirmed that seven anti-mP2X7 Nbs (from families 5, 12, 20, 22 and 23) inhibit P2X7-mediated shedding of CD62L at above threshold ATP and NAD⁺ concentrations, NAD⁺ and ATP-titration experiments were performed in order to determine whether higher nucleotide concentrations could overcome the inhibitory effects of the Nbs. Moreover, the capacity of the suspected enhancing effects of Nbs 14D5 (17) (**Fig. 5.17A**), 4B4 (4) and 7D6 (8) were likewise investigated. To this end, Yac-1 cells were pre-incubated with saturating doses of the respective Nbs and subsequently incubated with titrated amounts of ATP or NAD⁺ to induce shedding of CD62L (**Fig. 5.20**). Final concentration of Nbs was 2 μM. Analyses were carried out in two experiments (**Figs. 5.20A-B**).

The results show a competitive blockade of P2X7 activation by Nbs 13A7, 8G11, 8G12, 8F5, 13G9, 7H6 and 13B5 only over a limited range of ATP concentrations. P2X7 blockade was reversed by increasing ATP concentration. None of the Nbs was able to block shedding of CD62L at ATP concentrations of 900 μM and above. Nearly complete blockade of shedding of CD62L by Nbs was observed over the whole range of NAD⁺ concentrations used in the assay, whereas Nbs 8F5 and 13B5 only partially inhibited shedding of CD62L at higher NAD⁺ concentrations (**Fig. 5.20**). The order of potency to inhibit shedding of CD62L by increasing concentrations of ATP (13A7 > 8G11 > 8G12 = 13G9 = 7H6 > 8F5 = 13B5) was similar to results in the Nb dose-response analyses (**Fig. 5.19**). The results further confirm the capacity of Nbs 4B4, 7D6 and 14D5 to potentiate shedding of CD62L at sub-threshold levels of ATP (30 μM and less), Nb 14D5 showed a stronger synergistic effect than Nbs 7D6 and 4B4 (approximately five-fold vs two-fold reduction of the EC₅₀ of ATP-induced shedding of CD62L) (**Fig. 5.20B**). A comparatively weaker potentiation of the NAD⁺-induced shedding of CD62L was observed

(approximately two-fold reduction of the EC₅₀ of NAD⁺-induced shedding of CD62L by Nb 14D5 vs. little if any effect by Nbs 4B4 and 7D6).

On the basis of these results, the two strongest P2X7 antagonizing Nbs 13A7 and 8G11 and the strongest potentiating Nb 14D5 were selected for reformatting and further characterization.

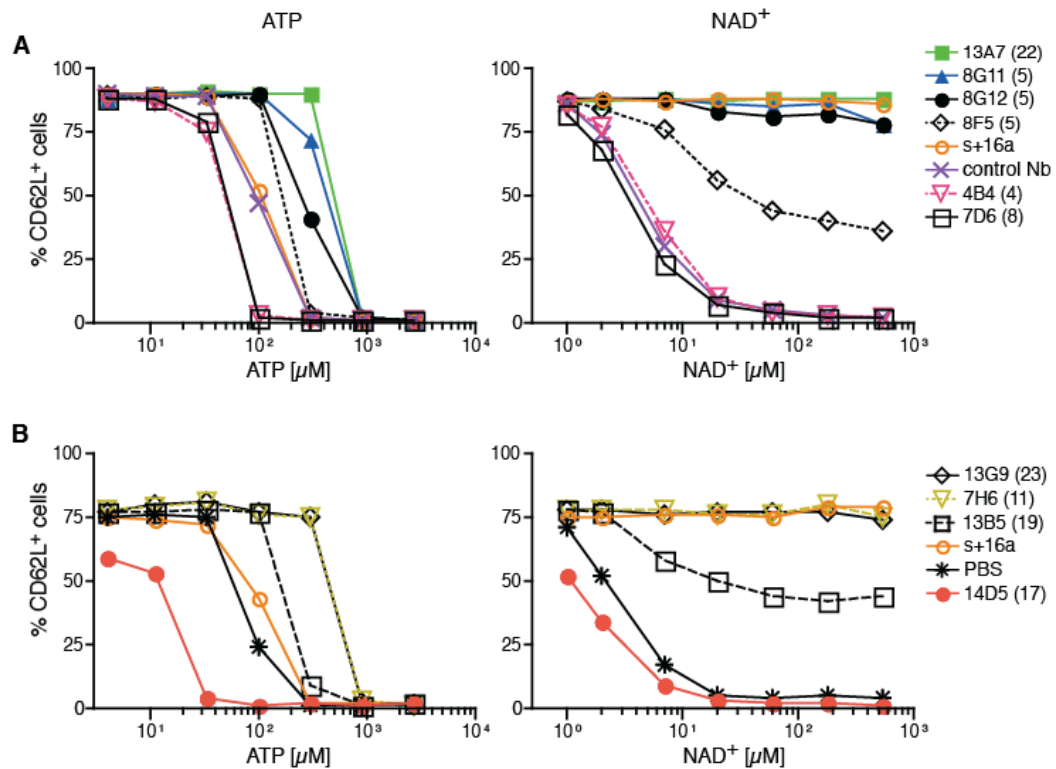


Figure 5.20. Analyses of inhibitory and potentiating effects of a saturating dose of Nbs on shedding of CD62L induced with titrated amounts of ATP and NAD⁺. 5×10^5 Yac-1 cells were incubated with 5 μ g of respective Nbs in 150 μ l complete RPMI medium for 15 min at room temperature. 15 μ l of ATP or NAD⁺ stock solutions titrated at 1:3 dilution series were added and the cells were incubated further for 20 min at 37°C. ATP concentrations ranged from 4 μ M – 2.7 mM whereas NAD⁺ concentrations ranged from 6 – 540 μ M. Final concentrations of Nb was 2 μ M (5 μ g in 165 μ l reaction volume). Cells were subsequently washed and stained for expression of CD62L (MEL-14 PE). Data collection was carried out by flow cytometry (FACS Calibur, BD). (s+16a inhibits NAD⁺- but not ATP-induced P2X7 activation (Koch-Nolte *et al*, 2007); the control Nb does not affect P2X7 activation). Nbs were tested in two experiments (A and B).

5.3.4 Reformatting of Nbs into dimeric molecules increases potency

The experiments shown so far were performed with monovalent Nbs. Considering the homotrimeric structure of the P2X7 ion channel it was hypothesized that an enhanced functional potency of the Nbs could be achieved by increasing the valency - and thereby the avidity - of the Nbs. Two approaches were followed to generate bivalent Nb formats:

(i) genetic fusion of two Nanobodies in a single polypeptide chain via a 35-amino acid linker, and (ii) genetic fusion to the hinge and Fc-domains of mouse IgG1 - thereby allowing formation of a whole antibody-like molecule covalently linked by disulfide bridges in the hinge region.

Homomeric dimers of Nbs 13A7, 8G11, and 14D5 were constructed by Ablynx by PCR amplification with primers encoding a 35GS linker sequence. To determine whether dimers of 13A7 and 8G11 show improved blocking potency, Yac-1 cells were pre-incubated with titrated monomeric or dimeric Nbs prior to treatment with 100 μ M ATP or 20 μ M NAD⁺ to induce shedding of CD62L as in **Fig. 5.18**. Cells were stained for expression of CD62L and analyzed by FACS (**Fig. 5.21**).

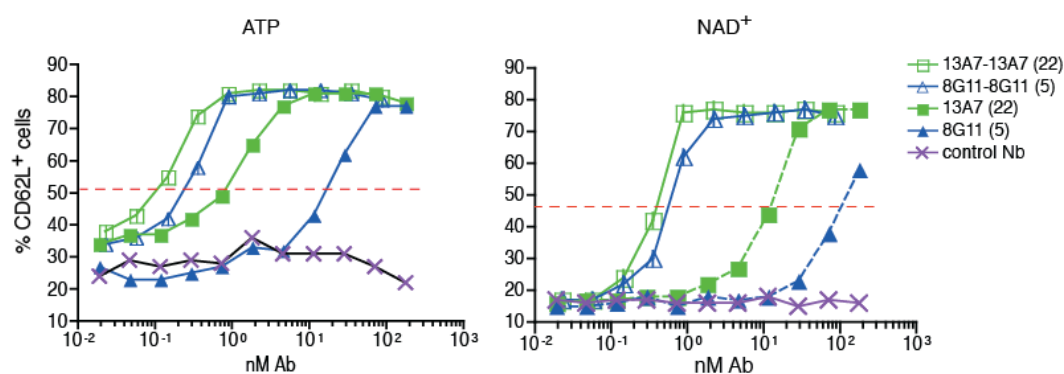


Figure 5.21. Analyses of the inhibitory effects of titrated amounts of monomeric and dimeric Nbs 13A7 and 8G11 on shedding of CD62L induced by 100 μ M ATP or 20 μ M NAD⁺. 5 x 10⁵ Yac-1 cells were pre-incubated with monomeric or dimeric antagonistic Nb molecules titrated down, 11 steps in a 1:2.5 dilution series in 135 μ L complete RPMI medium. Following addition of ATP or NAD⁺ stock solutions to final concentrations of 100 μ M ATP or 20 μ M NAD⁺, cells were incubated for 20 min at 37°C. Final concentrations of monomeric Nbs were titrated from 178 nM to 19 pM whereas dimeric Nbs were titrated from 86 nM to 22 pM for dimers. Cells were subsequently washed and stained for surface expression of CD62L (MEL-14 PE). Data collection was carried out by flow cytometry (FACS Calibur, BD). (The control Nb does not affect P2X7 activation). Red lines were used to estimate IC₅₀ values (**Table 5.6**). This figure is representative of two (ATP) and four (NAD⁺) experiments with similar results.

The results show that reformatting Nb into homodimers resulted in a 6-fold and 80-fold increase in the potency of Nbs 13A7-13A7 and 8G11-8G11 respectively, versus their corresponding monomeric counterparts to inhibit the ATP-induced shedding of CD62L. With regard to the NAD⁺-induced shedding of CD62L, a 20-fold and 120-fold increase in blocking potency vs. the respective monomeric counterparts were observed for Nbs 13A7-13A7 and 8G11-8G1,1 respectively (**Fig. 5.21**). Estimated IC₅₀ values compared well to previously estimated values for monomeric Nbs 13A7 and 8G11 (**Tables 5.6 vs 5.7**

Table 5.7. Estimated IC₅₀ values of anti-mP2X7 monomeric and dimeric Nbs in the blockade of shedding of CD62L by Yac-1 cells. IC₅₀ values were estimated from curves in **Figure 5.21** with half maximal blockade marked at dashed red line

	IC ₅₀ [nM]			
	13A7	13A7-13A7	8G11	8G11-8G11
ATP [100 μM]	0.9	0.15	20	0.25
NAD ⁺ [20 μM]	6.5	0.35	70	0.55

In parallel to screening of dimeric antagonists, P2X7-potentiating Nb 14D5-14D5 was compared with Nb 14D5 for improved synergy of P2X7 activation. To this end, Yac-1 cells were pre-incubated with titrated amounts of monomeric or dimeric Nbs prior to induction of shedding by treatment with sub-threshold levels of ATP (33 μM) or NAD⁺ (1.5 μM) (**Fig. 5.22**).

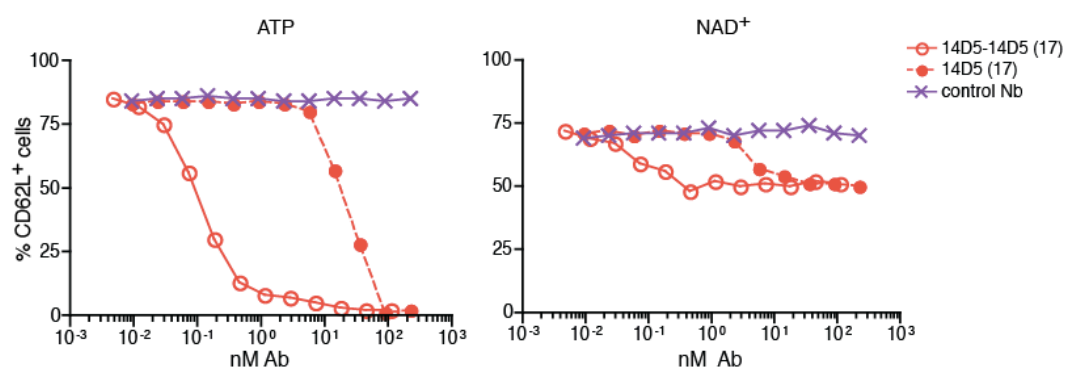


Figure 5.22. Analyses of the potentiating effects of titrated amounts of monomeric and dimeric Nb 14D5 on shedding of CD62L induced by sub-threshold concentrations of ATP and NAD⁺. 5 × 10⁵ Yac-1 cells were pre-incubated with monomeric or dimeric antagonistic Nb 14D5 titrated in 11 steps in a 1:2.5 dilution series (from 222 nM to 6 pM) in 135 μL RPMI medium containing 5% FCS. Following addition of 15 μL ATP or NAD⁺ stock solutions to final concentrations of 33 μM ATP or 1.5 μM NAD⁺, cells were incubated for 20 min at 37°C. Cells were subsequently washed and stained for cell surface expression of CD62L (MEL-14 PE). Data collection was carried out by flow cytometry (FACS Calibur, BD). (The control Nb does not affect P2X7 activation). This figure is representative of two experiments with similar results.

The results confirm that 33 μM ATP does not suffice to induce CD62L shedding by Yac-1 cells in the presence of a control Nb and that 1.5 μM NAD⁺ induces shedding of CD62L only on a small subset of cells. However, incubation of cells in the presence of 14D5 potentiated shedding of CD62L in a dose-dependent manner, thereby reducing the nucleotide threshold required for CD62L shedding (**Fig. 5.22**). Approximately 100-fold lower concentrations of the dimeric 14D5-14D5 Nb than the monomeric 14D5 were required to achieve similar potentiation effects. Note that a maximum percentage of only 55% of cells could be induced to shed CD62L with excess 14D5 monomers and dimers in

the presence of low amounts of exogenous NAD⁺ (1.5 μM in this assay) whereas nearly all cells could be induced to shed CD62L with 14D5 monomers and dimers in the presence of a sub-threshold concentration of ATP (33 μM).

5.3.5 Nb 13A7 and 8G11 block, Nb 14D5 potentiates nucleotide-induced shedding of CD62L by primary Balb/c T cells

Having demonstrated that mP2X7-specific Nbs 13A7 and 8G11 or 14D5 respectively blocked or potentiated shedding of CD62L by mouse Yac-1 lymphoma cells, it was investigated whether the same would hold true for primary T cells. Naive T cells of Balb/c mice have been shown to shed CD62L in response to activation of P2X7 by exogenously added ATP and NAD⁺ (Scheuplein *et al.*, 2009). Moreover, the majority of Foxp3⁺ regulatory T cells from B6 mice shed CD62L in response to low concentrations of NAD⁺ released during cell preparation (Hubert *et al.* 2011). NAD⁺ released during cell preparation serves as a substrate for ART2 even when cells are prepared or kept at 4°C, while gating of ADP-ribosylated P2X7 and subsequent shedding of CD62L require incubation of cells for several minutes at 37°C.

In order to visualize potential functional effects of mP2X7-specific Nbs on CD62L shedding by primary T cells, splenocytes from a wildtype BALB/c mouse were prepared and pre-incubated at 4°C with a saturating dose of monovalent Nbs (2 μg/sample, 0.9 μM final concentration) for 15 min and subsequently incubated further in the presence of moderate concentrations of exogenously added ATP (200 μM) or NAD⁺ (50 μM) for 30 min at 37°C. T cells were then stained with anti-CD3 and anti-CD62L and analyzed by FACS (**Fig. 5.23**).

The results confirm that treatment of splenocytes with ATP or NAD⁺ induces shedding of CD62L by the majority of CD3⁺ T cells but not by CD3⁻ cells (**Fig. 5.23**). Nbs 8G11 and 13A7 completely blocked both, ATP- and NAD⁺-induced shedding of CD62L by T cells. In the presence of Nb 14D5, on the other hand, a substantially larger fraction of T cells showed loss of cell surface CD62L (> 95% of cells in case of 200 μM ATP and approximately 80% of cells in case of 50 μM NAD⁺). As expected, the ART2-specific control Nb s+16a selectively inhibited NAD⁺-mediated but not ATP-mediated shedding of

CD62L. Thus, Nbs 13A7, 8G11 and 14D5 evidently can target and modulate function of P2X7 not only in lymphoma cell lines but also in primary lymphocytes.

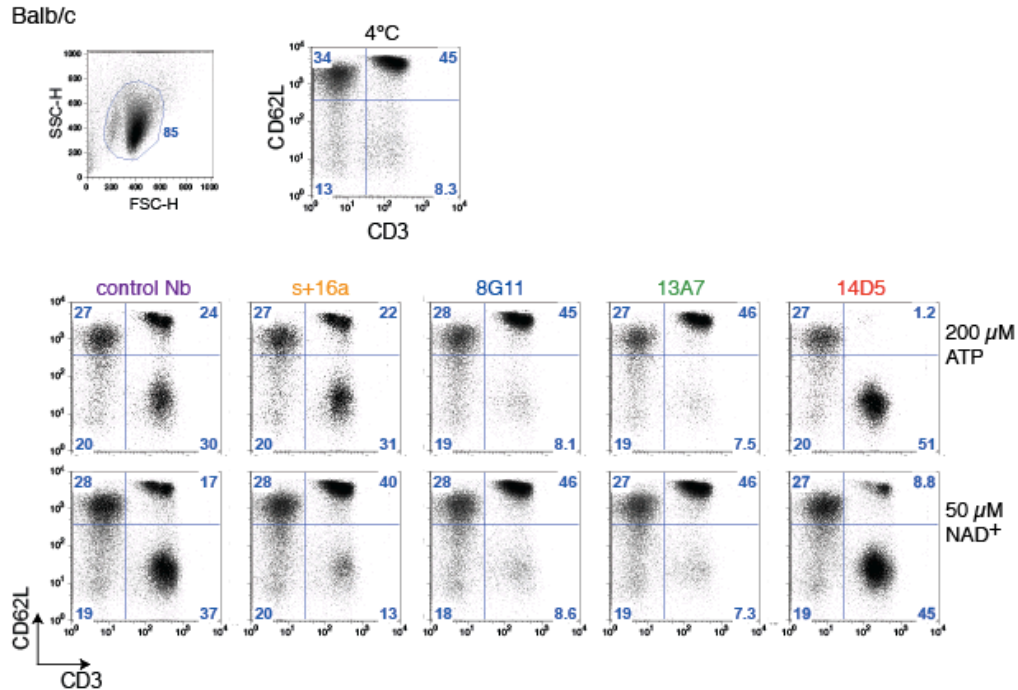


Figure 5.23. FACS analyses of functional effects of monovalent Nbs on ATP and NAD⁺ induced shedding of CD62L by primary Balb/c T cells. 10⁶ wildtype Balb/c splenocytes were pre-incubated with 2 μg Nbs in 75 μl of RPMI medium containing 5% FCS for 15 min at 4°C. 75 μl of ATP or NAD⁺ stock solutions were added to final ATP and NAD⁺ concentrations of 200 μM and 50 μM respectively (Final Nb concentration was 0.9 μM). Following further incubation at 37°C for 30 min, cells were washed and stained with anti-CD3e (145-2C11 APC) and anti-CD62L (MEL-14 PE) and analyzed by flow cytometry (FACS Calibur, BD). Control incubations were performed with a control Nb which does not affect P2X7 activation or with the ART2-blocking Nb, s+16a (Koch-Nolte *et al*, 2007).

5.3.6 Intraperitoneal injection of Nb 13A7-13A7 blocks P2X7 activation *ex vivo* in B6 mice

Results from **section 5.3.5** demonstrated that Nbs 8G11 and 13A7 inhibit P2X7-mediated shedding of CD62L by primary T cells *in vitro*. To investigate whether systemically injected Nbs would target and inhibit P2X7 *in vivo*, a pilot experiment was performed with the potent homodimeric Nb 13A7-13A7 (see **Fig. 5.21**). Female wildtype B6 mice were injected intraperitoneally with 50 μg of Nb 13A7-13A7 or PBS. Two and twenty-four hours post injection, mice were sacrificed and lymphocytes isolated from spleen and liver. Successful *in vivo* targeting of P2X7 by Nbs was verified by detection of the myc epitope tag of cell bound Nbs with fluorochrome-conjugated anti-myc mAb (**Fig. 5.24B**). Liver T cells (CD3⁺ NK1.1⁻), NK (CD3⁻ NK1.1⁺) and iNKT cells (CD3⁺ NK1.1^{int}) were

distinguished by respective cell surface markers (**Fig. 5.24A**). Splenocytic CD4⁺ T cells were delineated by anti-CD4 staining and the regulatory CD4⁺ T cell (Treg) subset (which are sensitive even to lower concentrations of nucleotides (Hubert *et al*, 2010)) were demarcated by counterstaining for CD25 (**Fig. 5.25**). Similar to shedding of CD62L, T cells and iNKT cells shed CD27 upon P2X7 activation (Moon *et al*, 2006). In order to examine effects of the injected dimeric Nb 13A7-13A7 on shedding of CD27 induced by endogenous NAD⁺ released during cell preparation (Scheuplein *et al*. 2009) cells were incubated at 4°C or at 37°C for 15 min in the absence of exogenously added NAD or ATP before FACS analysis (**Fig. 5.24**). Parallel aliquots of cells were incubated with exogenously added ATP (250 μM) or NAD⁺ (30 μM) (**Figs. 5.24C and 5.25B**).

Two hours after Nb injection, cell bound Nb 13A7-13A7 was detectable in liver lymphocytes targeting predominantly iNKT cells and a small subset of T cell but not NK cells (**Fig 5.24B**). Twenty-four hours after Nb injection, however, only a weak staining of liver lymphocytes was detected. Merely incubating cells at 37°C induced shedding of CD27 in the majority of NK1.1^{int} iNKT cells and CD25⁺ Tregs and in a small subset of T cells (**Figs. 5.24C and 5.25B**). This is a result of NAD⁺ released during cell preparation which serves as a substrate for ART2. ART2 ADP-ribosylates P2X7 even when cells are kept at 4°C, whereas gating of ADP-ribosylated P2X7 and subsequent shedding of CD27 ensues upon incubation at 37°C. Incubation of splenocytes with exogenous NAD⁺ and ATP aggravated shedding of CD27 in T cells (**Fig. 5.25B**). Systemically injected Nb 13A7-13A7, completely blocked shedding of CD27 mediated by endogenous and exogenous NAD⁺ and partially inhibited CD27 shedding mediated by exogenous ATP. Antagonism of P2X7 by Nbs was effective within two hours after injection of Nbs but reversed twenty-four after Nb injection (**Fig. 5.25B**). Thus systemically injected anti-mP2X7 Nb 13A7-13A7 specifically targets and blocks P2X7 *in vivo* but is also rapid excreted.

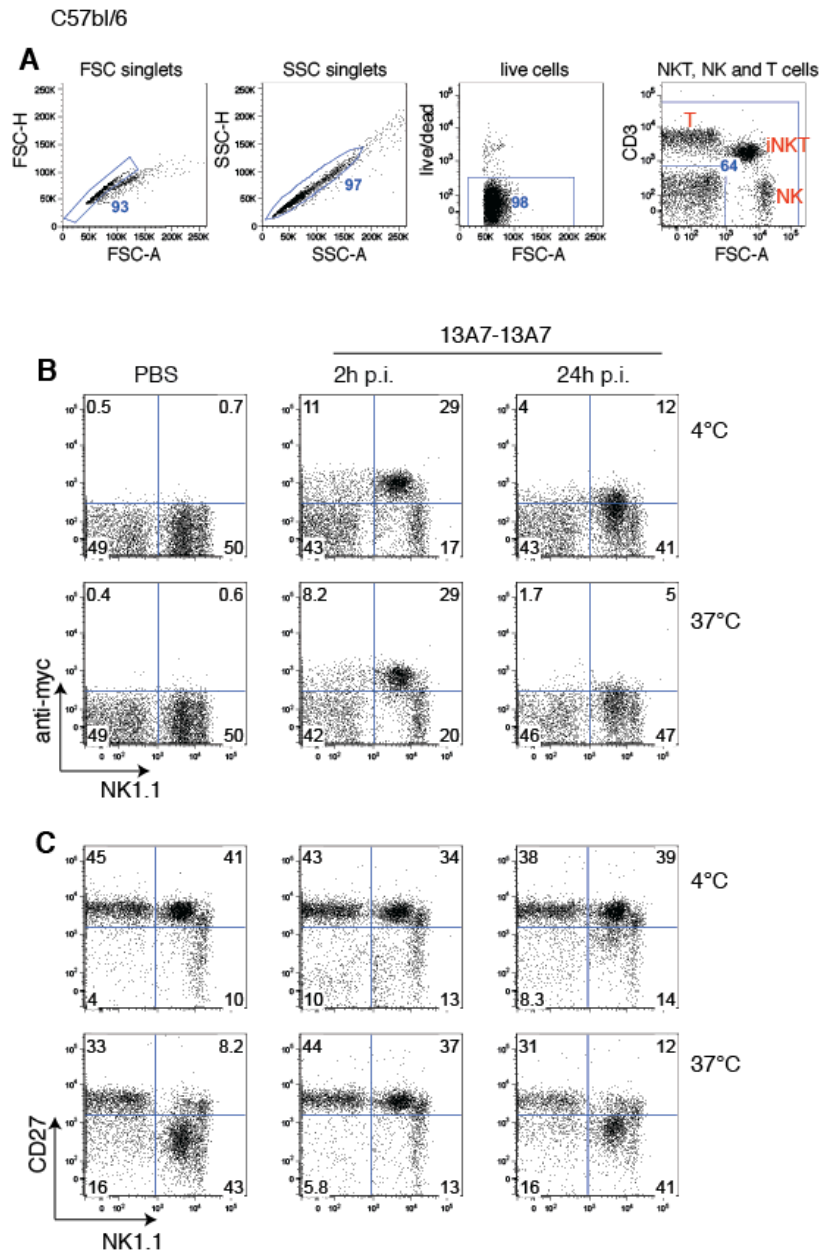


Figure 5.24. Ex vivo analyses of targeting and blockade of P2X7 in liver lymphocytes by intraperitoneally injected Nb 13A7-13A7. Eight weeks old female wildtype B6 mice were injected intraperitoneally with 50 μ g of Nb 13A7-13A7 or with PBS. Two and twenty-four hours post injection, mice were sacrificed and liver leukocytes prepared by Percoll gradient centrifugation. 10^5 liver leukocytes were incubated at 37°C for 15 min in complete RPMI without exogenous nucleotides to induce shedding of CD27. Cells were washed and stained with a mastermix of antibodies including CD27 PE (LG3A10), anti-myc APC (9B11) and CD3e V450 (eBio500A2), NK1.1 PE-Cy7 (PK136) and an amine reactive live/dead stain (BD). Cells were washed and data collection carried out by flow cytometry (FACS CantoII, BD). (A) Dead cells were excluded by live/dead staining, lymphocytes gated by FSC vs SSC properties and T, NK and iNKT cells delineated by surface expression of CD3 and NK1.1 molecules. (B) P2X7 expression on T (NK1.1⁻) iNKT (Nk1.1^{int}) and NK (NK1.1⁺) cells was visualized by anti-myc detection of cell-bound Nbs. (C) Shedding of CD27 was used as readout for the activation of P2X7 by endogenously released nucleotides.

C57b/6

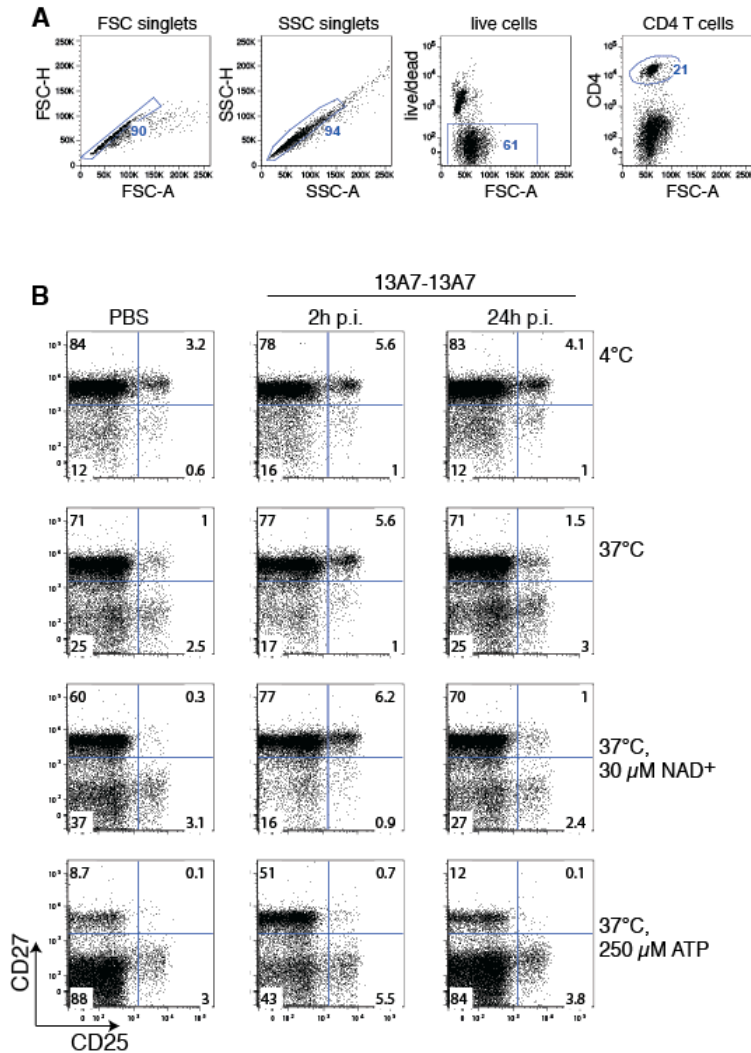


Figure 5.25. Ex vivo analyses of blockade of P2X7-mediated shedding of CD27 in splenocytes by Nb 13A7-13A7 following intraperitoneal injection. Eight weeks old female wildtype B6 mice were injected intraperitoneally with 50 μg of Nb 13A7-13A7 or with PBS. Two and twenty-four hours post injection, mice were sacrificed and splenocytes prepared. 10⁶ splenocytes were incubated with 30 μM NAD⁺ or 250 μM ATP in complete RPMI medium or with medium without exogenous nucleotides (37°). Cells were incubated at 37°C for 15 min, washed and stained with a mastermix of antibodies including CD27 PE (LG3A10), CD25 APC (PC61.5) and CD4 V450 (L3T4), and an amine reactive live/dead stain (BD). Cells were washed and data collection carried out by flow cytometry (FACS CantoII, BD). (A) Dead cells were excluded by live/dead staining, lymphocytes gated by FSC vs SSC properties and CD4⁺ T cells were delineated by surface expression of subset-specific molecules. (B) Shedding of CD27 in CD4⁺CD25⁺ Tregs and CD4⁺CD25⁻ T helper cells was used as readout of P2X7 activation.

5.3.7 Genetic fusion of dimers of Nbs 13A7 and 14D5 to albumin-specific Nb, ALB8, does not reduce the capacity of these Nbs to block or potentiate P2X7

To improve the *in vivo* half-life of P2X7-blocking Nbs, anti-mP2X7 dimeric Nbs 13A7-13A7, 8G11-8G11 and 14D5-14D5 were derivatized by C-terminal genetic linkage to ALB8, a Nb generated by Ablynx which binds to albumin leading to extension of systemic half-life by co-recycling with serum albumin (Tijink *et al*, 2008). To exclude loss of potency resulting from derivatization, the half-life extended Nbs (HLE-Nbs), 13A7-13A7-ALB, 8G11-8G11-ALB were evaluated *in vitro* in the presence of serum albumin. To this end, HLE-Nbs were serially diluted in RPMI medium supplemented with 20% B6 mouse serum as source of albumin. Yac-1 cells were pre-incubated with titrated Nbs prior to induction of CD62L shedding by treatment with 100 μ M ATP or 20 μ M NAD⁺.

The results indicate comparable blocking potencies for homodimeric Nbs and corresponding HLE-Nbs (Fig. 5.26). Similar to observation with homodimeric Nbs, HLE-Nb 13A7-13A7-ALB was also more potent than 8G11-8G11-ALB (see Fig. 5.21). A control HLE-Nb, Dum-ALB-Dum, had no effect on P2X7-mediated shedding of CD62L.

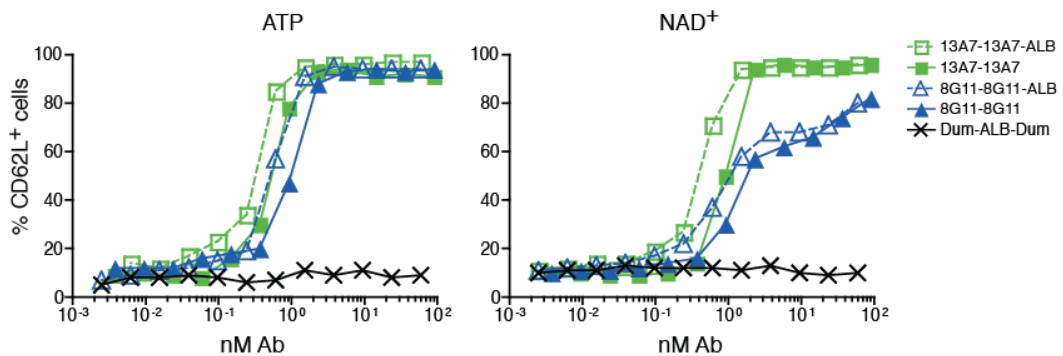


Figure 5.26. Analyses of the inhibitory effects of titrated amounts of homodimeric and half-life extended Nbs (HLE-Nbs) of anti-mP2X7 Nbs 13A7 and 8G11 on shedding of CD62L induced by 100 μ M ATP or 20 μ M NAD⁺ *in vitro*, in Yac-1 cells. 5 x 10⁵ Yac-1 cells were pre-incubated for 15 min at room temperature, with homodimeric or HLE-Nb antagonistic Nb molecules titrated down, 12 steps in a 1:2.5 dilution series in 135 μ L complete RPMI medium supplemented with 20% B6 mouse serum. (Homodimeric Nbs were titrated from 89 nM – 4 pM whereas ALB-derivatized HLE-Nbs were titrated from 59 nM – 2 pM). Following addition of ATP or NAD⁺ stock solutions to final concentrations of 100 μ M ATP or 20 μ M NAD⁺, cells were incubated for 20 min at 37°C. Cells were subsequently washed and stained for surface expression of CD62L (MEL-14 PE). Data collection was carried out by flow cytometry (FACS Calibur, BD). (The control HLE-Nb, Dum-ALB-Dum does not affect P2X7 activation).

5.3.8 Intravenous injections of ALB8-linked dimeric Nbs 13A7 and 8G11 block activation of P2X7 *ex vivo* 2 h post injection

In vitro analyses of blockade P2X7-mediated CD62L shedding by Yac-1 cells with HLE-Nbs indicated no loss in blocking potency as compared to bivalent counterparts in RPMI medium supplemented with mouse serum (Fig. 5.26). Subsequently, the short term *in vivo* blockade of P2X7 activation following systemic delivery of the HLE-Nbs 8G11-8G11-ALB (200 µg) and 13A7-13A7-ALB (200, 60 or 15 µg) was evaluated. Female wildtype B6 mice were injected intravenously with respective HLE-Nbs and sacrificed two hours after injection. Splenocytes were prepared and cell-bound Nbs detected by anti-myc staining (Fig. 5.27). P2X7 activation was induced by incubation of cells at 37°C with or without exogenous NAD⁺ (25 µM) or ATP (250 µM) using shedding of CD27 and the externalization of phosphatidylserine (visualized by Annexin V staining) in splenocytes as readouts (Fig. 5.28). CD4⁺ splenocytes were defined by expression of subset-specific molecules after demarcation according to FSC versus SSC properties. The Treg subset was further delineated by counterstaining for CD25 (Fig. 5.27A).

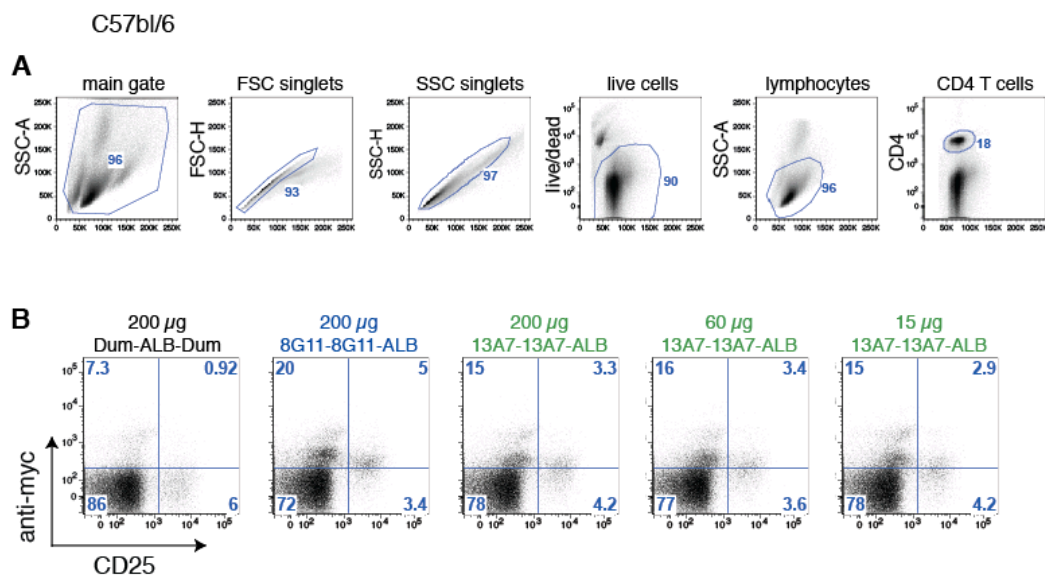


Figure 5.27. Detection of cell-bound HLE-Nbs in splenocytes 2 h post intravenous injection. Eight weeks old female wildtype B6 mice were injected intravenously with indicated doses of HLE-Nbs. Two hours post injection, mice were sacrificed and splenocytes prepared. 10^6 splenocytes were stained with a mastermix of antibodies including anti-myc FITC (9B11), CD4 V450 (L3T4) CD25 APC (PC61.5). Dead cells were excluded by an amine reactive live/dead stain (BD). Cells were washed and data collection carried out by flow cytometry (FACS CantoII, BD). (A) Dead cells were excluded by live/dead staining, lymphocytes gated by FSC vs SSC properties and CD4 T cells in spleen by surface expression of subset-specific molecules. (B) P2X7 expression was visualized by anti-myc detection of cell-bound Nbs.

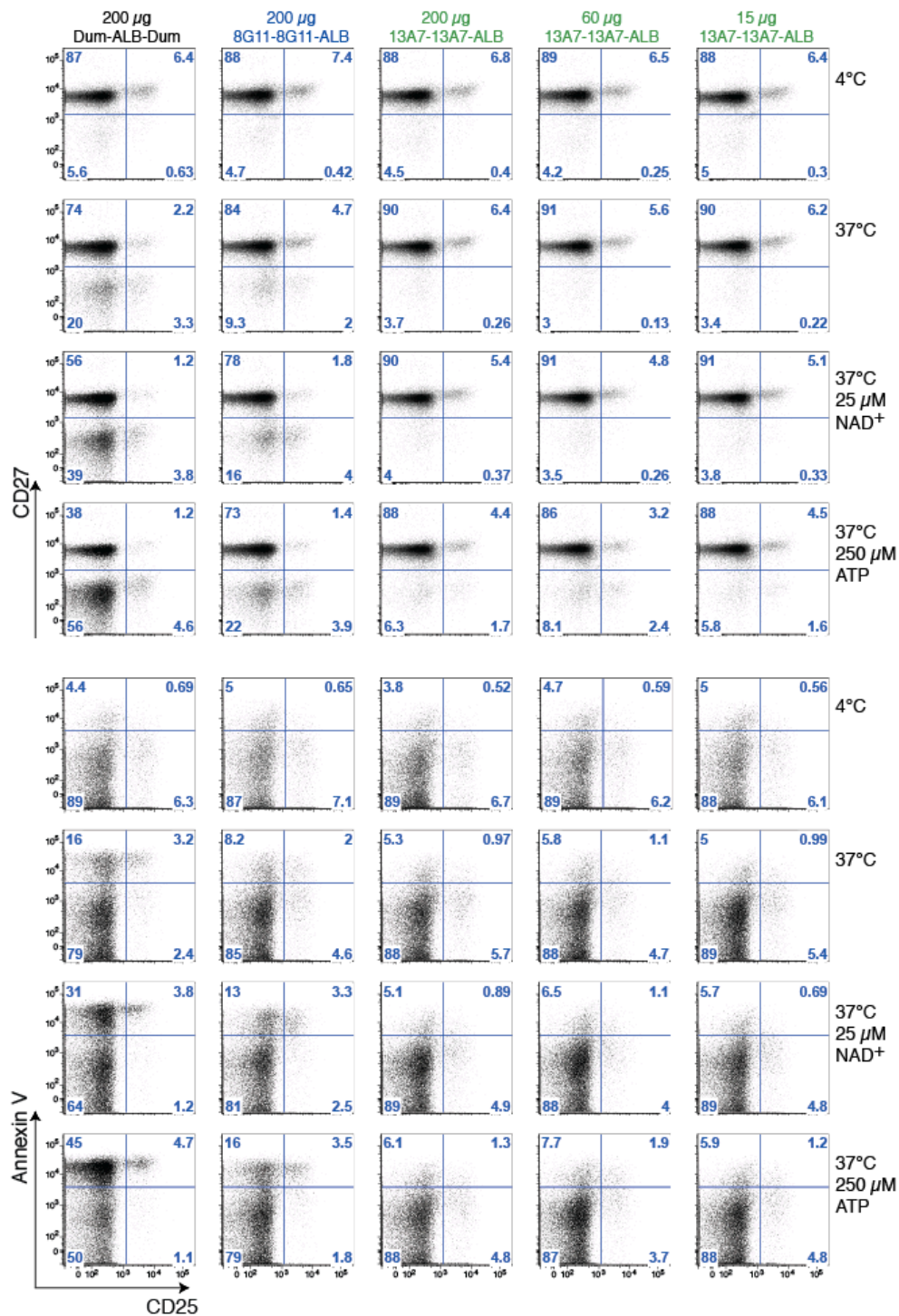


Figure 5.28. FACS analyses of blockade of P2X7-mediated shedding of CD27 and exposition of PS in splenocytes *in vivo*, following intravenous injection of HLE-Nbs. Eight weeks old female wildtype B6 mice were injected intravenously with indicated amounts of HLE-Nbs. Two hours post injection, mice were sacrificed and splenocytes prepared. 10^6 splenocytes were incubated with $30 \mu\text{M}$ NAD^+ or $250 \mu\text{M}$ ATP in complete RPMI medium or with medium without exogenous nucleotides (37°C). Cells were incubated at 37°C for 15 min, washed and stained with a mastermix of antibodies including Annexin V (FITC), CD27 PE (LG3A10), CD25 APC (PC61.5) and CD4 V450 (L3T4), and an amine reactive live/dead stain (BD). Cells were washed and data collection carried out by flow cytometry (FACS CantoII, BD). Analyses of CD27 shedding and PS-flashing as read-outs for P2X7 activation are shown. **Gated on CD4⁺ T cells.**

Detection of the c-terminal myc epitope tag showed targeting of HLE-Nbs to CD4⁺ CD25⁺ Tregs and a small subset of CD4⁺ CD25⁻ T helper cells in the spleen (**Fig. 5.27B**). HLE-Nb 8G11-8G11-ALB generally demonstrated higher staining signal intensities than HLE-Nb 13A7-13A7-ALB. Similar staining intensities was observed for all doses of 13A7-13A7-ALB injected. P2X7-mediated shedding of CD27 was induced by incubation of cells at 37°C for 15 min with or without exogenous NAD⁺ (30 μM) or ATP (250 μM) (**Figs. 5.28**)

P2X7 activation in CD4⁺ splenocytes by ADP-ribosylation via endogenously released NAD⁺ (37°C sample) induced shedding of CD27 and externalization of phosphatidylserine (PS-flashing) by the Treg subset and by a small population of T helper cells probably corresponding to the P2X7^{high} sub-population of T helper cells (**Fig. 5.28** and **Fig. 5.27B**). Shedding of CD27 and PS-flashing by the CD4⁺ splenocytes was further exacerbated by incubation with exogenous NAD⁺ and ATP. Intravenously injected HLE-Nb 8G11-8G11-ALB partially prevented nucleotide-mediated shedding of CD27 and PS-flashing by splenocytes whereas the HLE-Nb, 13A7-13A7-ALB, completely prevented both CD27 shedding and PS-flashing by splenocytes without dose-effect (**Fig. 5.28**).

The above results indicate that systemically injected HLE-Nbs effectively target P2X7 *in vivo* and block the *ex vivo* activation thereof two hours after injection. HLE-Nb 13A7-13A7-ALB showed more effective blockade of P2X7 than HLE-Nb 8G11-8G11-ALB confirming results from *in vitro* studies. Finally, no dose-effect was observed for HLE-Nb 13A7-13A7-ALB. Consequently, further *in vivo* blockade experiments were carried out with only HLE-Nb 13A7-13A7-ALB using a dose of 20 μg per mouse.

5.3.9 Intravenous injection of 13A7-13A7-ALB blocks P2X7 activation whereas 14D5-14D5-ALB results in loss of CD4⁺ CD25⁺ Tregs *in vivo*

The goal of investigating the *in vivo* efficacy of the HLE-Nbs is to apply the Nbs as therapeutics as well as tools to elucidate role of P2X7 in inflammation-based disease models such as experimental glomerulonephritis (EAG). Having demonstrated the efficacy of anti-mP2X7 HLE-Nbs to target and block P2X7 *in vivo* two hours after injection it was investigated whether a single dose of the antagonistic HLE-Nb 13A7-13A7-ALB or the synergistic HLE-Nb 14D5-14D5-ALB would suffice to block or potentiate P2X7 activation, respectively, *in vivo* over a longer term (i.e., 24 h after injection). Previous short

term analyses suggested that 20 μg of Nb 13A7-13A7-ALB was sufficient to antagonize P2X7 *in vivo* two hours after intravenous injection. Therefore, three female wildtype B6 mice per group were injected with 20 μg of HLE-Nb 13A7-13A7-ALB or 100 μg HLE-Nb 14D5-14D5-ALB. One mouse for each time point was also injected with 100 μg of the control HLE-Nb, Dum-ALB-Dum. Mice were sacrificed two and twenty-four hours after injection and splenocytes prepared. CD4⁺ splenocytes were delineated by expression of subset-specific molecules following gating based on FSC versus SSC properties. The Treg subset of the CD4⁺ T cells was defined by counterstaining for CD25 (Fig. 5.29A-B). Activation of P2X7 was induced by incubation of cells at 37°C in the absence or presence of exogenous NAD⁺ (25 μM) or ATP (250 μM) using shedding of CD27 as readouts.

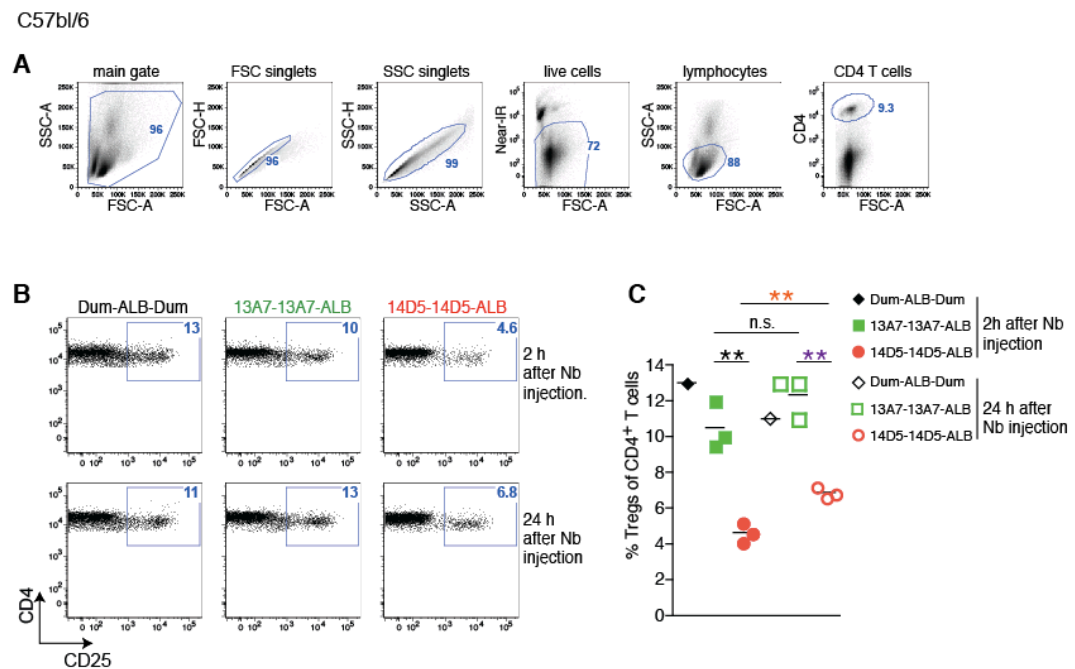


Figure 5.29. Analysis of Treg frequencies 2 h and 24 h after intravenous injection of HLE-Nbs 13A7-13A7-ALB and 14D5-14D5-ALB. Three 8-week old female wildtype B6 mice per group were injected intravenously with either 20 μg of 13A7-13A7-ALB, 100 μg of 14D5-14D5-ALB or 100 μg of a control HLE-Nb Dum-ALB-Dum. Two and twenty-four hours post injection, mice were sacrificed and splenocytes prepared. 10^6 splenocytes were stained with a mastermix of antibodies including CD25 APC (PC61.5) and CD4 V450 (L3T4), and an amine reactive live/dead stain (BD). Cells were washed and data collection carried out by flow cytometry (FACS CantoII, BD). (A) Lymphocytes were delineated based on FSC vs SSC properties and CD4⁺ T cells gated on based on expression of subset markers. (B) Representative FACS plots (one of three) showing frequencies of CD4⁺ CD25⁺ Tregs as percentage of CD4⁺ T cells. (C) Statistical analyses of Treg frequencies in HLE-Nb-injected mice using GraphPad Prism. Statistical significance was calculated using a two-tailed student t-test (** $p < 0.01$; ns = not significant). (p.i. = after injection).

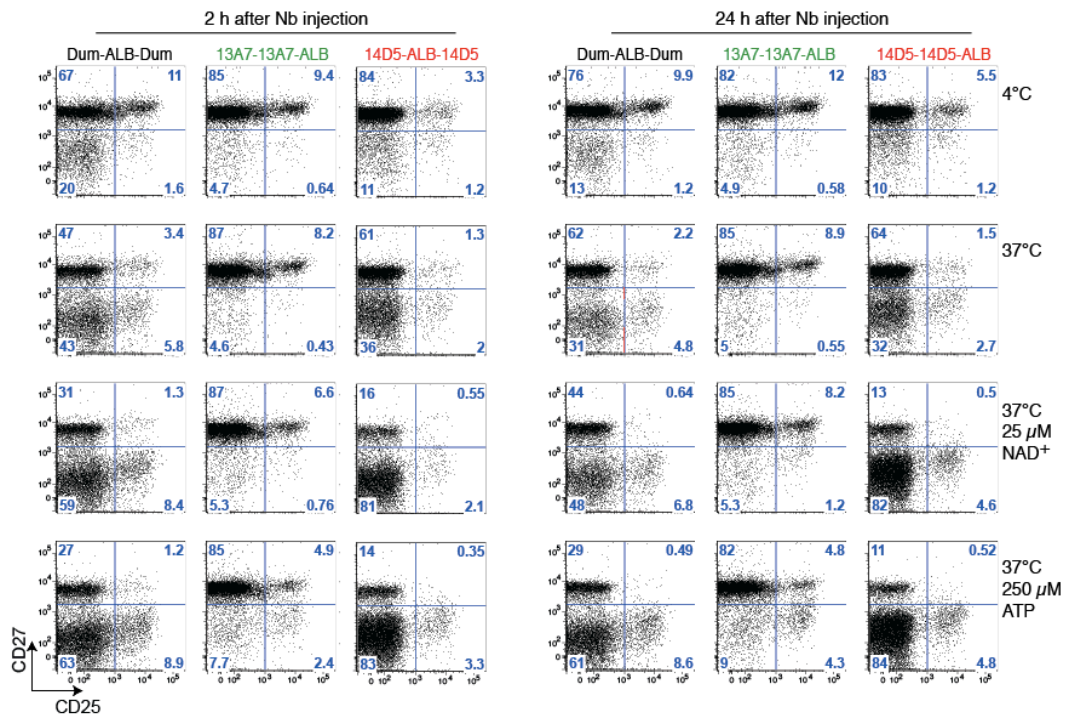


Figure 5.30. FACS analyses of blockade or potentiation of P2X7-mediated shedding of CD27 by splenocytes after intravenous injection of HLE-Nbs. Three 8-week old female wildtype B6 mice per group were injected intravenously with either 20 μg of 13A7-13A7-ALB, 100 μg of 14D5-14D5-ALB or 100 μg of a control HLE-Nb Dum-ALB-Dum. Two and twenty-four hours post injection, mice were sacrificed and splenocytes prepared. 10^6 splenocytes were incubated with 30 μM NAD^+ or 250 μM ATP in complete RPMI medium or with medium without exogenous nucleotides (37°). Cells were incubated at 37°C for 15 min, washed and stained with a mastermix of antibodies including CD27 PE (LG3A10), CD25 APC (PC61.5) and CD4 V450 (L3T4), and an amine reactive live/dead stain (BD). Cells were washed and data collection carried out by flow cytometry (FACS CantoII, BD). Representative FACS plot of 1 of 3 mice per group. CD27 shedding was used as read-out for P2X7 activation $\text{CD4}^+ \text{CD25}^+$ Tregs and $\text{CD4}^+ \text{CD25}^-$ T helper cells. **Gated on CD^+ T cells.** (p.i. = after injection)

A significant reduction in frequencies of $\text{P2X7}^{\text{high}} \text{CD4}^+ \text{CD25}^+$ Tregs in splenocytes was observed in mice injected with HLE-Nb 14D5-14D5-ALB as compared to HLE-Nb 13A7-13A7-ALB-injected mice two hours ($p = 0.0021$) and twenty-four hours ($p = 0.0014$) after injection of Nbs (**Fig. 5.29B-C**). A rebound in Treg frequencies ($p = 0.036$) was however observed twenty-four hours after injection. As previously observed, P2X7 activation induced by ART2-mediated ADP-ribosylation via endogenously released NAD^+ (37°C samples) resulted in shedding of CD27 by the majority of $\text{CD4}^+ \text{CD25}^+$ Tregs and by a small subset of $\text{CD4}^+ \text{CD25}^-$ T helper cells. Shedding of CD27 by the splenocytes was further increased following incubation with exogenous NAD^+ and ATP (**Fig. 5.30**). Representative FACS plots (one of three mice from each group) demonstrate complete blockade of CD27 shedding by T helper cells and partial blockade of CD27 shedding by Tregs mediated by injected HLE-Nb 13A7-13A7-ALB. Conversely, HLE-Nb 14D5-14D5-ALB enhanced shedding of CD27. Difference between samples two and twenty-four hours

after injection was little if any. Thus injection of 20 µg of HLE-Nb 13A7-13A7-ALB demonstrates persisting blockade of P2X7 24 h post injection whereas systemic injection of P2X7-synergistic antibody, HLE-Nb 14D5-14D5-ALB ablates the Treg compartment.

5.3.10 Targeting P2X7 with HLE-Nbs 13A7 and 14D5 attenuates or exacerbates disease course in a mouse model of in experimental glomerulonephritis

Taylor *et al* reported an attenuated course of experimental glomerulonephritis (EAG) in P2X7 knockout mice and in rats treated with a broad spectrum P2X7 antagonist, suggesting that antagonizing P2X7 with Nbs might provide a useful therapeutic strategy (Taylor *et al*, 2009). To further probe the role of P2X7 in EAG and to assess the potential therapeutic utility of a P2X7-antagonistic Nb in this disease, a pilot experiment was performed in collaboration with the Meyer-Schwesinger group using their established model of EAG induced with anti-podocyte antibodies (Meyer-Schwesinger *et al*, 2011). In this model, the systemic injection of serum from sheep immunized with mouse podocytes causes a slowly progressing inflammation of the kidney. Groups of 5 – 6 animals each received 5 intraperitoneal injections of HLE-Nbs 13A7-13A7-ALB, 14D5-14D5-ALB or a control HLE-Nb, Dum-ALB-Dum (at an initial dose of 50 µg on day 0 and 25 µg each, on days 3, 6, 9, and 12) (see **Fig. 4.1**). To induce EAG, mice were injected intravenously with 300 µl of two fold concentrated anti-podocyte nephritis (APN) or pre-immune (PI) serum from the same sheep, two hours after the first dose of HLE-Nb. Animals were monitored and was collected in metabolic cages on days 0, 3, 6, 9, 12, and 15 to determine urine levels of albumin and creatinine. Animals were sacrificed on day 15 and blood samples were collected to determine serum levels of cholesterol, triglycerides and creatinine.

The results of urine analyses show detectable albuminuria in animals treated with APN serum and the control HLE-Nb Dum-ALB-Dum at day 9 and increased levels on days 12 and 15. Differences in albuminuria of mice receiving APN vs PI serum reached significance on day 15 ($p = 0.024$) (**Fig. 5.31**). Mice treated with the P2X7 antagonistic HLE-Nb 13A7-13A7-ALB and the APN serum showed little if any albuminuria, indicating an attenuated disease development. In marked contrast, mice treated with the P2X7-potentiating HLE-Nb 14D5-14D5-ALB developed detectable albuminuria already on day 3 after APN serum injection and displayed significantly elevated albuminuria in comparison to mice treated with the control Nb on days 9, 12 15 ($p = 0.024$). Mice treated

with 14D5-14D5-ALB and the PI serum did not develop albuminuria indicating that the HLE-Nb 14D5-14D5-ALB by itself does not induce kidney disease (Fig. 5.31). Consistent with a more severe nephrotic syndrome in 14D5-14D5-ALB and APN-treated mice, these mice also exhibited elevated serum levels of creatinine, triglycerides and cholesterol on day 15 (Fig. 5.32). In contrast, the corresponding serum parameters for mice treated with APN serum and the P2X7 blocking HLE-Nb 13A7-13A7-ALB were similar to those of mice that had received PI serum, consistent with a therapeutic effect of HLE-Nb 13A7-13A7-ALB (Fig. 5.32).

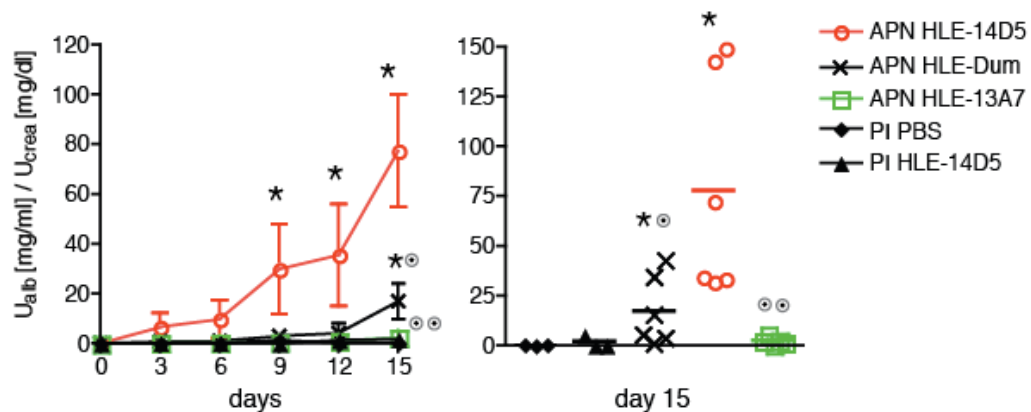


Figure 5.31. Monitoring albuminuria in mice after injection of anti-podocyte nephritis (APN) or preimmune (PI) sheep serum in conjunction with half-life extended, dimeric formats of P2X7-blocking Nb 13A7, P2X7 potentiating Nb 14D5 and a control Nb Dum. Groups of 6-8 week old C57BL/6 mice ($n = 5$ or 6) received intravenous injections of $300 \mu\text{l}$ of two-fold concentrated sheep anti-mouse podocyte nephritis serum (APN). Mice each received 5 intraperitoneal injections of HLE-Nbs: an initial dose of $50 \mu\text{g}$ in 1ml PBS on day 0, 2 h before injection of APN serum, and $25 \mu\text{g}$ each on days 3, 6, 9, and 12. Groups of control mice ($n = 3$) received injections of $300 \mu\text{l}$ of two-fold concentrated pre-immune (PI) serum. These mice also received 5 intraperitoneal injections of PBS or of HLE-14D5 in PBS at the same dosage and time schedule as in the APN-injected groups. Mice were monitored daily and urine was collected in metabolic cages for 24 h after each HLE-Nb injection and for the last 24 h before sacrifice of mice on day 15. Albumin in urine was measured by ELISA (Bethyl labs) and urine creatine levels were determined in the central diagnostic lab (UKE, Hamburg). Results were analyzed with GraphPad Prism. Significance was assessed with the Mann Whitney U test in comparison to control PI PBS group (* $p < 0.05$) or to APN HLE-Nb-14D5 group (\odot $p < 0.05$; $\odot\odot$ $p < 0.01$). (HLE-Dum = Dum-ALB-Dum; HLE-14D5 = 14D5-14D5-ALB; HLE-13A7 = 13A7-ALB-13A7).

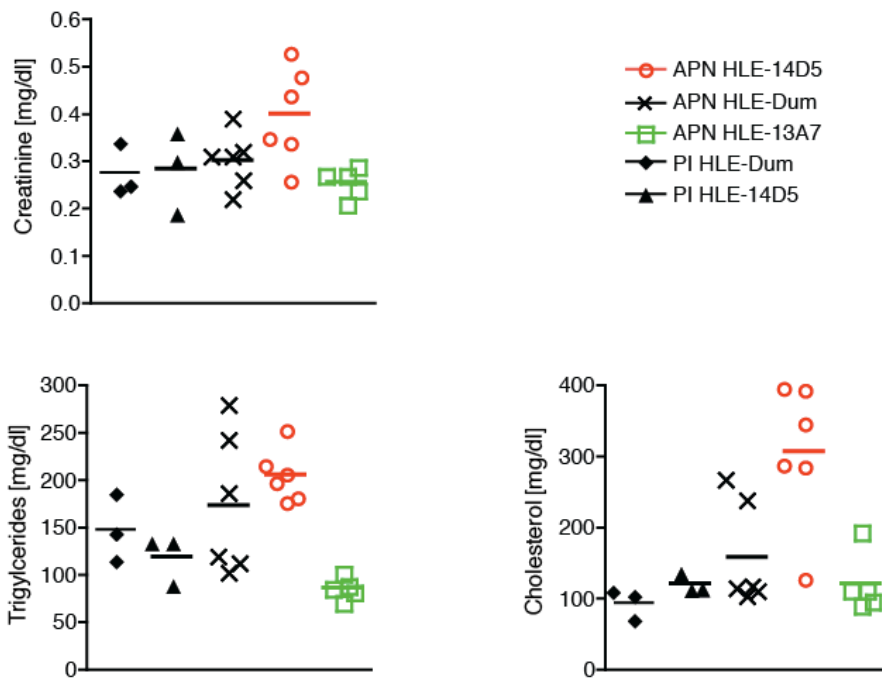


Figure 5.32. Serum creatinine, triglycerides and cholesterol levels at d15 after treatment of mice with anti-podocyte nephritis (APN) or preimmune (PI) serum . Groups of were treated with sheep serum and Nbs as in Fig. 5.31. Blood was collected on day 15 and serum levels of creatinine, triglycerides and cholesterol determined in the central diagnostic lab (UKE, Hamburg). Results were analyzed with GraphPad Prism. (HLE-Dum = Dum-ALB-Dum; HLE-14D5 = 14D5-14D5-ALB; HLE-13A7 = 13A7-ALB-13A7).

6 Discussion

This study provides a novel proof of principle that Nbs can serve as tools to block an ion channel. The Nbs selected in this project show effective antagonism and potentiation of P2X7-mediated shedding of cell surface molecules and cell death, both *in vitro* and *in vivo*. Application of the Nbs in an inflammatory disease model point to a possible therapeutic benefit of P2X7-antagonistic Nbs. In this section, the scope of the selected Nbs and their potential application in research and therapy are discussed.

6.1 Selected Nbs modulate P2X7 activation

Nbs specific for mouse and/or human P2X7 were selected by panning phage libraries generated from immunized llamas on cells expressing P2X7 (**Figs. 5.3**). Eighteen of twenty-three Nb families selected on mouse P2X7 expressing cells were confirmed to specifically bind to mP2X7 (**Fig. 5.4**). Similarly, three of eight Nb families selected on cells expressing human P2X7 showed specific binding to human P2X7 (**Fig. 5.5**). None of the selected anti-mP2X7 Nbs demonstrated cross-reactivity with P2X7 orthologs of human and rat whereas one of three anti-hP2X7 Nb families (fam a, Nb 1c81) showed cross-reactivity to both mouse and rat orthologs of P2X7 (**Fig. 5.7**). These results show that the use of cDNA and cell immunizations permitted the induction of immune responses against an ion channel such as P2X7 in its native confirmation (Möller *et al*, 2007).

Nbs from six of the eighteen anti-mP2X7 Nb families (families 5, 7, 11, 19, 22 and 23) were found to inhibit ATP- and NAD-induced activation of P2X7 while another three demonstrated potentiation of the activation of P2X7 (families 8, 10 and 11) (**Figs. 5.18 – 5.20; Table 5.2**). All anti-hP2X7 specific Nb clones showed inhibition of ATP-induced P2X7 activation with two Nb families (families a and e) showing complete blockade at saturating concentrations (**Figs. 5.12 and 5.13; Table 5.3**). Therefore, half of the mP2X7-specific Nb-families, and all of the human P2X7-specific Nb families functionally modulated activation of P2X7. This high proportion of functional Nbs concurs with previous reports by our own and other groups on anti-enzyme Nbs: Lauwereys *et al* reported that 40% of isolated Nb clones inhibited the carbonic anhydrase or porcine pancreatic α -amylase enzymatic activity. De Genst *et al* demonstrated that six of eight anti-lysozyme Nbs isolated were inhibitory while similarly generated mouse monoclonal antibodies did not. Similarly, our group found that all selected anti-SpvB Nbs inhibited the

bacterial toxin and that three of four of the anti-ART2 Nbs isolated blocked the cytotoxic activity of the transferase while none of twelve anti-ART2 rat monoclonal antibodies (mAbs) generated was able to block the enzymatic activity (Lauwereys *et al*, 1998; De Genst *et al*, 2006; Alzogaray *et al*, 2011; Koch-Nolte *et al*, 2007).

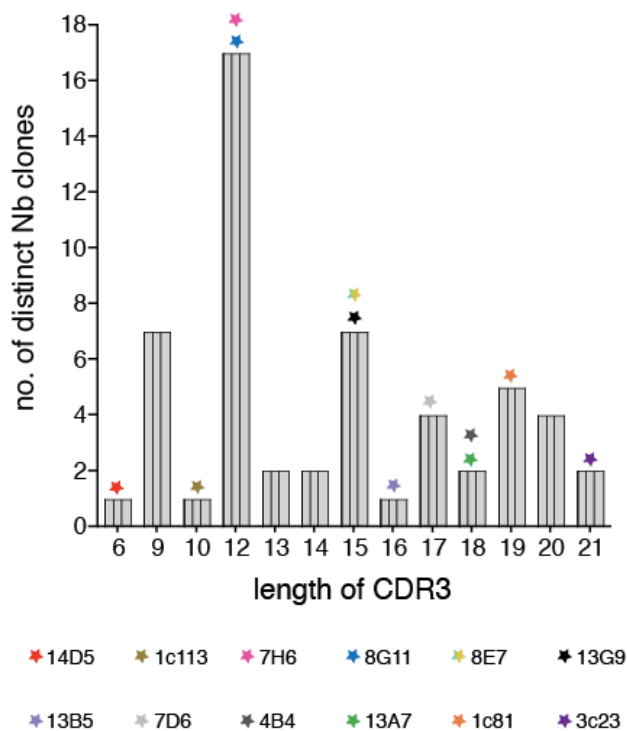


Figure 6.1. Nbs demonstrate long CDR3 regions. The distribution of number of amino acids in CDR3 regions (length) of mP2X7- and hP2X7-specific Nbs combined was analyzed using GraphPad Prism. Each distinct Nb is represented once irrespective of number of hits. Nanobodies characterized as antagonists or synergists of P2X7 are shown as colored stars (mP2X7 antagonists in order of potency: 13A7 > 8G11 > 13G9 > 7H6 > 13B5 > 8E7; hP2X7 antagonists in order of potency: 3c23 > 1c81 > 1c113; and mP2X7 synergists in order of potency: 14D5 > 4B4 = 7D6)

The tendency of Nbs to inhibit their target antigen presumably stems from the long CDR3 regions which form finger-like structures that reach hidden epitopes of proteins, e.g. substrate-binding or ligand-binding clefts, whereas the paratope of classical antibodies tend to be of planar conformation (Laskowski *et al*, 1996; Lauwereys *et al*, 1998; De Genst *et al*, 2006). An analysis of the CDR3 loop of the isolated anti-P2X7 Nb families shows a bias toward CDR3 regions comprising 12 amino acids or longer (**Figs. 6.1**). Interestingly, the most potent P2X7 blocking Nbs show very long CDR3 sequences of 18 (13A7, mP2X7), 19 (1c81, m/hP2X7) and 21 (3c23, hP2X7) amino acid residues whereas the less effective blocking Nbs had a CDR3 of intermediate lengths of 10 (1c113, hP2X7), 12 (8G11 and 7H6, mP2X7), 15 (8E7 and 13G9, mP2X7) and 16 (13B5, mP2X7) residues.

On the other hand, Nb 14D5 which potentiated mP2X7 possesses a CDR3 region comprising merely 6 amino acids whereas weaker potentiators 4B4 (mP2X7) and 7D6 (mP2X7) possessed longer CDR3 regions comprising 18 and 17 amino acids respectively. On the basis of these observations, it is tempting to speculate that the longer CDR3 region of the blocking Nbs permits the formation of finger-like domains that target clefts on P2X7 such as the ATP-binding pocket or the lateral vestibules (Kawate *et al*, 2009; Hattori & Gouaux, 2012) while the potentiating Nbs may allosterically modulate P2X7 by binding to an epitope outside of the ligand binding pocket (**Fig. 2.1**).

Results of cross blocking experiments provided further insight into the relative location of the binding sites of the P2X7-specific Nbs. Fc-fusion proteins of two anti-hP2X7 Nbs (1c81 and 1c113) blocked binding of each other and of the L4 mAb, indicating that these proteins bind to overlapping epitopes on human P2X7 (**Fig. 5.8**). Nb 3c23, isolated after masking the epitopes of Nbs 1c81 and 1c113 with purified Nbs on cells used for panning, recognized an independent P2X7 binding site. Interestingly, the Nbs 1c81 and 3c23 each completely blocked activation of hP2X7 at saturating Nb concentrations despite binding to independent epitopes (**Figs. 5.12 – 5.16**). This observation that two unique Nbs isolated from two different llamas (llama 405 = Nb 1c81 and llama 418 = Nb 1c113) and a mouse mAb (L4) recognize overlapping epitopes on hP2X7 indicates that the corresponding region of P2X7 may contain immunodominant epitopes.

Similarly, the anti-mP2X7 Nbs 13A7 (blocker) and 14D5 (enhancer) each block the binding epitope of a monoclonal rat anti-mP2X7 mAb, Hano44 (not shown) (Adriouch *et al*, 2008). Hano44 has been demonstrated to require an arginine at position 151 for binding – mutation of this arginine to lysine (R151K) resulted in a loss of binding by mAb Hano44. R151 is located on a prominent bulge in the head domain of mP2X7 outside of the ATP binding site (**Figs. 6.3 and 6.4**) (Kawate *et al*, 2009; Hattori & Gouaux, 2012; Schwarz *et al*, 2012). It is remarkable, that two functional P2X7 Nbs, one inhibitory (13A7) the other potentiating (14D5) and a nonfunctional mAb (Hano44) would bind to overlapping epitopes. Of note, Nb 13A7 blocks the binding epitope of the Nb 1c81, the only Nb which cross-reacts with both human and mouse P2X7 (not shown).

To better define the binding sites of the isolated Nbs, chimeric human-mouse P2X7 constructs could be generated by grafting modular domains of the ectodomain of one ortholog on the other and vice versa. Since all but one Nb (1c81) specifically bind to either mouse or human P2X7, such constructs would aid delineate the binding sites of individual Nbs. Nb 1c81 is expected to bind to all chimeras and could be used as control to monitor expressibility of the chimeras in transiently transfected cells. Mouse or human P2X7-specific Nbs would be expected to bind only the one chimeras, i.e. the one containing its binding epitope and not to the *mirror-image* chimera. Models of mouse and human P2X7 based on the recently solved 3D-structures of zebra fish P2X4 with and without bound ATP, can serve as convenient guide for delineating domains of P2X7 containing non-conserved amino acids that might be swapped between mouse and human P2X7 while maintaining overall structural integrity and functionality (**Fig. 6.4**). Using PCR-based domain-swapping technology, defined regions of various sizes could be transplanted between mouse and human P2X7 orthologs. For example, larger regions corresponding to the *head* (light purple) or *body* (gold) regions of P2X7 could be grafted (**Figs. 6.2 and 6.4**). Alternatively, smaller regions could be grafted. Finally, single amino acid residues within and outside of the *head* and *body* regions of P2X7 could be generated by site directed mutagenesis (**Figs. 6.3 and 6.4**). Following transient transfection of the mouse/human P2X7 chimeras into HEK cells, FACS analyses with Nb 1c81 shall reveal successful expression on the cell surface and parallel analyses with other Nbs shall reveal the domains, regions, and single amino acid residues that are essential for binding of a particular Nb to mouse or human P2X7.

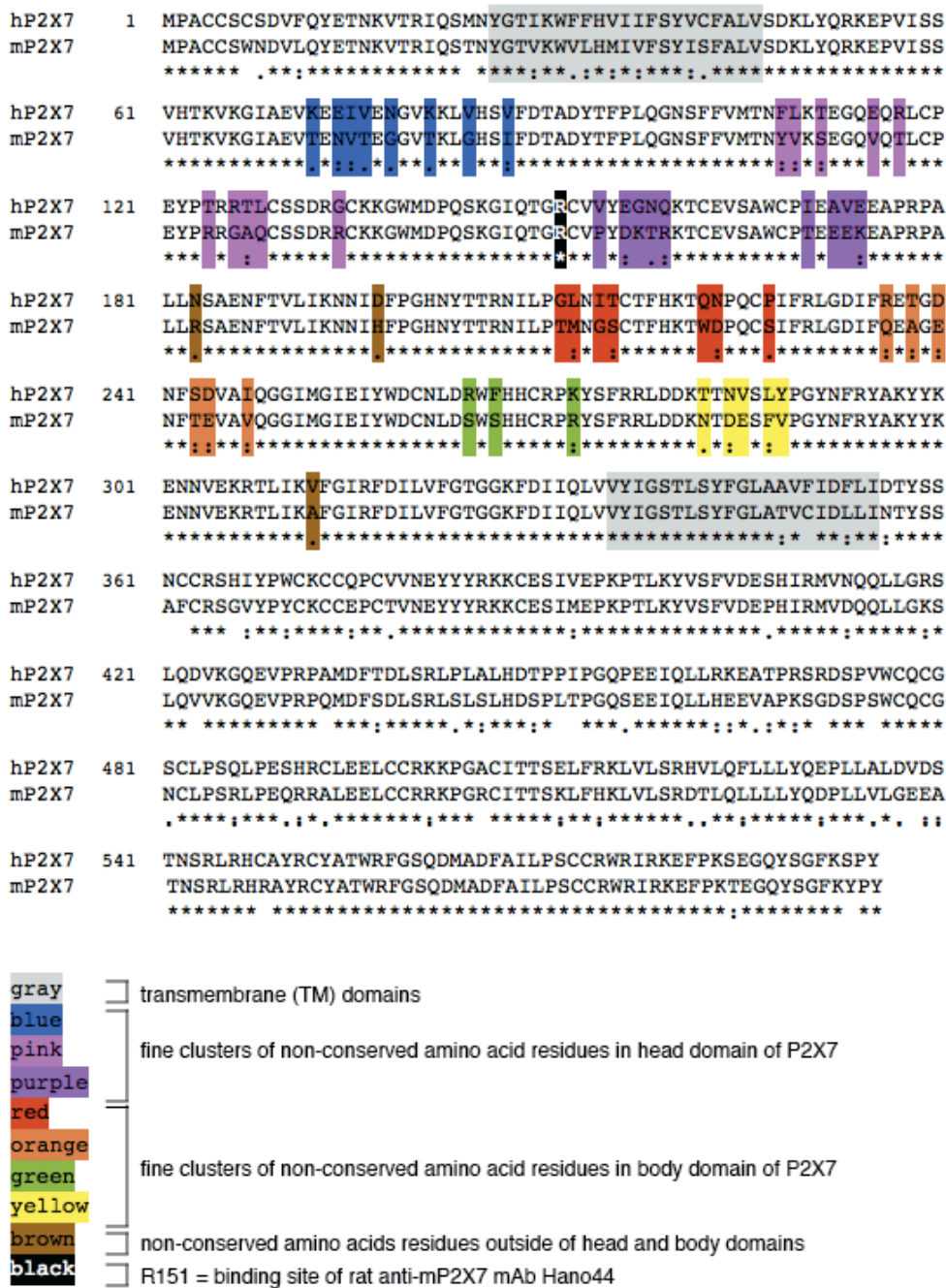


Figure 6.3. P2X7 orthologs of human versus mouse showing fine clusters of non-conserved amino acid residues. The polypeptide sequences of human versus mouse P2X7 using the reference sequences NP_002553.3 (hP2X7) and NP_035157.2 (mP2X7) were aligned using ClustalW. Clusters of non-conserved amino acid residues in smaller domains of the head and body regions of the ectodomains are color-coded as in the 3D model of P2X7 in **Figure 6.4**. Amino acid residue R151, important for P2X7-binding by mAb Hano44 is coded black. The transmembrane domains are shaded gray.

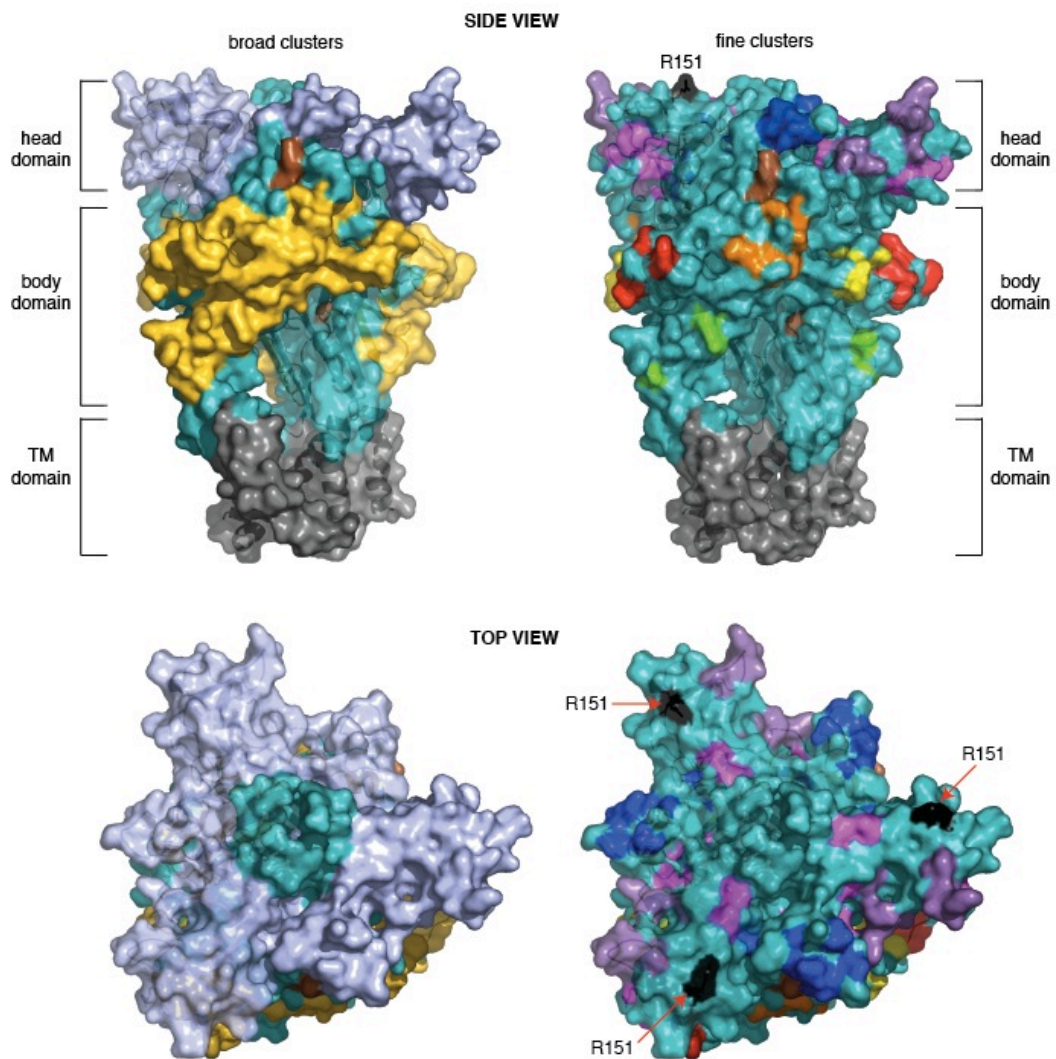


Figure 6.4. Schematic representation of P2X7 clusters of non-conserved amino acid residues in a 3D structure model of mouse P2X7. The 3D structure of mouse P2X7 was modeled based on the zebrafish P2X4 crystal structure (pdb code 4DW1) using PyMOL. Broad and fine clusters of non-conserved amino acids in the head and body domains of P2X7 are color coded as in **Figures 6.2 and 6.3**. Both the side and top view of the purine receptor are shown. Amino acid residue R151, important for P2X7-binding by Hano44 is marked with an arrow (black). (TM = transmembrane domain).

6.2 Applications of anti-P2X7 Nbs in research

6.2.1 Nbs permit detection of P2X7 in native conformation

The Nbs selected in this study present useful research tools for future studies of P2X7, e.g. for the detection of native P2X7 on normal and neoplastic cells. Most of the presently available anti-P2X7 antibodies were raised by immunizing animals with peptide epitopes of P2X7. These antibodies are useful for detecting denatured P2X7, e.g. in western blot analyses but provide unreliable detection of native P2X7 (Anderson & Nedergaard, 2006). The range of anti-P2X7 Nbs generated in this study present alternative tools for the

detection of P2X7 in native conformation, e.g., in flow cytometry and immunohistochemistry and for purification of P2X7, e.g., by immunoprecipitation (**Fig. 6.5**)

Monomeric, dimeric and Nb-Fc constructs

While the monovalent single domain Nbs isolated permit detection of P2X7, bivalent dimeric and Nb-Fc constructs present potentially increased binding avidity to P2X7, permitting enhanced visualization of the receptor. P2X7-bound monomeric and dimeric Nbs can be stained indirectly by detection of the hexa-histidine or c-myc-derived epitope tags with fluorochrome-conjugated secondary antibodies while Nb-Fc constructs can be detected with anti-Fc secondary antibodies. Furthermore, the Nbs and Nb-Fc proteins can be conjugated to fluorochromes permitting direct detection of P2X7 without the requirement of a secondary antibody (**Fig. 5.8**). Results presented here indicate that a strategy of combining Nb-Fc fusion proteins of Nbs which target independent epitopes on P2X7 provides an additive effect, increasing the staining intensity of P2X7 and permitting, for example, a clear detection of low levels of the receptor expressed on T cells (**Figs. 5.9 and 5.10**). This experimental approach allows direct assessment of expression levels of P2X7 on the cell surface and may help to resolve controversies regarding P2X7 expression on astrocytes and neurons (Anderson & Nedergaard, 2006).

Nb-Alkaline phosphatase (PhoA, ALPP) fusion proteins

Fusion of a Nb to alkaline phosphatases from *E. coli* (PhoA) or human (ALPP) may provide an alternative strategy to improve detection of P2X7 in histology. Molecular cloning using the pQuantagen cloning protocol provides a means for genetic linkage of Nbs to the *E. coli* alkaline phosphatase (PhoA). In the pQuantagen cloning and expression system, Nb-PhoA fusion proteins are directed by the PhoA signal peptide to the periplasma (Inouye *et al*, 1981; Ducancel *et al*, 1993). The spontaneous dimerization of the phosphatase in the periplasma, allows formation of dimeric (from monomeric Nbs) and tetrameric (from dimeric Nbs) Nb molecules (**Fig. 6.5**). Nb-PhoA fusion proteins can be purified from periplasma lysates in which the fusion proteins often constitute the major protein (Inouye *et al*, 1981). Additionally to the increased avidity for P2X7, such Nb-PhoA fusion constructs provide a direct detection system via the inherent enzymatic activity of PhoA. P2X7 detection by immunohistochemistry on cells and tissue sections

can be performed using such molecules. Furthermore, signal intensity can be enhanced by combining detection by Nb-ALPP fusion proteins with the alkaline-phosphatase-anti-alkaline phosphatase (APAAP) amplification system suited for human placental alkaline phosphatase (Hohmann *et al.*, 1988).

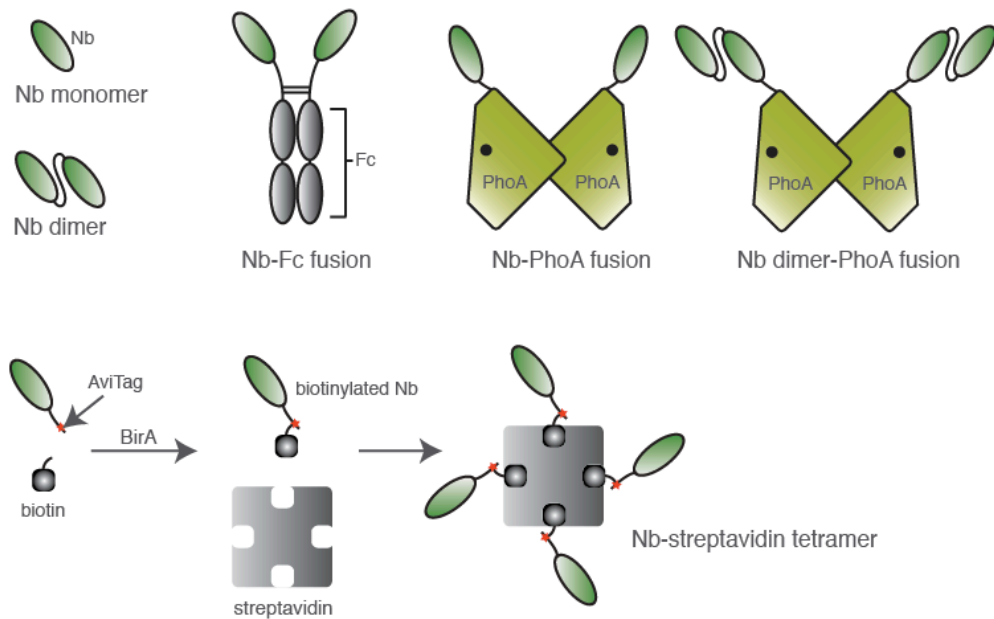


Figure 6.5. Nb formats for improved detection of native P2X7.

Nb-AviTag-biotin-streptavidin constructs

The biotin-streptavidin system allows formation of tetrameric binding modules. Nbs biotinylated at a single specific site can be generated using the AviTag technology from Avidity (Schatz, 1993). Subsequent to molecular fusion of the AviTag (GLNDIFEAQ**K**IEWHE) either N- or C-terminally to the Nb, Nb-AviTag constructs are expressed and purified from eukaryotic or prokaryotic expression systems. The purified Nb-AviTag constructs are incubated with the *E. coli*-derived biotin ligase (BirA) in the presence of biotin. BirA specifically biotinylates the lysin residue of the AviTag (**K**, bold). Such biotinylated Nbs-can be incubated with streptavidin in a molar ratio of 4:1 to generate streptavidin-linked Nb-tetramers (**Fig. 6.5**). Nb tetramers could be used for P2X7 detection by flow cytometry or immunohistochemistry or for immunoprecipitation and affinity purification of native P2X7.

6.2.2 Anti-P2X7 Nbs as specific inhibitors *in vitro* and *in vivo*

Three of the anti-P2X7 Nbs described in this study (13A7, 3c23, 1c81) represent robust specific inhibitors applicable both *in vitro* and *in vivo* in research. These Nbs provide numerous advantages over small molecule inhibitors of P2X7 (Guile *et al*, 2009; Friedle *et al*, 2010). Nbs demonstrate low *in vivo* toxicity, are stable under harsh pH and temperature conditions, show biodegradability, high specificity and selectivity for their targets and flexibility in reformatting (Wesolowski *et al*, 2009). Small molecule inhibitors, in contrast, often pose *in vivo* toxicity problems and often are non-selective for closely related proteins. In fact, initially reported P2X7 inhibitors did not discriminate well between P2X7 and other members of the P2X family (Guile *et al*, 2009). Recently reported more selective small molecule P2X7 antagonists are yet to be extensively probed *in vivo* (Friedle *et al*, 2010). The results presented in this study show that the Nbs specifically target and block P2X7 *in vivo* and *in vitro*. Following an intraperitoneal or intravenous injection, the Nbs specifically targeted P2X7 *in vivo* and inhibited the activation of P2X7 on liver and spleen lymphocytes within two hours after Nb injection. Loss of inhibition was observed 24 h after injection of dimeric Nbs (**Figs. 5.24** and **5.25**). Similarly, it was observed in our own group that anti-ART2 Nbs demonstrate *in vivo* blockade of the ecto-enzyme on lymph node T cells within 15 min post injection, which was partially reversed 6 h after injection (Koch-Nolte *et al*, 2007). The rapid tissue penetration and the quick systemic clearance of monomeric Nbs is due to their small size (15 kDa). With a molecular weight below the kidney filtration molecular weight cut-off, monomeric and dimeric Nbs are rapidly excreted by the kidneys (Wesolowski *et al*, 2009; Muyldermans, 2001). This could be advantageous for applications in acute disease or imaging studies. For applications in chronic diseases such as autoimmune diabetes or experimental autoimmune glomerulonephritis, Nb serum half-life can be tailor-extended by various strategies (Scheuplein *et al*, 2010; Tijink *et al*, 2008).

Extending the in vivo half-life of Nbs

Firstly, *in vivo* half-life of Nbs can be extended by molecular linkage to other Nbs which target abundant serum proteins such as albumin (Tijink *et al*, 2008). Binding to serum albumin confers an increased virtual size to the Nbs and also permit FcRn-mediated co-recycling of Nbs with albumin (Kim *et al*, 2006). Constructs in which the anti-albumin Nb ALB8 was genetically fused to dimeric versions of mouse P2X7 specific Nbs 13A7, 8G11

and 14D5 were provided by Ablynx. The results presented here show that such derivatization of Nbs did, indeed result in prolonged *in vivo* half-life without compromising their functional potency (**Fig. 5.30**). Secondly, the molecular fusion to the Fc domain of a classical antibody can increase the *in vivo* half-life of Nbs due to increase in molecular weight – Nb-Fc fusion proteins have a molecular weight of 80 kDa, i.e., above the filtration threshold of a healthy kidney (Holliger & Hudson, 2005). Moreover, point mutations in the C_{H2} domain (T252L, T254S, T256F) that enhance the affinity to the neonatal Fc-receptor expressed on endothelial and kidney tubule cells have been demonstrated to further enhance *in vivo* half life (Ghetie *et al*, 1997). In case of the ART2-specific Nb s+16a, our group found that fusion to such an LSF mutant of the Fc domain of mouse IgG1 sufficed to extend the duration of an effective blockade of ART2 *in vivo* from less than 6 h to more than 7 d (Scheuplein *et al*, 2010). A caveat in the application of fusion to Fc domains as a method of extending the serum half-life of Nbs is that, other effector functions of the Fc domain, e.g. binding to Fc receptors on NK cells or macrophages and/or complement proteins *in vivo*, may ensue. It has been demonstrated that a single point mutation (D265A) in the C_{H2} domain of the Fc tail of the murine IgG as well as the human IgG3 can drastically attenuate these effector functions (Baudino *et al*, 2008). Such point mutations can be incorporated during generation of Nb-Fc fusion proteins intended for *in vivo* applications.

6.2.3 Use of P2X7-blocking Nbs to protect Tregs from NAD-induced cell death in experimental set-ups

Previously, our group demonstrated that NAD is released during cell preparation from spleen or lymph nodes, in sufficient quantities to allow ART2-catalyzed ADP-ribosylation of P2X7 even when cells are prepared at 4°C (Scheuplein *et al*, 2009). ADP-ribosylation of P2X7 during cell preparation results in activation of P2X7 when cells are subsequently returned to 37°C, inducing apoptosis of a substantial fraction of the P2X7^{high} Treg subset (Hubert *et al*, 2010). This ART2-mediated activation of P2X7 undermines the suppressive function of Tregs in subsequent assays. Injection of the ART2-blocking Nbs+16a, shortly before sacrifice of mice and cell preparation prevented the cytotoxic effect of endogenously released NAD (Rissiek, 2012). The results presented in this study demonstrate that systemic injection of P2X7-blocking Nbs 8G11 and 13A7 similarly block the effect of endogenous NAD released during cell preparation and also prevent P2X7

activation upon subsequent exposure to exogenous NAD and ATP (Figs. 5.24 and 5.25). Moreover, incubation of T cell preparations with anti-P2X7 Nbs post cell preparation at 4°C prevented the subsequent activation of ADP-ribosylated P2X7 upon return to 37°C while the ART2 inhibitory Nb, s+16a, did not (Fig. 5.23). Therefore, anti-P2X7 Nb inhibitors present a more effective means to protect Tregs than anti-ART2 Nb inhibitors with the former preventing both NAD- and ATP-mediated P2X7 activation and activation of P2X7 post ADP-ribosylation while the latter blocks ADP-ribosylation of P2X7 and other cell surface proteins. Either of these Nbs can be injected shortly before preparation of Tregs to protect Treg viability and preserve suppressive effects. It must however be noted that some authors have suggested a contribution of P2X7 to T cell activation (Yip *et al*, 2009). It is thus, important to determine whether coating of Tregs with P2X7-blocking Nbs, affects activation of these cells in subsequent suppression assays and other experiments.

6.3 Nb-mediated antagonism of P2X7 as a therapeutic approach

Several reports have proposed antagonism of P2X7 as a therapeutic approach in various inflammatory-diseases (Table 6.1). Up to date, elucidating the role of P2X7 in disease models has been carried out mainly by using knock-out mice or small molecule inhibitors. Small molecule inhibitors often lack selectivity and present with complex toxic side effects (Friedle *et al*, 2010). Nbs generally demonstrate high target-specificity and low toxicity. In this section, the possible therapeutic applications of Nb-based P2X7 antagonists in glomerulonephritis and multiple sclerosis are discussed.

Table 6.1. Role of P2X7 in disease

Disease	Summary of findings	Reference(s)
rodent disease models		
Anti-collagen-induced arthritis	P2X7 knockout mice show lower incidence and lower severity of disease	(Labasi <i>et al</i> , 2002)
Antibody-induced glomerulonephritis	P2X7 knockout mice develop milder disease; treatment of rats with a high dose of a P2X7 antagonist ameliorates disease	(Taylor <i>et al</i> , 2009)
MOG peptide-induced experimental autoimmune encephalopathy (EAE)	Lower incidence of EAE in P2X7 knockout mice; treatment with P2X7 antagonists ameliorates disease	(Sharp <i>et al</i> , 2008; Matute <i>et al</i> , 2007)

Disease	Summary of findings	Reference(s)
Chronic pulmonary obstructive disease induced by cigarette smoke	P2X7 knockout mice and mice treated with P2X7 antagonists show reduced lung inflammation and emphysema	(Lucattelli <i>et al</i> , 2011)
Hypertension induced by deoxycorticosterone acetate (DOCA) and high salt diet	Wildtype but not P2X7 knockout mice develop hypertension	(Ji <i>et al</i> , 2012)
Skin cancer induced by application of DMBA/TPA	Co-application of a P2X7 agonist, BzATP, with DMBA/TPA, reduced incidence of cancer	(Fu <i>et al</i> , 2009)
Nerve-injury-induced pain behavior	Balbc/c mice with more sensitive P451 variant of P2X7 demonstrated higher pain sensation in mechanical allodynia that C57bl/6 mice with L451 variant	(Sorge <i>et al</i> , 2012)
human studies		
Chronic pain	After mastectomy, patients with less sensitive P2X7 allelic variant His270 reported reduced sensation of pain as compared to R270 patients	(Sorge <i>et al</i> , 2012)
Extrapulmonary tuberculosis	Populations with the 1513c allele leading to the E496A loss-of-function point mutation were more susceptible to tuberculosis linked with ablated ATP-mediated killing of mycobacterium	(Fernando <i>et al</i> , 2007)

6.3.1 Potential application of P2X7-blocking Nbs in Glomerulonephritis

Glomerulonephritis (GN) causes end-stage renal failure treated currently, in part, with broad immunosuppressive regimens accompanied with severe side effects (Tam, 2006). Pathologically, GN is marked by glomerular deposition of immune complexes encompassing autoantibodies which mediate kidney inflammation. In the experimental model of autoimmune glomerulonephritis (EAG) used in this study, mice develop anti-podocyte nephritis (APN) following intravenous injection of immune serum from sheep immunized with cultivated mouse podocytes (Meyer-Schwesinger *et al*, 2011). The disease course is marked by the development of albuminuria and increases in serum cholesterol and triglycerides. Treatment of mice with a dimer of the P2X7 antagonistic Nb 13A7 fused to the anti-albumin Nb ALB8, prior to injection of the sheep anti-podocyte serum and at regular intervals (every three days) during the course of disease, attenuated EAG (**Figs. 5.31 and 5.32**). Conversely, treatment with a P2X7-potentiating Nb resulted in an early onset and adverse course of disease. These results are in line with those of previous reports suggesting a role of P2X7 and of the P2X7-induced pro-inflammatory cytokines IL-1 β and IL-18 in the development and severity of GN. Prophylactic or therapeutic treatment with

IL-1 receptor antagonists attenuated crescentic glomerulonephritis in the rat model of GN (Lan *et al*, 1995; 1993). Furthermore, it was observed that IL-18 promoted local renal inflammation and mediated infiltration of leukocytes in the same model (Kitching *et al*, 2005). Macrophages play a pivotal effector role in the human as well as experimental forms of GN (Tam *et al*, 1996). Monocyte chemoattractant protein 1 (MCP-1) released by intrinsic renal cells upon immune complex deposition mediates the initial kidney infiltration of macrophages (Tang *et al*, 1996). Activation of P2X7 in macrophages induces assembly of the NALP3 inflammasome, resulting in activation of caspase-1, leading to release of active IL-1 β and IL-18 (Di Virgilio, 2007). The pro-inflammatory cytokines, IL-1 β and IL18, mediate further infiltration of leukocytes and exacerbate the inflammation. Activated macrophages also produce more MCP-1 leading to enhanced recruitment of macrophages. While P2X7 blockade with Nbs may not prevent renal deposition of immune complexes and the initial recruitment of macrophages, the subsequent activation of P2X7 in macrophages which plays a major role in the secondary inflammation and the severity of GN, can be blocked. Taylor *et al* reported that P2X7 knock-out mice and rats treated with broad P2X7-inhibitors develop a milder form of antibody-induced GN with reduced overall macrophage infiltration accompanied by lower levels of urinal MCP-1 (Taylor *et al*, 2009). Targeting P2X7 with antagonistic Nbs may present a more specific, alternative therapeutic approach with lower risks of side effects than small molecule antagonists or immunosuppressants.

6.3.2 Potential application of P2X7-blocking Nbs in Multiple sclerosis

Multiple sclerosis (MS) is a an inflammatory autoimmune demyelinating disease of the central nervous system (CNS) the cause of which is not known (Loma & Heyman, 2011). An estimated 400,000 individuals in the United States are affected by forms of MS. Patients present with heterogenous degrees in the loss of motoric, cognitive and autonomic functions (Sospedra & Martin, 2005). Onset of symptoms of MS is usually in the young adult years of life. Mounting evidence points to role of P2X7 in the etiology of MS: (i) elevated levels of P2X7 expression is observed in activated microglia (the resident macrophages in the CNS) in MS lesions contributing to tissue damage (Yiangou *et al*, 2006); (ii) P2X7-deficient mice demonstrate attenuated development of experimental autoimmune encephalomyelitis (EAE, mouse disease model of MS) (Sharp *et al*, 2008); (iii) treatment of mice with small molecule P2X7 antagonist ameliorates disease

progression in EAE (Matute *et al*, 2007); and (iv) treatment of MS patients with DSMD glatiramer acetate results in downregulation of P2X7 on monocytes (Caragnano *et al*, 2012). Thus P2X7 is increasingly recognized as a therapeutic target in MS and other neurological disorders (Friedle *et al*, 2010). The anti-P2X7 Nbs selected and characterized in this study demonstrate effective blockade of P2X7 and provide attractive alternatives for the treatment of EAE and MS. Application of anti-P2X7 Nbs in multiple sclerosis and other neurological conditions may, however, be hampered by the inability of antibodies to cross the blood brain barrier (BBB). The challenge of transmigration across the BBB might be overcome by molecular linkage of anti-P2X7 Nbs to other Nbs which target receptors on the brain endothelium and mediate transcytosis. The Nbs FC5 and FC44 which were selected on human cerebro-microvascular endothelia cells were shown to be detectable in brain tissues following intravenous injection in mice (Muruganandam *et al*, 2002). Fusion of anti-P2X7 Nbs to either FC5 or FC44 may permit the application of the P2X7 antagonistic Nbs in multiple sclerosis and other neurological disorders. Moreover, it was recently demonstrated that Nbs with inherent alkaline isoelectric points (pI) can transmigrate across the BBB in a receptor-independent manner (Li *et al*, 2012). The authors demonstrated that an alkaline Nb (pI = 9.4), specific for the astrocyte glial fibrillary acidic protein (GFAP), traversed the BBB and penetrated astrocytes to bind this intracellular target protein. Indeed, molecular linkage of the Nb to green fluorescent protein (GFP) resulted in the fluorescent labeling of astrocytes *in vivo*. The pI of a Nb can be rendered more alkaline by site directed insertion of the basic amino acids arginine and lysine. It will be important to determine whether and under which conditions the P2X7-antagonizing Nbs described in this report can translocate into the CNS.

6.4 Nb potentiation of P2X7 activation as a therapeutic approach

Next to P2X7-blocking Nbs, three Nbs (14D5, 4B4, 7D6) that potentiate nucleotide-induced activation of mouse P2X7 were selected from the immunized llamas (**Fig. 5.20**). While blocking Nbs find potential applications in inflammation-mediated conditions, such P2X7-synergistic Nbs may find therapeutic application in tumor therapy or clearance of intracellular pathogens.

6.4.1 Combining Nb-mediated potentiation of P2X7 activation with chemotherapy to improve tumor therapy

Enhancing uptake and reducing expulsion of chemotherapeutic compounds

Chemotherapy is the primary method of treatment of cancer. However multidrug resistance in neoplastic cells increasingly impedes therapeutic successes (Szakács *et al*, 2006). Cancer cells employ molecular pumps such as P-glycoprotein and ABC-transporters to exude cytotoxic drugs out into the exterior thereby evading cell death (Gottesman & Ling, 2006; Gottesman *et al*, 2002). Methods to enhance uptake or to reduce the expulsion of drugs by neoplastic cells would benefit patients. Preliminary experiments from our lab indicate that P2X7 activation mediates enhanced uptake of the cytostatic drug, doxorubicin, and increases cell death in the Yac-1 lymphoma cell line *in vitro*. Moreover, in the presence of the Nb 14D5, lesser doses of doxorubicin suffice to induce substantial cell death of Yac-1 cells (Becher *et al*, 2012). The group of di Virgilio has reported that several tumors upregulate P2X7, a basal activation of which presumably supports tumor growth *in vivo* (Di Virgilio *et al*, 2009; Adinolfi *et al*, 2012). The high expression of P2X7 on tumors may pave the way for use of P2X7-potentiating Nbs as an adjuvant to chemotherapy. To this end, molecular linkage of such P2X7-synergistic Nbs to a Nb specific for a tumor antigen may permit further selectivity in tumor targeting (Tijink *et al*, 2008).

Depletion of Tregs

It has been observed that in the microenvironment of tumors *in vivo*, elevated levels of immunosuppressive regulatory T cells are present (Hiraoka *et al*, 2006; Zou *et al*, 2005). Tregs secrete cytokines such as IL-10 and TGF- β which dampen the anti-tumor immune response. In the DEREK mouse model, in which Tregs express the sensitive diphtheria toxin receptor (DTR), depletion of Tregs by intraperitoneal injection of diphtheria toxin (DT) leads to enhanced clearance of tumors by cytotoxic TILs (Klages *et al*, 2010; Li *et al*, 2010). Similarly, depletion of Tregs by systemic injection of NAD⁺ resulted in enhanced tumor clearance (Hubert *et al*, 2010). Considering the findings presented here that systemic injection of the P2X7-potentiating HLE-Nb, 14D5-14D5-ALB, leads to partial depletion Tregs (**Fig. 5.29**), it is conceivable that such treatments may also enhance tumor clearance. Thus, P2X7-potentiating Nbs may exert synergistic effects: Nb-mediated Treg depletion

and Nb-enhanced uptake of chemotherapeutic drugs to improve outcome of cancer treatments.

6.4.2 Nb-mediated potentiation of P2X7 as a therapeutic approach in the clearance of intracellular pathogens

Among cells of hematopoietic lineage, macrophages express the highest levels of P2X7 (Sluyter & Stokes, 2011). ATP-mediated activation of P2X7 in macrophages is important for signaling the fusion of pathogen-containing phagosomes with lysosomes and for the ensuing killing of intracellular mycobacteria in pulmonary tuberculosis and of the intracellular parasite, *Toxoplasma gondii* in toxoplasmosis (Fairbairn *et al*, 2001; Corrêa *et al*, 2010). Impaired killing of these intracellular pathogens is linked with reduced or abrogated activation of P2X7 associated with loss-of-function polymorphisms in the P2X7 gene (Fernando *et al*, 2007; Lees *et al*, 2010; Jamieson *et al*, 2010). Our own group recently observed that murine macrophages express the less sensitive P2X7a splice variant which is insensitive to activation by NAD via ART2-mediated ADP-ribosylation (Schwarz *et al*, 2012). Preliminary experiments indicate that the P2X7-potentiating Nb, 14D5 may not only enhance activation of wildtype P2X7 (**Figs. 5.20 and 5.22**), but may also promote nucleotide-induced activation of low sensitive splice isoforms and allelic variants of P2X7. These observations suggest possible application of such Nbs to promote killing of intracellular pathogens by macrophages via augmentation of P2X7 activation or even restoration of P2X7 activation in loss-of-function variants.

6.5 Perspectives

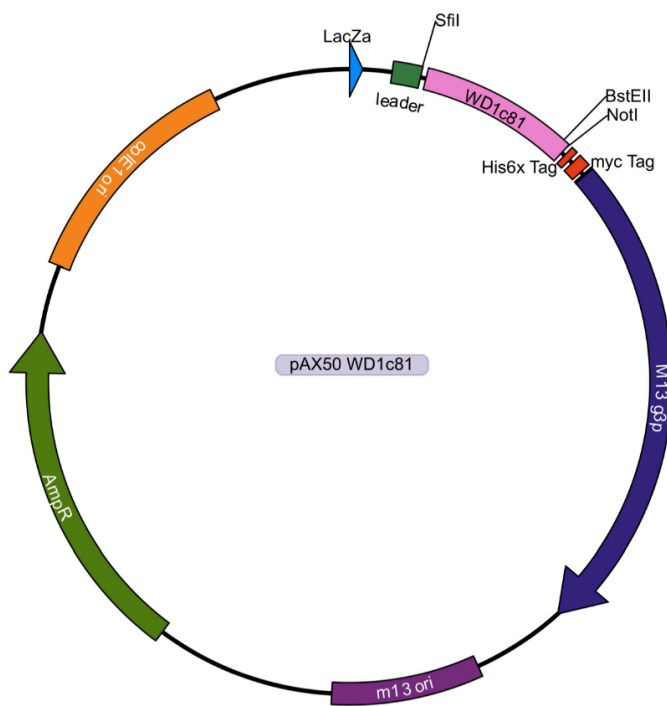
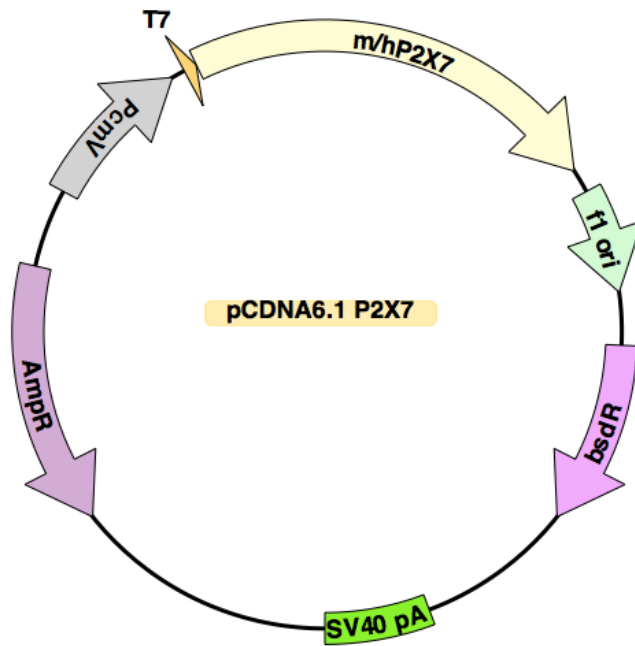
The P2X7-specific Nbs generated and characterized in this study demonstrate utility as new research tools. These Nbs also hold promise as new therapeutic tools for combating inflammation, cancer and infection.

7 Appendix

7.1 Oligonucleotides (Primers)

Primer name	Sequence (5' - 3')	description
ABL050	CATTTGAGTT GGCCTAGCCG GCCATGGCAG AGGTGCAATT GGTGGAGTCT	forward primer for nested PCR amplification of V _H H fragments. SfiI site in blue
ABL051	GGCTGAGCTGGGTGGTCCTGG	forward primer for V _H H amplification from CDNA
ABL052	GGCTGAGTTTGGTGGTCCTGG	forward primer for V _H amplification from CDNA
ABL003	GGTACGTGCT GTTGAAGTGT TCC	reverse primer for V _H H amplification; anneals to C _H 2
VHH1 for_WD	TGCG GCC CAG CCG GCC ATG GCA GAG GTG CAG CTG	forward primer for amplification of Nbs from pAX50; Sfi site in blue
VHH1 rev 20 GS	ACC CGG ATC CCCC GCC ACC GCT GCC TCC ACC GCC GCT ACC CCC GCC ACC GCT GCC TCC ACC GCC CGA GGA GAC GGT GAC	reverse primer for Nb amplification for Nb-Nb dimer cloning into pHEN2; entails 20GS sequence; BamHI site in blue
VHH2 for 15 GS	TCTTGGATCCGGCGGGGAGGTAG TGGGGGTGGGGGCTCAGGTGGCGG CGGCTCAATGGCAGAGGTGCAGCT G	forward primer for Nb2 amplification for Nb-Nb dimer cloning into pHEN2; entails 15GS sequence; BamHI site in blue
VHH2 rev	ATGTGGCGCCGTGAGGAGACGGT GA	reverse primer for amplification of Nbs from pAX50; NotI site in blue
VHH mFc for	TCCAGATCTATGGCAGAGGTGCAG CTGGTG	forward primer for the amplification of Nbs for cloning as Nb-mIgG1 Fc into pME; BglII site in blue
VHH mFc rev	AGGCTCGAGTGAGGAGACGGTGAC	reverse primer for the amplification of Nbs for cloning as Nb-mIgG1 Fc into pME; XhoI site in blue
Ala348Thr_ for	GGTCTGGCCACTGTGTTTCATCGAC	forward primer for the mutagenesis of pcDNA6 hP2X7 Y155 A348 to Y155 T348
Ala348Thr_ rev	GTCGATGAACACAGTGGCCAGACC	reverse primer for the mutagenesis of pcDNA6 hP2X7 Y155 A348 to Y155 T348

7.2 Plasmid maps



7.3 Sequences of isolated Nanobody clones

Isolated anti-mouse P2X7 Nb families

compared with human VH3-23:JH5

evqlllesggglvqpggsrlr1scaasgftfs---wvraqpdkglewss-----rftisrdshskntlylqmns1raedtavvyakc-----wgggtlvtvss
 2C4 ...v...dv...a...l...dDYAIG.f...er.gi.-CISSTGNVFYADSVKQ...s.ke...h.agHFTVDSGKVLRLTDISS-----wgggtlvtvss
 2A6 ...v...dv...a...l...dDYAIG.f...er.gi.-CISSTGNVFYADSVKQ...s.ke...h.agHFTVDSGKVLRLTDISS-----wgggtlvtvss
 4D5 ...m...v...dv...a...l...dDYAIG.f...er.gi.-CISSTGNVFYADSVKQ...s.ke...h.agHFTVDSGKVLRLTDISS-----wgggtlvtvss
 4G6 ...v...dv...a...l...dDYAIG.f...er.gi.-CISSTGNVFYADSVKQ...s.ke...h.agHFTVDSGKVLRLTDISS-----wgggtlvtvss
 1A8 ...v...t...t...l...dDYAIA.f...er.g.-ILSSIGKTFYADSVKQ.s.ta.ga.t.vf...kp.g...i...vaGHFVYNDGALSLNNTARGSGF...aq
 1C9 ...v...t...t...l...dDYAIA.f...er.g.-ILSSIGKTFYADSVKQ.s.ta.ga.t.vf...kp.g...i...vaGHFVYNDGALSLNNTARGSGF...aq
 5A1 ...v...a...a...er.y.--MG.f...er.f.aGSGWDGIPTRYADSVKQ.l...a...vs...sg.kp...i...t-----GTSVVHYQY...q
 5B1 ...v...a...a...er.y.--MG.f...er.f.aGSGWDGIPTRYADSVKQ...a...vs...sg.kp...i...t-----GTSVVHYQY...q
 5F1 ...v...a...a...er.y.--MG.f...er.f.aGSGWDGIPTRYADSVKQ...a...vs...sg.kp...i...t-----GTSVVHYQY...q
 7E2 ...v...a...a...per.y.--MG.f...er.f.aGSGWDGIPTRYADSVKQ...a...vs...sg.kp...i...t-----GTSVVHYQY...q
 7F1 ...v...a...a...er.y.--MG.f...er.f.aGSGWDGIPTRYADSVKQ...a...vs...sg.kp...i...t-----GTSVVHYQY...q
 7F3 ...v...r...a...er.y.--MG.f...er.f.aGSGWDGIPTRYADSVKQ...a...vs...sg.kp...i...t-----GTSVVHYQY...q
 11G1 ...v...a...a...er.y.--MG.f.r...er.f.aGSGWDGIPTRYADSVKQ...a...vs...sg.kp...i...t-----GTSVVHYQY...q
 4B4 ...v...a...a...r.v.DYGMG.f...lr.f.aSINWSGIYTRYIDSVEG...t...n.k...n.k...y--FLGPNWYSNYGRPSSYDFY...q
 4G4 ...m...a...p...r.v.DYGMG.f...er.f.aSINWSGIYTRYIDSVEG...t...n.k...n.k...y--FLGPNWYSNYGRPSSYDFY...q
 8G11 a...v...a...a...nf.rVNTMA.Y...qr.l.a-DITRGRDRTNYADTVNG...vr.v...g.p...a...ya-----VIELGVLEPRDY...q
 6A11 ...v...a...a...nf.rVNTMA.Y...qr.l.a-DITRGRDRTNYADTVNG...vr.v...g.kp...a...ya-----RIELGVLEPRDY...q
 6H10 ...v...a...a...sf.rVNNMA.Y...qr.l.a-DITRGRDRTNYADTVNG...vr.v...g.kp...a...ya-----RIELGVLEPRDY...q
 8E6 ...v...a...p...nf.rVNTMA.Y...qr.l.a-DITRGRDRTNYADTVNG...vr.v...g.kp...a...ya-----RIELGVLEPRDY...q
 8F5 ...vk...a...a...sf.rVNNMA.Y...qr.l.a-DITRGRDRTNYADTVNG...vr.v...g.kp...a...ya-----RIELGVLEPRDY...q
 8B4 ...v...a...a...nf.rVNTMA.Y...qr.l.a-DITRGRDRTNYADTVNG...vr.v...g.kp...a...ya-----RIELGVLEPRDY...q
 14G4 ...v...a...g...nf.rVNTMA.Y...qr.l.a-DITRGRDRTNYADTVNG...vr.v...g.kp...a...ya-----RIELGVLEPRDY...q
 8H5 ...m...a...a...nf.rVNTMA.Y...qr.l.a-DITRGRDRTNYADTVNG...vr.v...g.kp...a...ya-----RIELGVLEPRDY...q
 14F10 ...v...a...l...sf.rVNNMA.Y...qr.l.a-DITRGRDRTNYADTVNG...vr.v...g.kp...s.ya-----RIELGILEPRDY...q
 8A11 ...v...a...a...sf.rVNNMA.Y...qr.l.a-DITRGRDRTNYADTVNG...vr.v...g.kp...g.kp...ya-----RIELGVLEPRDY...q
 8H6 ...v...a...a...sf.rVNNMA.Y...qr.l.a-DITRGRDRTNYADTVNG...vr.v...g.kp...g.kp...ya-----RIELGVLEPRDY...q
 8G12 k...v...a...a...sf.rVNNMA.Y.g...qr.l.a-DITRGRDRTNYADTVNG...vr.v...g.kp...ya-----RIELGVLEPRDY...q
 14F6 ...v...a...p...sf.rVNNMA.Y...qr.l.a-DITRGRDRTNYADTVNG...vr.v...g.kp...ya-----RIELGVLEPRDY...q
 8B12 ...v...a...a...sf.rVNNMA.Y.g...qr.l.a-DITRGRDRTNYADTVNG...vr.v...g.kp...ya-----RIELGVLEPRDY...q
 14G11 ...v...k...a...sf.rVNNMA.Y.g...qr.l.a-DITRGRDRTNYADTVNG...vr.v...g.kp...ya-----RIELGVLEPRDY...q
 8C12 ...v...a...a...sf.rVNNMA.Y...qr.l.a-DITRGRDRTNYADTVNG...vr.v...g.kp...ya-----RIELGVLEPRDY...q
 8H4 ...v...a...a...sf.rVNNMA.Y.g...qr.l.a-DITRGRDRTNYADTVNG...vr.v...g.kp...dg.kp...ya-----RIELGVLEPRDY...q
 8H10 ...v...a...a...sf.rVNNMA.Y.g...qr.l.a-DITRGRDRTNYADTVNG...vr.v...g.kp...g.kp...ya-----RIELGVLEPRDY...q
 8D10 ...v...a...a...sf.rVNNMA.Y...qr.l.a-DITRGRDRTNYADTVNG...vr.v...g.kp...g.kp...ya-----RIELGVLEPRDY...q
 4B3 ...v...d...a...k...vv.v..dDGTIG.f...er.giaCISRVDGTYTYRDSVKQ...v.s.sa.t.vn...kp...a--DYASLCITETGYSGLDY.k...q

Isolated anti-mouse P2X7 Nb families

compared with human VH3-23:JH5

evqllesggglvqpggslrlscaasgftfs-----wvrqapqgkglewvs-----rftisrdnskntlylqmnslraedtavyyca-----wgqgtlvtvss
 8C7 .m.v.....a.....f...**SLAMG**.l.....er.f.GISRGGSTYYADSVKG.....a.m.....kp.....g---SPVLSIVLDTTRGLEIY---.....g.....
 8E7v.....a.....**I...SLAMG**.l.....er.f.GISRGGSTYYADSVKG.....a.m.....kp.....g---SPVLSIVLDTTRGLEIY---.....g.....
 6D7v.....a.....**I...SLAMG**.l.....er.f.GISRGGSTYYADSVKG.l.....a.m.....kp.....g---SPVLSIVLDTTRGLEIY---.....g.....
 7E8v.....a.....**I...SSPYG**.f.....erdf.aTISWNGVDTHYLDVSKG.....al.vh..hi.kp...l....a---STSGSAYLFPYRVYQYDS.....g.....
 7D6v.....a.....**I...gSSPYG**.f.....erdf.aTISWNGVDTHYLDVSKG.....a.vh..hi.kp...l....a---STSGSVLLFPYRVYQYDS.....g.....
 7F5v.....a.....**I...SSPYG**.f.....erdf.aTISWNGVDTHYLDVSKG.....al.vh..hi.kp...l....a---STSGSAYLFPYRVHGYDS.....g.....
 7A4v.....a.....**aI.g.-YSMG**.f.....er.f.TISWNGADTYADSVKG.....a.d.v.....kp.....g-----SITSYVSTWQHDYEX.....g.....
 13E8v.....a.....**aI.g.-YTMG**.f.....er.f.TISWNGASTYYADSVKG.....a.vs.....kp.....g-----SISYSRRWQDDYEX.....g.....
 7B4v.....a.....**rn.gSYTMA**.f.....r.f.TINWSGGDTYADSVKG.....a.v...d.kp.....a-----GLEYMSTIRYTYEY.....g.....
 7H6v.....**vv...smyrIDNMG**.y.....qr.l.a-TVTRGDIYADSVKG.....g.a.v.....kpa.....ni-----DSYIIGAGVRDY..r.g.....
 7G5v.....s.....**g...syy--IIG**.f.....er.e.CIRVTDGSTYYTNSVKG...m...ae.v.....kp.....s.t-----ECORWAYPNRIGA-I.....g.....
 13F4v.....s.....**g...syy--IIG**.f.....er.e.CIRVTDGSTYHTNSVKG...m...ae.v.....kp.....s.t-----ECORWAYPNRIGA-I.....g.....
 7D8v.....**l.leYXNIG**.f.....er.g.aCIDWTEGTFYVDSVKG...t.a.v...h...ep.....agMGRVITVQHMCAADRSLFTS.....g.....
 13B8v.....**l.ltYXNIG**.f.....er.g.CIDWTDGTFYADSVKG...t.a.v...hl...ep.....agMGRVMTVQHMCADRSLFTS.....g.....
 7D5v.....a.d.....**I...SVAVG**.f.....erdf.aWISWGSBITYADSVKG...a...vn.v.....kp...d....a---AWKYDRASVDFPEAYDY.....g.....
 1G6v.....a.....**pga...SFNMG**.f.t...er.f.aATSWSDISTYYADSVKG.....a.vt.e...kp.....agYYRGYLGRLTLEGSYDV.....g.....
 6B7v.....a.....**pga...SFNMG**.f.t...er.f.aATSWSDISTYYADSVKG.....a.vt.e...kp.....agYYRGYLGRLTLEGSYDV.....g.....
 14D5 k...v.....a.....**spi.SYAMG**.y.....pr.l.a-RIYTGTAHVEDSVKG.....aq.v.....ks.....hg-----RVRYDY.....g.....
 13G5v.....a.....**dr...gSSAMG**.f.....drdf.aAISWGSSTHYADSVKG.....a.m.....kpa...t..a-----SRRAYLPAKVGEYDF.....g.....
 13B5v.....a.d.....**I...SYAMG**.f.....er.f.aAISLGSMTYYADSMKG.....a.v.....kp.....a-----BELGDGLGYLAYRYDY.....g.....
 13F6v.....**.....TNIMT**.....i.TINSGGFTTYADSVRG.....a.m.....s.kp...l...it-----PRGV---k.r.g.....
 13G4v.....a.....**dr...gSSTMG**.f.p...nr.f.aTIAMSAATTHYADAVKG...v...al.v.....kp.....a-----TLTWLGIHEYEYNT.....g.....
 13A7v.....**e.....t.r.mlqYDIDG**.f.....er.g.CRFVNDGSTYYADSVKG.....iv.h.v.....qp.....a---GPITKRRQCVPGFDFSMDF..e.....
 13E9v.....**e.....t.r.dIqYDIA**.f.....er.g.CSFTNDGSTYYADSVKG...m..n.dhr.v...t..qp.....t.v---GPITKRRQCVPGFDFSMDF..e.....
 13G9v.....a.....**v...I.ITMG**.f.....er.f.a-AISGIGAIHYADSVKG...l....ar..vs.h...kp.....a-----KANVESPRESYAY.....g.....

Isolated anti-human P2X7 Nb families

compared with human VH3-23:JH5

evqllesggglvqpggslrlscaasgftfs-----wvraqpkglewsv-----ftisrdnskntlylqmslraedtaavycak-----wgggtlvtvss
1c81 EVQLVESGGGLVQAGGSLRLSCASAGRTFSFSTSTMGWFRQAPGKELRFVAADMSDFNTYYADSVKGRFTISRHNPRNSVYLQLSLKPEDTAVYYCAA--HSETRGGTRFDRPSLYNYWGQGTQVTVSS
3c22 EVQLVESGGGLVQAGGSLRLSCASAGRTFSFSTSTMGWFRQAPGKELRFVAADMSDFNTYYADSVKGRFTISRHNPRNSVYLQLSLKPEDTAVYYCAA--HSETRDGTTRFDRPSLYNYWGQGTQVTVSS
3c29 EVQLVESGGGLVQAGGSLRLSCASAGRTFSFSTSTMGWFRQAPGKELRFVAADMSDFNTYYADSVKGRFTISRHNPRNSVYLQLSLKPEDTAVYYCAA--HSETRGGTRFDRPSLYNYWGQGTQVTVSS
1c113 EVQLVESGGGLVQPGGSLRLSCAASGIAFNYYMS--WHRQAPGKORLVA-DISPGGHTEYEDSVKGRFTISRDNFKNTMTLHMNSLKPEDTAVYYCAA-----RLRFEVSNYWGQGTQVTVSS
1c121 EVQLVESGGGLVQPGGSLRLSCAASGFTFRNYDMS--WVROAPGKPEWVSYMNSGGGTAYADSVKGRFTISRDNKNTLCLQMNSLKPEDTAVYYCAAT-----EKPLGGAMGQGTQVTVSS
1c126 RGAAGGYWRLGAGWGSLSLCAASGTFNNSVMG--WYRQAPGKORLVA-DISGGGVITNYADSVKGRFTISRDNKNNVYLQMHILKPEDTAVYYCNV-----KRRFPIWRDWGKGLITVTVSS
3c23 EVQLVESGGGLVQAGGSLRLSCAASGRTFRHYAMG--WFRQAPGKERFVA-AISSYGSITDYGDSVKGRFTISRDDAKNTVPLQMSLKPEDTAVYYCAAADETILGAVPNFRLHEKYEYEWGQGTQVTVSS
3c28 EMQLVESGGGLVQAGGSLRLSCAASGRTFRHYAMG--WFRQAPGKERFVA-AISSYGSITDYGDSVKGRFTISRDDAKNTVPLQMSLKPEDTAVYYCAAADETILGAVPNFRLHEKYEYEWGQGTQVTVSS
3c31 EVQLVESGGGLVQPGGSLRLSCVVSGFVDDYAIG--WFRQAPGKERGISCTITSSDGNITYALSVKGRFTASSDNKNTVYLQMSLNPEDTAVYYCAA-----DPVRRGWGRDHYKYWGQGTQVTVSS
3c34 EVQLVESGGGLVQPGGSLRLSCVTSGSIFFTSAMA--WFRQVPGKERLVA-TITRDGFTNYIDSVQGRFTISRDNKNNIYLRMNSLKPEDTAVYYCVT-----ILSGKKTWGQGTQVTVSS
3c36 EVQLVESGGGLVQAGGSLRLSCAAGRSIRNYVMS--WFRQAPGKORLVA-DISSGIFTTYQSSVKGRFTISRDNARNAVYLQMSLKPEDTAVYYCVT-----ILSGKKTWGQGTQVTVSS
3c40 EVQLVESGGGLVQAGGSLRLSCAASGNIFFNRMG--WFRQAPGKORLVA-DITSGGRTSYTSSVKGRFTISRDNKNTVYLQMSLKPEDTAVYYCAVA-----ILAGKKSWGQGTQVTVSS
3c39 EVQLVESGGGLVQAGSLRLSCAASGTFSSAYVS--WFRQAPGKORLVA-GLSSGGSFYDDSDVQGRFTISRDNKNTVYLQMSLKPEDTAVYYCART-----YTOAHYYWGQGTQVTVSS

7.4 Abbreviations

3D	three dimensional
ADAM	A disintegrin and metalloprotease
ADP	adenosine diphosphate
AEBSF	4-(2-Aminoethyl) benzenesulfonyl fluoride
AF647	Alexa Fluor 647
ALPP	placental alkaline phosphatase
APAAP	alkaline phosphatase anti-alkaline phosphatase
APC	Allophycocy
ART2	ADP-ribosyl transferase 2
ATP	adenosine triphosphate
BCA	bca bicinchoninic acid
BCR	B cell receptor
BSA	bovine serum albumin
BzATP	benzoyl ATP
CD	cluster of differentiation
cDNA	complementary DNA
CDR	complementary determining region
CH	constant domain of the antibody heavy chain
CHO	chinese hamster ovary
CL	constant domain of the light chain
Cy7	cyanine 7
DAMP	danger-associated molecular pattern
DMBA	7,12-dimethylbenz[α]anthracene
DMEM	Dulbecco's modified Eagle medium
DNA	deoxyribonucleic acid
dNTP	deoxyribonucleotide triphosphate
DOCA	deoxycortisterone acetate
DTR	diphtheria receptor
EAE	Experimental autoimmune encephalomyelitis
EAG	Experimental autoimmune glomerulonephritis
ELISA	Enzyme-linked immunosorbent assay
Fab	fragment antigen binding
FACS	fluorescence-activated cell sorting
Fc	Fragment of crystallization
FCS	foetal calf serum
Fig.	figure
FITC	Fluorescein isothiocyanate
FR	framework regions
FSC	forward scatter
GN	glomerulonephritis
GPCR	G protein-coupled receptor
HCl	hydrochloric acid
HEK	human embryonal kidney cells
HEK hP2X7	human P2X7-transfected HEK cells
HEK mP2X7	mouse P2X7-transfected HEK cells
HEPES	4-(2-hydroxyethyl)-1-piperazineethanesulfonic acid
HLE	half-life extended
hP2X7	human P2X7
Ig	immunoglobulin
IL-10	interleukin-10

IL-18	interleukin-18
IL-1 β	interleukin-1 β
IMAC	Immobilized metal ion affinity chromatography
iNKT	invariant natural killer T cells
IPTG	isopropylthio- β -galactoside
kDa	kilodalton
LB	Luria broth
mAb	monoclonal antibody
MES	2-(N-morpholino)ethanesulfonic acid
mP2X7	mouse P2X7
MS	multiple sclerosis
NaCl	sodium chloride
NAD ⁺	nicotinamide adenine dinucleotide
NALP3	NACHT, LRR and PYD domains-containing protein 3
Nb	Nanobody
Ni-NTA	nickel-nitriloacetic acid
PBS	phosphate buffer saline
PCR	polymerase chain reaction
PE	R-Phycoerythrin
PhoA	alkaline phosphatase
PI	propidium iodide
PS	phosphatidylserine
RNA	ribonucleic acid
RPMI	Roswell Park Memorial Institute (medium)
SDS-PAGE	sodium dodecyl sulfate polyacrylamide
SNP	single nucleotide polymorphism
SOC	super optimal broth with catabolite repression
SSC	sideward scatter
TACE	Tumor necrosis factor- α converting enzyme
TGF- β	tumor growth factor- β
TNF- α	tumor necrosis factor- α
TPA	12-O-tetradecanoylphorbol-13-acetate
TS	tris-HCl sucrose
UV	ultraviolet
V	volt
VH	variable domain of the heavy chain
VHH	variable domain of the heavy chain only antibody
VL	variable domain of the light chain
w/v	weight per volume
wt	wildtype

8 References

- Adinolfi E, Raffaghello L, Giuliani AL, Cavazzini L, Capece M, Chiozzi P, Bianchi G, Kroemer G, Pistoia V & Di Virgilio F (2012) Expression of P2X7 Receptor Increases In Vivo Tumor Growth. *Cancer Res*
- Adriouch S, Bannas P, Schwarz N, Fliegert R, Guse AH, Seman M, Haag F & Koch-Nolte F (2008) ADP-ribosylation at R125 gates the P2X7 ion channel by presenting a covalent ligand to its nucleotide binding site. *FASEB J.* **22**: 861–869
- Adriouch S, Dox C, Welge V, Seman M, Koch-Nolte F & Haag F (2002) Cutting edge: a natural P451L mutation in the cytoplasmic domain impairs the function of the mouse P2X7 receptor. *J. Immunol.* **169**: 4108–4112
- Adriouch S, Haag F, Boyer O, Seman M & Koch-Nolte F (2012) Extracellular NAD(+): a danger signal hindering regulatory T cells. *Microbes Infect.*
- Adriouch S, Hubert S, Pechberty S, Koch-Nolte F, Haag F & Seman M (2007) NAD⁺ released during inflammation participates in T cell homeostasis by inducing ART2-mediated death of naive T cells in vivo. *J. Immunol.* **179**: 186–194
- Alzogaray V, Danquah W, Aguirre A, Urrutia M, Berguer P, García Véscovi E, Haag F, Koch-Nolte F & Goldbaum FA (2011) Single-domain llama antibodies as specific intracellular inhibitors of SpvB, the actin ADP-ribosylating toxin of *Salmonella typhimurium*. *FASEB J.* **25**: 526–534
- Anderson CM & Nedergaard M (2006) Emerging challenges of assigning P2X7 receptor function and immunoreactivity in neurons. *Trends Neurosci.* **29**: 257–262
- Arulkumaran N, Unwin RJ & Tam FW (2011) A potential therapeutic role for P2X7 receptor (P2X7R) antagonists in the treatment of inflammatory diseases. *Expert Opin Investig Drugs* **20**: 897–915
- Azzazy HME & Highsmith WE (2002) Phage display technology: clinical applications and recent innovations. *Clin. Biochem.* **35**: 425–445
- Barbas CF, Kang AS, Lerner RA & Benkovic SJ (1991) Assembly of combinatorial antibody libraries on phage surfaces: the gene III site. *Proc. Natl. Acad. Sci. U.S.A.* **88**: 7978–7982
- Baroja-Mazo A, Barberà-Cremades M & Pelegrín P (2012) The participation of plasma membrane hemichannels to purinergic signaling. *Biochim. Biophys. Acta*
- Baudino L, Shinohara Y, Nimmerjahn F, Furukawa J-I, Nakata M, Martínez-Soria E, Petry F, Ravetch JV, Nishimura S-I & Izui S (2008) Crucial role of aspartic acid at position 265 in the CH2 domain for murine IgG2a and IgG2b Fc-associated effector functions. *J. Immunol.* **181**: 6664–6669
- Becher J, Nader S, Nicola J, Danquah W, Koch-Nolte F & Haag F (2012) P2X7-mediated ATP release by lymphoma cells. In Glasgow
- Beck LH, Bonegio RGB, Lambeau G, Beck DM, Powell DW, Cummins TD, Klein JB & Salant DJ (2009) M-type phospholipase A2 receptor as target antigen in idiopathic membranous nephropathy. *N. Engl. J. Med.* **361**: 11–21
- Becker D, Woltersdorf R, Boldt W, Schmitz S, Braam U, Schmalzing G & Markwardt F (2008) The P2X7 carboxyl tail is a regulatory module of P2X7 receptor channel activity. *J. Biol. Chem.* **283**: 25725–25734
- Blobel CP (2005) ADAMs: key components in EGFR signalling and development. *Nat. Rev. Mol. Cell Biol.* **6**: 32–43

- Buell G, Chessell IP, Michel AD, Collo G, Salazzo M, Herren S, Gretener D, Grahames C, Kaur R, Kosco-Vilbois MH & Humphrey PP (1998) Blockade of human P2X7 receptor function with a monoclonal antibody. *Blood* **92**: 3521–3528
- Burnstock G (2007) Purine and pyrimidine receptors. *Cell. Mol. Life Sci.* **64**: 1471–1483
- Cabrini G, Falzoni S, Forchap SL, Pellegatti P, Balboni A, Agostini P, Cuneo A, Castoldi G, Baricordi OR & Di Virgilio F (2005) A His-155 to Tyr polymorphism confers gain-of-function to the human P2X7 receptor of human leukemic lymphocytes. *J. Immunol.* **175**: 82–89
- Caragnano M, Tortorella P, Bergami A, Ruggieri M, Livrea P, Specchio LM, Martino G, Trojano M, Furlan R & Avolio C (2012) Monocytes P2X7 purinergic receptor is modulated by glatiramer acetate in multiple sclerosis. *J. Neuroimmunol.* **245**: 93–97
- Clackson T, Hoogenboom HR, Griffiths AD & Winter G (1991) Making antibody fragments using phage display libraries. *Nature* **352**: 624–628
- Corrêa G, Marques da Silva C, de Abreu Moreira-Souza AC, Vommaro RC & Coutinho-Silva R (2010) Activation of the P2X(7) receptor triggers the elimination of *Toxoplasma gondii* tachyzoites from infected macrophages. *Microbes Infect.* **12**: 497–504
- Csóka B, Himer L, Selmeczy Z, Vizi ES, Pacher P, Ledent C, Deitch EA, Spolarics Z, Németh ZH & Haskó G (2008) Adenosine A2A receptor activation inhibits T helper 1 and T helper 2 cell development and effector function. *FASEB J.* **22**: 3491–3499
- Davies DR & Chacko S (1993) Antibody structure. *Accounts of chemical research* **26**: 421–427
- Davies DR & Cohen GH (1996) Interactions of protein antigens with antibodies. *Proc. Natl. Acad. Sci. U.S.A.* **93**: 7–12
- De Genst E, Silence K, Decanniere K, Conrath K, Loris R, Kinne J, Muyltermans S & Wyns L (2006) Molecular basis for the preferential cleft recognition by dromedary heavy-chain antibodies. *Proc. Natl. Acad. Sci. U.S.A.* **103**: 4586–4591
- Debiec H, Guignonis V, Mougnot B, Decobert F, Haymann J-P, Bensman A, Deschênes G & Ronco PM (2002) Antenatal membranous glomerulonephritis due to anti-neutral endopeptidase antibodies. *N. Engl. J. Med.* **346**: 2053–2060
- Desmyter A, Transue TR, Ghahroudi MA, Thi MH, Poortmans F, Hamers R, Muyltermans S & Wyns L (1996) Crystal structure of a camel single-domain VH antibody fragment in complex with lysozyme. *Nat. Struct. Biol.* **3**: 803–811
- Di Virgilio F (2007) Liaisons dangereuses: P2X(7) and the inflammasome. *Trends Pharmacol. Sci.* **28**: 465–472
- Di Virgilio F, Ferrari D & Adinolfi E (2009) P2X 7: a growth-promoting receptor—implications for cancer. *Purinergic Signal.* **5**: 251–256
- Dorsam RT & Kunapuli SP (2004) Central role of the P2Y12 receptor in platelet activation. *J. Clin. Invest.* **113**: 340–345
- Dubyak GR (2007) Go it alone no more—P2X7 joins the society of heteromeric ATP-gated receptor channels. *Molecular pharmacology* **72**: 1402–1405
- Ducancel F, Gillet D, Carrier A, Lajeunesse E, Ménez A & Boulain JC (1993) Recombinant colorimetric antibodies: construction and characterization of a bifunctional F(ab)2/alkaline phosphatase conjugate produced in *Escherichia coli*. *Biotechnology (N.Y.)* **11**: 601–605
- Durvasula RV & Shankland SJ (2003) Models of glomerulonephritis. *Methods Mol. Med.* **86**: 47–66

- Edelman GM (1971) ANTIBODY STRUCTURE AND MOLECULAR IMMUNOLOGY*. *Annals of the New York Academy of Sciences* **190**: 5–25
- Fadeel B (2004) Plasma membrane alterations during apoptosis: role in corpse clearance. *Antioxid. Redox Signal.* **6**: 269–275
- Fairbairn IP, Stober CB, Kumararatne DS & Lammas DA (2001) ATP-mediated killing of intracellular mycobacteria by macrophages is a P2X(7)-dependent process inducing bacterial death by phagosome-lysosome fusion. *J. Immunol.* **167**: 3300–3307
- Farrell AW, Gadeock S, Pupovac A, Wang B, Jalilian I, Ranson M & Sluyter R (2010) P2X7 receptor activation induces cell death and CD23 shedding in human RPMI 8226 multiple myeloma cells. *Biochim. Biophys. Acta* **1800**: 1173–1182
- Fernando SL, Saunders BM, Sluyter R, Skarratt KK, Goldberg H, Marks GB, Wiley JS & Britton WJ (2007) A polymorphism in the P2X7 gene increases susceptibility to extrapulmonary tuberculosis. *Am. J. Respir. Crit. Care Med.* **175**: 360–366
- Fredholm BB, Abbracchio MP, Burnstock G, Daly JW, Harden TK, Jacobson KA, Leff P & Williams M (1994) Nomenclature and classification of purinoceptors. *Pharmacol. Rev.* **46**: 143–156
- Friedle SA, Curet MA & Watters JJ (2010) Recent patents on novel P2X7 receptor antagonists and their potential for reducing central nervous system inflammation. *Recent patents on CNS drug discovery* **5**: 35
- Fu W, McCormick T, Qi X, Luo L, Zhou L, Li X, Wang B-C, Gibbons HE, Abdul-Karim FW & Gorodeski GI (2009) Activation of P2X(7)-mediated apoptosis Inhibits DMBA/TPA-induced formation of skin papillomas and cancer in mice. *BMC Cancer* **9**: 114
- Garbers C, Jänner N, Chalaris A, Moss ML, Floss DM, Meyer D, Koch-Nolte F, Rose-John S & Scheller J (2011) Species specificity of ADAM10 and ADAM17 proteins in interleukin-6 (IL-6) trans-signaling and novel role of ADAM10 in inducible IL-6 receptor shedding. *J. Biol. Chem.* **286**: 14804–14811
- Ghetie V, Popov S, Borvak J, Radu C, Matesoi D, Medesan C, Ober RJ & Ward ES (1997) Increasing the serum persistence of an IgG fragment by random mutagenesis. *Nat. Biotechnol.* **15**: 637–640
- Glasscock RJ (2010) The pathogenesis of idiopathic membranous nephropathy: a 50-year odyssey. *American Journal of Kidney Diseases* **56**: 157–167
- Gottesman MM & Ling V (2006) The molecular basis of multidrug resistance in cancer: the early years of P-glycoprotein research. *FEBS letters* **580**: 998–1009
- Gottesman MM, Fojo T & Bates SE (2002) Multidrug resistance in cancer: role of ATP-dependent transporters. *Nat. Rev. Cancer* **2**: 48–58
- Guile SD, Alcaraz L, Birkinshaw TN, Bowers KC, Ebdon MR, Furber M & Stocks MJ (2009) Antagonists of the P2X7 receptor. From lead identification to drug development. *Journal of medicinal chemistry* **52**: 3123–3141
- Gulbransen BD, Bashashati M, Hirota SA, Gui X, Roberts JA, MacDonald JA, Muruve DA, McKay DM, Beck PL, Mawe GM, Thompson RJ & Sharkey KA (2012) Activation of neuronal P2X7 receptor-pannexin-1 mediates death of enteric neurons during colitis. *Nat. Med.* **18**: 600–604
- Haag F, Adriouch S, Brass A, Jung C, Möller S, Scheuplein F, Bannas P, Seman M & Koch-Nolte F (2007) Extracellular NAD and ATP: Partners in immune cell modulation. *Purinergic Signal.* **3**: 71–81
- Hamers-Casterman C, Atarhouch T, Muyldermans S, Robinson G, Hamers C, Songa EB, Bendahman N & Hamers R (1993) Naturally occurring antibodies devoid of light chains. *Nature* **363**: 446–448

- Hattori M & Gouaux E (2012) Molecular mechanism of ATP binding and ion channel activation in P2X receptors. *Nature* **485**: 207–212
- Hiraoka N, Onozato K, Kosuge T & Hirohashi S (2006) Prevalence of FOXP3+ regulatory T cells increases during the progression of pancreatic ductal adenocarcinoma and its premalignant lesions. *Clin. Cancer Res.* **12**: 5423–5434
- Hohmann A, Hodgson AJ, Di W, Skinner JM, Bradley J & Zola H (1988) Monoclonal alkaline phosphatase-anti-alkaline phosphatase (APAAP) complex: production of antibody, optimization of activity, and use in immunostaining. *J. Histochem. Cytochem.* **36**: 137–143
- Holliger P & Hudson PJ (2005) Engineered antibody fragments and the rise of single domains. *Nat. Biotechnol.* **23**: 1126–1136
- Hoque R, Malik AF, Gorelick F & Mehal WZ (2012) Sterile inflammatory response in acute pancreatitis. *Pancreas* **41**: 353–357
- Hubert S, Rissiek B, Klages K, Huehn J, Sparwasser T, Haag F, Koch-Nolte F, Boyer O, Seman M & Adriouch S (2010) Extracellular NAD⁺ shapes the Foxp3+ regulatory T cell compartment through the ART2-P2X7 pathway. *J. Exp. Med.* **207**: 2561–2568
- Inouye H, Michaelis S, Wright A & Beckwith J (1981) Cloning and restriction mapping of the alkaline phosphatase structural gene (phoA) of *Escherichia coli* and generation of deletion mutants in vitro. *J. Bacteriol.* **146**: 668–675
- Jamieson SE, Peixoto-Rangel AL, Hargrave AC, Roubaix L-A de, Mui EJ, Boulter NR, Miller EN, Fuller SJ, Wiley JS, Castellucci L, Boyer K, Peixe RG, Kirisits MJ, Elias L de S, Coyne JJ, Correa-Oliveira R, Sautter M, Smith NC, Lees MP, Swisher CN, et al (2010) Evidence for associations between the purinergic receptor P2X(7) (P2RX7) and toxoplasmosis. *Genes Immun.* **11**: 374–383
- Janeway C Jr, Travers P, Walport M & Shlomchik M (2005) Immunobiology: the immune system in health and disease 6th ed. Garland Science Publishing
- Jennette JC (2003) Rapidly progressive crescentic glomerulonephritis. *Kidney Int.* **63**: 1164–1177
- Jin C & Flavell RA (2010) Molecular mechanism of NLRP3 inflammasome activation. *J. Clin. Immunol.* **30**: 628–631
- Ji X, Naito Y, Weng H, Endo K, Ma X & Iwai N (2012) P2X7 deficiency attenuates hypertension and renal injury in deoxycorticosterone acetate (DOCA)-salt hypertension. *Am. J. Physiol. Renal Physiol.*
- Kabat EA & Wu TT (1991) Identical V region amino acid sequences and segments of sequences in antibodies of different specificities. Relative contributions of VH and VL genes, minigenes, and complementarity-determining regions to binding of antibody-combining sites. *J. Immunol.* **147**: 1709–1719
- Kawate T, Michel JC, Birdsong WT & Gouaux E (2009) Crystal structure of the ATP-gated P2X4 ion channel in the closed state. *Nature* **460**: 592–598
- Kieffmann R, Islam MN, Lindert J, Parthasarathi K & Bhattacharya J (2009) Paracrine purinergic signaling determines lung endothelial nitric oxide production. *Am. J. Physiol. Lung Cell Mol. Physiol.* **296**: L901–10
- Kim J, Bronson CL, Hayton WL, Radmacher MD, Roopenian DC, Robinson JM & Anderson CL (2006) Albumin turnover: FcRn-mediated recycling saves as much albumin from degradation as the liver produces. *Am. J. Physiol. Gastrointest. Liver Physiol.* **290**: G352–60
- Kitching AR, Turner AL, Wilson GRA, Semple T, Odobasic D, Timoshanko JR, O'Sullivan KM, Tipping PG, Takeda K, Akira S & Holdsworth SR (2005) IL-12p40 and IL-18 in crescentic glomerulonephritis: IL-12p40 is the key Th1-defining cytokine chain, whereas IL-18 promotes local inflammation and leukocyte recruitment. *J. Am. Soc. Nephrol.* **16**: 2023–2033

- Klages K, Mayer CT, Lahl K, Loddenkemper C, Teng MWL, Ngiow SF, Smyth MJ, Hamann A, Huehn J & Sparwasser T (2010) Selective depletion of Foxp3⁺ regulatory T cells improves effective therapeutic vaccination against established melanoma. *Cancer Res* **70**: 7788–7799
- Koch-Nolte F, Reyelt J, Schössow B, Schwarz N, Scheuplein F, Rothenburg S, Haag F, Alzogaray V, Cauerhff A & Goldbaum FA (2007) Single domain antibodies from llama effectively and specifically block T cell ecto-ADP-ribosyltransferase ART2.2 in vivo. *FASEB J.* **21**: 3490–3498
- Kumar H, Kawai T & Akira S (2011) Pathogen recognition by the innate immune system. *International reviews of immunology* **30**: 16–34
- la Sala A, Ferrari D, Di Virgilio F, Idzko M, Norgauer J & Girolomoni G (2003) Alerting and tuning the immune response by extracellular nucleotides. *J. Leukoc. Biol.* **73**: 339–343
- Labasi JM, Petrushova N, Donovan C, McCurdy S, Lira P, Payette MM, Brissette W, Wicks JR, Audoly L & Gabel CA (2002) Absence of the P2X7 receptor alters leukocyte function and attenuates an inflammatory response. *J. Immunol.* **168**: 6436–6445
- Lan HY, Nikolic-Paterson DJ, Mu W, Vannice JL & Atkins RC (1995) Interleukin-1 receptor antagonist halts the progression of established crescentic glomerulonephritis in the rat. *Kidney Int.* **47**: 1303–1309
- Lan HY, Nikolic-Paterson DJ, Zarama M, Vannice JL & Atkins RC (1993) Suppression of experimental crescentic glomerulonephritis by the interleukin-1 receptor antagonist. *Kidney Int.* **43**: 479–485
- Laskowski RA, Luscombe NM, Swindells MB & Thornton JM (1996) Protein clefts in molecular recognition and function. *Protein Sci.* **5**: 2438–2452
- Lauwereys M, Arbabi Ghahroudi M, Desmyter A, Kinne J, Hölzer W, De Genst E, Wyns L & Muyldermans S (1998) Potent enzyme inhibitors derived from dromedary heavy-chain antibodies. *EMBO J.* **17**: 3512–3520
- Le Gall SM, Bobé P, Reiss K, Horiuchi K, Niu X-D, Lundell D, Gibb DR, Conrad D, Saftig P & Blobel CP (2009) ADAMs 10 and 17 represent differentially regulated components of a general shedding machinery for membrane proteins such as transforming growth factor alpha, L-selectin, and tumor necrosis factor alpha. *Mol. Biol. Cell* **20**: 1785–1794
- Lees MP, Fuller SJ, McLeod R, Boulter NR, Miller CM, Zakrzewski AM, Mui EJ, Witola WH, Coyne JJ, Hargrave AC, Jamieson SE, Blackwell JM, Wiley JS & Smith NC (2010) P2X7 receptor-mediated killing of an intracellular parasite, *Toxoplasma gondii*, by human and murine macrophages. *J. Immunol.* **184**: 7040–7046
- Lemieux GA, Blumenkron F, Yeung N, Zhou P, Williams J, Grammer AC, Petrovich R, Lipsky PE, Moss ML & Werb Z (2007) The low affinity IgE receptor (CD23) is cleaved by the metalloproteinase ADAM10. *J. Biol. Chem.* **282**: 14836–14844
- Li T, Bourgeois J, Celli S & Glacial F (2012) Cell-penetrating anti-GFAP VHH and corresponding fluorescent fusion protein VHH-GFP spontaneously cross the blood-brain barrier and specifically recognize *The FASEB Journal*
- Li X, Kostareli E, Suffner J, Garbi N & Hämmerling GJ (2010) Efficient Treg depletion induces T-cell infiltration and rejection of large tumors. *Eur. J. Immunol.* **40**: 3325–3335
- Loma I & Heyman R (2011) Multiple sclerosis: pathogenesis and treatment. *Curr Neuropharmacol* **9**: 409–416
- Lucattelli M, Cicko S, Müller T, Lommatzsch M, De Cunto G, Cardini S, Sundas W, Grimm M, Zeiser R, Dürk T, Zissel G, Sorichter S, Ferrari D, Di Virgilio F, Virchow JC, Lungarella G & Idzko M (2011)

- P2X7 receptor signaling in the pathogenesis of smoke-induced lung inflammation and emphysema. *Am. J. Respir. Cell Mol. Biol.* **44**: 423–429
- Matute C, Torre I, Pérez-Cerdá F, Pérez-Samartín A, Alberdi E, Etxebarria E, Arranz AM, Ravid R, Rodríguez-Antigüedad A, Sánchez-Gómez M & Domercq M (2007) P2X(7) receptor blockade prevents ATP excitotoxicity in oligodendrocytes and ameliorates experimental autoimmune encephalomyelitis. *J. Neurosci.* **27**: 9525–9533
- Mead DA & Kemper B (1988) Chimeric single-stranded DNA phage-plasmid cloning vectors. *Biotechnology* **10**: 85–102
- Mehta VB, Hart J & Wewers MD (2001) ATP-stimulated release of interleukin (IL)-1 β and IL-18 requires priming by lipopolysaccharide and is independent of caspase-1 cleavage. *J. Biol. Chem.* **276**: 3820–3826
- Meyer-Schwesinger C, Dehde S, Klug P, Becker JU, Mathey S, Arefi K, Balabanov S, Venz S, Endlich K-H, Pekna M, Gessner JE, Thaiss F & Meyer TN (2011) Nephrotic syndrome and subepithelial deposits in a mouse model of immune-mediated anti-podocyte glomerulonephritis. *J. Immunol.* **187**: 3218–3229
- Moon H, Na H-Y, Chong KH & Kim TJ (2006) P2X7 receptor-dependent ATP-induced shedding of CD27 in mouse lymphocytes. *Immunol. Lett.* **102**: 98–105
- Möller S, Jung C, Adriouch S, Dubberke G, Seyfried F, Seman M, Haag F & Koch-Nolte F (2007) Monitoring the expression of purinoceptors and nucleotide-metabolizing ecto-enzymes with antibodies directed against proteins in native conformation. *Purinergic Signal.* **3**: 359–366
- Muruganandam A, Tanha J, Narang S & Stanimirovic D (2002) Selection of phage-displayed llama single-domain antibodies that transmigrate across human blood-brain barrier endothelium. *FASEB J.* **16**: 240–242
- Muyldermans S (2001) Single domain camel antibodies: current status. *J. Biotechnol.* **74**: 277–302
- Muyldermans S, Cambillau C & Wyns L (2001) Recognition of antigens by single-domain antibody fragments: the superfluous luxury of paired domains. *Trends Biochem. Sci.* **26**: 230–235
- Nguyen VK, Su C, Muyldermans S & van der Loo W (2002) Heavy-chain antibodies in Camelidae; a case of evolutionary innovation. *Immunogenetics* **54**: 39–47
- Nicke A (2008) Homotrimeric complexes are the dominant assembly state of native P2X7 subunits. *Biochem. Biophys. Res. Commun.* **377**: 803–808
- Nicke A, Kuan Y-H, Masin M, Rettinger J, Marquez-Klaka B, Bender O, Górecki DC, Murrell-Lagnado RD & Soto F (2009) A functional P2X7 splice variant with an alternative transmembrane domain 1 escapes gene inactivation in P2X7 knock-out mice. *J. Biol. Chem.* **284**: 25813–25822
- Noelle RJ, Roy M, Shepherd DM, Stamenkovic I, Ledbetter JA & Aruffo A (1992) A 39-kDa protein on activated helper T cells binds CD40 and transduces the signal for cognate activation of B cells. *Proc. Natl. Acad. Sci. U.S.A.* **89**: 6550
- Pasqualini R & Ruoslahti E (1996) Organ targeting in vivo using phage display peptide libraries. *Nature* **380**: 364–366
- Pelegri P & Surprenant A (2006) Pannexin-1 mediates large pore formation and interleukin-1 β release by the ATP-gated P2X7 receptor. *EMBO J.* **25**: 5071–5082
- Perregaux DG, McNiff P, Laliberte R, Conklyn M & Gabel CA (2000) ATP acts as an agonist to promote stimulus-induced secretion of IL-1 beta and IL-18 in human blood. *J. Immunol.* **165**: 4615–4623

- Pétrilli V, Papin S, Dostert C, Mayor A, Martinon F & Tschopp J (2007) Activation of the NALP3 inflammasome is triggered by low intracellular potassium concentration. *Cell Death Differ.* **14**: 1583–1589
- Prunotto M, Carnevali ML, Candiano G, Murtas C, Bruschi M, Corradini E, Trivelli A, Magnasco A, Petretto A & Santucci L (2010) Autoimmunity in membranous nephropathy targets aldose reductase and SOD2. *J. Am. Soc. Nephrol.* **21**: 507–519
- Pusey CD & Peters DK (1993) Immunopathology of glomerular and interstitial disease. In *Diseases of the kidney*, Schrier RW & Gottschalk CW (eds) pp 1647–1680. Boston: Little, Brown and Co.
- Reeves G & Todd I (1996) Immunology 3rd ed.
- Richards-Williams C, Contreras JL, Berecek KH & Schwiebert EM (2008) Extracellular ATP and zinc are co-secreted with insulin and activate multiple P2X purinergic receptor channels expressed by islet beta-cells to potentiate insulin secretion. *Purinergic Signal.* **4**: 393–405
- Rissiek B (2012) Untersuchung des Einflusses von extrazellulärem Nikotinamidadenindinukleotid (NAD⁺) auf regulatorische T Zellen der Maus (*Mus musculus*, Linnaeus, 1758) Koch-Nolte F (ed) Hamburg
- Rodríguez RM, López-Vázquez A & López-Larrea C (2012) Immune systems evolution. *Adv. Exp. Med. Biol.* **739**: 237–251
- Russel M (1991) Filamentous phage assembly. *Mol. Microbiol.* **5**: 1607–1613
- Schatz PJ (1993) Use of peptide libraries to map the substrate specificity of a peptide-modifying enzyme: a 13 residue consensus peptide specifies biotinylation in *Escherichia coli*. *Biotechnology (N.Y.)* **11**: 1138–1143
- Scheuplein F (2005) PhD Thesis: Molecular mechanism and role of the ADP-ribosyltransferase mediated apoptosis in T cells Koch-Nolte F (ed)
- Scheuplein F, Rissiek B, Driver JP, Chen Y-G, Koch-Nolte F & Serreze DV (2010) A recombinant heavy chain antibody approach blocks ART2 mediated deletion of an iNKT cell population that upon activation inhibits autoimmune diabetes. *J. Autoimmun.* **34**: 145–154
- Scheuplein F, Schwarz N, Adriouch S, Krebs C, Bannas P, Rissiek B, Seman M, Haag F & Koch-Nolte F (2009) NAD⁺ and ATP released from injured cells induce P2X7-dependent shedding of CD62L and externalization of phosphatidylserine by murine T cells. *J. Immunol.* **182**: 2898–2908
- Schwarz N, Drouot L, Nicke A, Fliegert R, Boyer O, Guse AH, Haag F, Adriouch S & Koch-Nolte F (2012) Alternative Splicing of the N-Terminal Cytosolic and Transmembrane Domains of P2X7 Controls Gating of the Ion Channel by ADP-Ribosylation. *PLoS One* **7**
- Seman M, Adriouch S, Scheuplein F, Krebs C, Freese D, Glowacki G, Deterre P, Haag F & Koch-Nolte F (2003) NAD-induced T cell death: ADP-ribosylation of cell surface proteins by ART2 activates the cytolytic P2X7 purinoceptor. *Immunity* **19**: 571–582
- Sharp AJ, Polak PE, Simonini V, Lin SX, Richardson JC, Bongarzone ER & Feinstein DL (2008) P2x7 deficiency suppresses development of experimental autoimmune encephalomyelitis. *J Neuroinflammation* **5**: 33
- Sluyter R & Stokes L (2011) Significance of P2X7 receptor variants to human health and disease. *Recent Pat DNA Gene Seq* **5**: 41–54
- Smart ML, Gu B, Panchal RG, Wiley J, Cromer B, Williams DA & Petrou S (2003) P2X7 receptor cell surface expression and cytolytic pore formation are regulated by a distal C-terminal region. *J. Biol. Chem.* **278**: 8853–8860

- Smith GP (1985) Filamentous fusion phage: novel expression vectors that display cloned antigens on the virion surface. *Science* **228**: 1315–1317
- Sorge RE, Trang T, Dorfman R, Smith SB, Beggs S, Ritchie J, Austin J-S, Zaykin DV, Vander Meulen H, Costigan M, Herbert TA, Yarkoni-Abitbul M, Tichauer D, Livneh J, Gershon E, Zheng M, Tan K, John SL, Slade GD, Jordan J, et al (2012) Genetically determined P2X7 receptor pore formation regulates variability in chronic pain sensitivity. *Nat. Med.* **18**: 595–599
- Sospedra M & Martin R (2005) Immunology of multiple sclerosis*. *Annu. Rev. Immunol.* **23**: 683–747
- Stokes L, Fuller SJ, Sluyter R, Skarratt KK, Gu BJ & Wiley JS (2010) Two haplotypes of the P2X(7) receptor containing the Ala-348 to Thr polymorphism exhibit a gain-of-function effect and enhanced interleukin-1beta secretion. *FASEB J.* **24**: 2916–2927
- Surprenant A & North RA (2009) Signaling at purinergic P2X receptors. *Annual review of physiology* **71**: 333–359
- Suzuki T, Hide I, Ido K, Kohsaka S, Inoue K & Nakata Y (2004) Production and release of neuroprotective tumor necrosis factor by P2X7 receptor-activated microglia. *J. Neurosci.* **24**: 1–7
- Szakács G, Paterson JK, Ludwig JA, Booth-Genthe C & Gottesman MM (2006) Targeting multidrug resistance in cancer. *Nature Reviews Drug Discovery* **5**: 219–234
- Tam FW, Karkar AM, Smith J, Yoshimura T, Steinkasserer A, Kurrle R, Langner K & Rees AJ (1996) Differential expression of macrophage inflammatory protein-2 and monocyte chemoattractant protein-1 in experimental glomerulonephritis. *Kidney Int.* **49**: 715–721
- Tam FWK (2006) Current pharmacotherapy for the treatment of crescentic glomerulonephritis.
- Tang WW, Qi M & Warren JS (1996) Monocyte chemoattractant protein 1 mediates glomerular macrophage infiltration in anti-GBM Ab GN. *Kidney Int.* **50**: 665–671
- Taylor SRJ, Turner CM, Elliott JI, McDaid J, Hewitt R, Smith J, Pickering MC, Whitehouse DL, Cook HT, Burnstock G, Pusey CD, Unwin RJ & Tam FWK (2009) P2X7 deficiency attenuates renal injury in experimental glomerulonephritis. *J. Am. Soc. Nephrol.* **20**: 1275–1281
- Tesch GH, Yang N, Yu H, Lan HY, Foti R, Chadban SJ, Atkins RC & Nikolic-Paterson DJ (1997) Intrinsic renal cells are the major source of interleukin-1 beta synthesis in normal and diseased rat kidney. *Nephrol. Dial. Transplant.* **12**: 1109–1115
- Tijink BM, Laeremans T, Budde M, Stigter-van Walsum M, Dreier T, de Haard HJ, Leemans CR & van Dongen GAMS (2008) Improved tumor targeting of anti-epidermal growth factor receptor Nanobodies through albumin binding: taking advantage of modular Nanobody technology. *Mol. Cancer Ther.* **7**: 2288–2297
- Torres GE, Egan TM & Voigt MM (1999) Hetero-oligomeric assembly of P2X receptor subunits. Specificities exist with regard to possible partners. *J. Biol. Chem.* **274**: 6653–6659
- Trang T, Beggs S & Salter MW (2012) ATP receptors gate microglia signaling in neuropathic pain. *Exp. Neurol.* **234**: 354–361
- Turner CM, Tam FWK, Lai P-C, Tarzi RM, Burnstock G, Pusey CD, Cook HT & Unwin RJ (2007) Increased expression of the pro-apoptotic ATP-sensitive P2X7 receptor in experimental and human glomerulonephritis. *Nephrol. Dial. Transplant.* **22**: 386–395
- Unger M (2012) Klonierung und molekulare Charakterisierung von einzeldomänen Antikörpern gegen das membranständige Ekto-Enzym CD38 aus Homo sapiens und gegen toxine aus Clostridium difficile Koch-Nolte F (ed) Hamburg: University of Hamburg

- Vallé A, Zuber CE, Defrance T, Djossou O, Riem MD & Banchereau J (1989) Activation of human B lymphocytes through CD40 and interleukin 4. *Eur. J. Immunol.* **19**: 1463–1467
- Vu KB, Ghahroudi MA, Wyns L & Muyldermans S (1997) Comparison of llama VH sequences from conventional and heavy chain antibodies. *Mol. Immunol.* **34**: 1121–1131
- Wang X, Arcuino G, Takano T, Lin J, Peng WG, Wan P, Li P, Xu Q, Liu QS, Goldman SA & Nedergaard M (2004) P2X7 receptor inhibition improves recovery after spinal cord injury. *Nat. Med.* **10**: 821–827
- Weber FC, Esser PR, Müller T, Ganesan J, Pellegatti P, Simon MM, Zeiser R, Idzko M, Jakob T & Martin SF (2010) Lack of the purinergic receptor P2X(7) results in resistance to contact hypersensitivity. *J. Exp. Med.* **207**: 2609–2619
- Wesolowski J, Alzogaray V, Reyelt J, Unger M, Juarez K, Urrutia M, Cauerhff A, Danquah W, Rissiek B, Scheuplein F, Schwarz N, Adriouch S, Boyer O, Seman M, Licea A, Serreze DV, Goldbaum FA, Haag F & Koch-Nolte F (2009) Single domain antibodies: promising experimental and therapeutic tools in infection and immunity. *Med. Microbiol. Immunol.* **198**: 157–174
- Wiley JS, Sluyter R, Gu BJ, Stokes L & Fuller SJ (2011) The human P2X7 receptor and its role in innate immunity. *Tissue Antigens* **78**: 321–332
- Wilhelm K, Ganesan J, Müller T, Dürr C, Grimm M, Beilhack A, Krempl CD, Sorichter S, Gerlach UV, Jüttner E, Zerweck A, Gärtner F, Pellegatti P, Di Virgilio F, Ferrari D, Kambham N, Fisch P, Finke J, Idzko M & Zeiser R (2010) Graft-versus-host disease is enhanced by extracellular ATP activating P2X7R. *Nat. Med.* **16**: 1434–1438
- Yiangou Y, Facer P, Durrenberger P, Chessell IP, Naylor A, Bountra C, Banati RR & Anand P (2006) COX-2, CB2 and P2X7-immunoreactivities are increased in activated microglial cells/macrophages of multiple sclerosis and amyotrophic lateral sclerosis spinal cord. *BMC Neurol* **6**: 12
- Yip L, Woehrle T, Corriden R, Hirsh M, Chen Y, Inoue Y, Ferrari V, Insel PA & Junger WG (2009) Autocrine regulation of T-cell activation by ATP release and P2X7 receptors. *FASEB J.* **23**: 1685–1693
- Young MT (2010) P2X receptors: dawn of the post-structure era. *Trends Biochem. Sci.* **35**: 83–90
- Zou W, Curiel T & Zou L (2005) Specific recruitment of regulatory T cells in ovarian carcinoma fosters immune privilege and predicts reduced survival. ... *for Cancer Research*